DESIGN AND ANALYSIS OF MILLIMETER-WAVE BACKHAUL NETWORKS IN URBAN ENVIRONMENTS

A Dissertation
Presented to
The Academic Faculty

By

Qiang Hu

In Partial Fulfillment
of the Requirements for the Degree
Doctor of Philosophy in the
School of Electrical and Computer Engineering

Georgia Institute of Technology

December 2019

DESIGN AND ANALYSIS OF MILLIMETER-WAVE BACKHAUL NETWORKS IN URBAN ENVIRONMENTS

Approved by:

Dr. Douglas M. Blough, Advisor
School of Electrical and Computer Engineering
Georgia Institute of Technology

Dr. Raghupathy Sivakumar
School of Electrical and Computer Engineering
Georgia Institute of Technology

Dr. Gee-Kung Chang
School of Electrical and Computer Engineering
Georgia Institute of Technology

Dr. Yusun Chang
School of Electrical and Computer Engineering
Georgia Institute of Technology

Dr. David Goldsman
School of Industrial and Systems Engineering
Georgia Institute of Technology

Date Approved: August 15, 2019

The definition of genius is taking the complex and making it simple.

Albert Einstein

To my family, for your endless love and support.

ACKNOWLEDGEMENTS

It has been 5 year since I came to Atlanta from Nanjing to start my graduate study at Georgia Tech. During this wonderful PhD journey, I have been always grateful for the endless help and support from Jesus Christ, family, advisor, and friends. This surely is not a short journey and I almost gave up at several points in the middle of it, but every time, because of Him and His amazing grace, I figured a way out and went back on the right track. All thanks to the LORD and Jesus Christ!

My father, Qishan Hu, I miss you so much. Thank you and mom for giving me life, teaching me to live it, and loving me every step of the way. I hope I do not let you down and I know you are always looking at me and smiling in the heaven. You will always be with me. My mom, Kexia Qing, and my sister, Xuyan Hu, thank you so much for always supporting me to continue my study far far away from home. Thank you for taking care of dad when I was not there. Wish I can take care of you both in the rest of our lives. I have to express my special thanks to Dr. Blough, who is my advisor during my PhD study. Without his patient coaching and helpful advice, I cannot make it here today. From every aspect, you are the best advisor I can expect. My lab mates, Mengyao, Chuanji, Huiye, Yuchen, Yan, Hemin, Ang, and Lei: I enjoy every minute we spent together in the lab, and thank you all for the help and support in this thesis work. To my dear friends: Manchen, Liang, Long, Yimeng, and Yun: with you all, I feel I am not alone, and those joy and fun we shared together will always be remembered. To my church family: you are the great cloud surrounding me and thank you for being my family here in Atlanta. In the end, the support of the U.S. National Science Foundation for my research is gratefully acknowledged.

TABLE OF CONTENTS

LIST OF TABLES

LIST OF FIGURES

SUMMARY

With the pervasive deployment of small cells in the 5G era, the crucial challenge of providing backhaul to the gateway node arises, because of the construction limitations and prohibitive cost of connecting all small-cell base stations (BSs) through wired connections such as fiber. Millimeter-wave (mmWave) band based wireless backhaul becomes a promising solution to this challenge due to the massive available bandwidth and the advantages brought by the use of high-gain highly-directional antennas. However, the poor propagation characteristics and severe blockage effect of mmWave signals must be considered and overcome within the design and optimization of mmWave backhaul networks. To address the backhaul challenge, we propose a new relay-assisted network architecture for mmWave backhaul in urban environments. Through deploying mmWave relays dedicated to the backhaul usage, multi-hop relay paths with multi-Gbps capacity are established between BSs, where direct line-of-sight (LoS) paths are not available.

The objective of this dissertation is to design and analyze the relay-assisted mmWave backhaul network in the urban environment for 5G communication systems. First, for constructing a multi-hop relay path between a pair of BSs in the dense urban area, a novel algorithm is proposed to select relays from a set of candidate relay locations so that ultra-high end-to-end throughput can be maintained to support the large backhaul traffic demand. We design an optimal scheduling algorithm for physical links along the multi-hop relay path, and integrate the optimal scheduling algorithm into the relay selection algorithm to find the hop-limited interference-minimal throughput-optimal path. Second, to build a relay-assisted mmWave backhaul network with a tree topology, which contains a set of pre-defined logical links between BSs, the relay selection algorithm is upgraded to not only consider controlling the mutual interference within a multi-hop path, but also have the ability to minimize the mutual interference among different paths. Two methods are proposed to improve the feasibility of constructing a backhaul network where all logical

links are interference-minimal and meet the pre-defined link rate requirement. Third, upon a new interference model, through linear programming, we can find the maximum uniform traffic demand of small-cell BSs and the maximum aggregated traffic demand at the macro-cell BS that can be supported by the given relay-assisted mmWave backhaul network in either the downlink or uplink case. An efficient distributed scheduling algorithm is also proposed, which can be installed easily in the practical system. Fourth, as for deploying mmWave backhaul networks along the urban roadside environment to provide 5G services to vehicles, a novel interference-minimal throughput-optimal backhaul topology is proposed and analyzed. Fifth, to enable the simulation of mmWave out-of-band backhaul networks, we propose a new design of mmWave backhaul module in ns-3. On the other hand, we implement the optimal scheduling algorithm in the existing mmWave in-band backhaul module in ns-3 to evaluate the performance of a single multi-hop logical link.

CHAPTER 1
INTRODUCTION

Facing the shortage of available spectrum in microwave bands and the increasing global mobile data traffic demand, millimeter-wave (mmWave) technology obtains a lot attention and is being heavily researched due to its potential of enabling broadband radio access and backhaul with ultra-high data speed in future 5G wireless networks [1, 2, 3, 4].

1.1 Motivations and Research Objectives

In the 5G era, the cell size becomes smaller, and operators will deploy a large number of small-cell base stations (BSs), which cooperate with legacy macro-cell BSs, to provide better coverage and higher data rate to cellular users in urban environments. However, most of small-cell BSs may not have wired connections to the core network due to the construction limits and prohibitive cost in many places such as North America, so that small-cell BSs can only connect to the core network with the help from nearby macro-cell BSs acting as gateway nodes. Thus, this small-cell trend brings the *backhaul challenge* of transferring the huge amount of data between small-cell BSs and macro-cell BSs. Being able to support multi-Gbps wireless links, mmWave backhauling has been regarded as a promising solution to the backhaul challenge in 5G cellular systems.

However, a few obstacles need to be overcome before mmWave communication and backhauling can be widely accepted and deployed. For example, mmWave signals experience higher free-space path loss than sub-6 GHz wireless signals. Atmospheric absorption and rain attenuation [5] compound the path loss problem[1]. Another significant problem of mmWave links is the significant communication loss when an obstacle blocks the line-of-

[1]Note that the proposed mmWave backhaul architecture in this dissertation can work closely with other types of wireless backhaul such as backhaul using free space optics to provide enhanced robustness and throughput performance [6, 7, 8].

sight (LoS) path between transmitter and receiver, which is known as the *blockage effect*. These propagation issues limit the communication range for very high rate mmWave links to a few hundred meters or less.

There are also positive aspects of mmWaves beyond the potential for high rates. One advantage is the ability to integrate a large number of antenna elements into wireless nodes, which can be used to produce narrow beam width directional antennas with high antenna gain. It helps alleviate signal propagation problems and reduces the interference footprint.

To make the mmWave backhaul network feasible, all these unique propagation features of mmWave signals and the development of mmWave communication technologies have to be taken into account. Besides, we need to figure out the way that the backhaul tier interacts with the access tier in the 5G small-cell cellular system, the backhaul network architecture and topology design, and the method used to optimize the performance of mmWave backhaul networks.

Nowadays, mmWave backhaul networks can be categorized into two types, the "in-band" backhaul and the "out-of-band" backhaul, based on the sharing policy of frequency bands used by the access and backhaul tiers. If both tiers share the same frequency band, it is the in-band case; while in the out-of-band backhaul, both the access and backhaul tiers operate on their dedicated frequency bands that do not overlap with each other. The out-of-band mmWave backhaul solution is adopted for the research work in this dissertation, because it provides more flexibility on the design of mmWave backhaul networks, as well as more room to enhance the backhaul network performance.

On the other hand, some research work use the mmWave "self-backhaul" network architecture, in which small-cell BSs connect with each other directly through mmWave wireless links. However, considering the abundant obstacles (e.g., buildings, billboards, trees, etc.) in dense urban environments, it may not be always possible to find LoS paths between intended BS pairs. The NLoS mmWave links cannot support the ultra-high data rate required in backhaul due to the severe reflection attenuation. Thus, we anticipate a number

of dedicated mmWave relays are deployed to form a sequence of relatively short but very high rate LoS mmWave links combining to connect a pair of BSs, and we refer to this as the *relay-assisted mmWave backhaul* architecture.

Since the backhaul traffic demand is ultra-high, the performance of the mmWave backhaul network has to be well analyzed and optimized. The placement of mmWave relays and the scheduling of individual physical links greatly impact the construction and throughput performance of interference-minimal multi-hop relay paths between BSs in the dense urban area. Moreover, when multiple mmWave relay paths need to be established simultaneously in the mmWave backhaul network, the challenge of intelligent relay selection approaches to the next level, because the mutual interference both within and between paths has to be minimized; meanwhile the relay sharing issue has to be resolved as well, since relays are relatively simple devices which are assumed not to be shared by multiple paths. After the mmWave backhaul network topology has been constructed, the overall system performance is largely affected by the scheduling of all logical links between BSs in the network, when practical factors are considered. Finding an efficient scheduling scheme is not trivial under different mmWave backhaul network settings.

Our focus is on the system design and performance analysis of the relay-assisted mmWave backhaul network in the urban environment. The objective of this thesis is to address the challenges therein and establish the fundamentals of the relay-assisted mmWave backhauling for 5G cellular systems.

1.2 Contributions

The primary contributions of this thesis are listed below:

- The first contribution (Chapter 3) is that using a 3D model for buildings targeted at urban environments, we provide optimal and efficient algorithms both for scheduling communications along a single mmWave relay-assisted path and for choosing the relay-assisted path with maximum throughput among all candidate paths connect-

ing a given base station pair. In addition to proving optimality of these algorithms, we evaluate their performance through simulations based on a real urban topology. Simulation results show that our algorithms can produce short relay paths with end-to-end throughputs of around 10 Gbps and higher that are capable of providing virtual mmWave links for a wireless backhaul use case.

- The second contribution (Chapter 4) is that we investigate problem of constructing multiple mmWave backhaul logical links between a set of BSs in urban areas. We propose an algorithm to find high-throughput LoS relaying paths for all logical links by minimizing interference within and between paths. We also propose methods to modify the backhaul topology to increase the probability of finding high-throughput paths using our algorithm. Extensive simulations, based on a 3-D model of a section of downtown Atlanta, are conducted to show the effectiveness of our algorithms and models. Some insights on the network design problem are also provided.

- The third contribution (Chapter 5) is that a novel interference model is proposed which reflects the characteristics of proposed relay-assisted mmWave backhaul networks. Based on the proposed interference model, we can obtain the maximum uniform downlink or uplink traffic demand of each small-cell BS and the maximum aggregated downlink or uplink traffic demand at the macro-cell BS, which are supported by the tree-style backhaul network, through linear programming. Different mutual interference and radio chain resource conditions are considered.

- The fourth contribution (Chapter 6) is that an efficient distributed scheduling algorithm is proposed, which can be easily implemented into the relay-assisted mmWave backhaul network in practice. The simulation results show that the throughput performance of the proposed scheduling algorithm is very close to the maximal values obtained through theoretic analysis in certain traffic settings, and it can adapt to the scenario where dynamic traffic demand is applied to small-cell BSs in the backhaul

network.

- The fifth contribution (Chapter 7) is that we investigate mmWave backhaul networks that use relay nodes and a regular triangular-wave topology to meet the very high data rates necessary to handle backhaul traffic in the roadside scenario. The challenge is to manage the self interference that can occur due to the near- straight-line topology that arises from a roadside deployment. The triangular-wave is a regular topology that can be deployed on regularly-spaced lampposts alongside a road. We derive conditions necessary for the triangular-wave topology to be interference-minimal and throughput-optimal. We also investigate how the proposed topology performs using lamppost positions taken from a 12 km stretch of highway in Atlanta. Results show that the topology can achieve throughputs very close to the ideal case and is capable of supporting backhaul throughputs of 10+ Gbps in real roadside environments.

- The sixth contribution (Chapter 8) is that we address the issue of realizing end-to-end simulation of mmWave out-of-band backhaul networks in ns-3. A novel design for integrating mmWave out-of-band backhaul in ns-3 is proposed, which includes a custom network backhaul device that can be added to nodes to enable the out-of-band backhaul transmissions. We also implement an extension to the existing mmWave integrated-access-and-backhaul (IAB) module in ns-3 to simulate the basic functionalities of the out-of-band backhaul and produce some preliminary results on the throughput performance. The existing scheduler in the IAB module is modified to support customizable scheduling for logical links in out-of-band backhaul networks.

1.3 Organization of the Thesis

The rest of the thesis is organized as follows. In Chapter 2, we provide a brief introduction on the mmWave communication technology, the mmWave backhaul use case, and the novel mmWave relay-assisted backhaul network architecture. Then, in Chapter 3, a novel

relay selection algorithm is proposed to construct a hop-limited relay path with optimal throughput between a pair of BSs in the dense urban area. Moreover, in Chapter 4 the problem of constructing multiple mmWave backhaul logical links simultaneously in the dense urban area is addressed via an enhanced relay selection algorithm that can minimize the mutual interference within and between paths and avoid the relay sharing between logical links as well. In addition, the maximum uniform traffic demand of small-cell BSs and the maximum aggregated traffic demand at the macro-cell BS that can be supported by a given tree-style mmWave backhaul are obtained using linear programming in Chapter 5. The distributed scheduling algorithm for the mmWave relay-assisted backhaul network is discussed in Chapter 6. In Chapter 7, we propose and analyze the triangular-wave topology, which is a regular topology well-suited for the deployment along the roadside environment. Additionally, in Chapter 8, we introduce our approach to simulate mmWave out-of-band backhaul networks in ns-3. Finally, in Chapter 9, our conclusions and suggestions for future work are provided.

CHAPTER 2
BACKGROUND AND PRELIMINARIES

In this chapter, we will review the preliminary knowledge of mmWave communication and networking technologies, and the current status of mmWave backhaul related research.

2.1 Characteristics of mmWave wireless communications

The research on mmWave wireless communications can be traced back to 1960s, when researchers started to investigate the propagation characteristics of wireless signals on the mmWave band [9, 10]. Some of them also explored applications of mmWave wireless transmissions in the satellite communication system [11] and the radar system [12]. Nowadays, as the fast development in electronic circuits and antenna technologies, it becomes more likely that mmWave wireless communications can be applied to the next generation of cellular systems. Therefore, the research on mmWave wireless communications has again attracted a lot attention from both academia and industry. In this section, we will go through some of the latest research results on the characteristics of mmWave wireless communications.

2.1.1 Propagation characteristics of mmWave wireless signals

As one of the key enabling technologies of 5G cellular systems, mmWave communications can enjoy more than giga-Hertz (GHz) available frequency spectrum from 30 GHz to 300 GHz, which has been quite scarce in the sub-6GHz band. Because the mmWave frequency range is very large and different mmWave sub-bands have different propagation characteristics, only a few mmWave sub-bands, such as 28 GHz, 38 GHz, 60 GHz, and E-band (71-76 GHz and 81-86 GHz), will be selected to use in the 5G cellular system. The propagation features of mmWave signals in different sub-bands have been extensively researched

by both academia and industry. Here we provide some significant research results in this area.

Rain attenuation and atmospheric absorption

Compared with the wireless signals in the sub-6 GHz band, mmWave signals suffer from huge propagation loss. One main reason is that the propagation loss of wireless signals is quadratic to the signal frequency. Another significant reason is the weather condition may contribute greatly to the path loss of mmWave signals. It is well known that the rain attenuation and atmospheric and molecular absorption limit the range of mmWave communications [13, 14, 15]. Figure 2.1 and 2.2 show the measured attenuation features of mmWave signals in different bands due to atmospheric and molecular absorption and rain attenuation respectively.

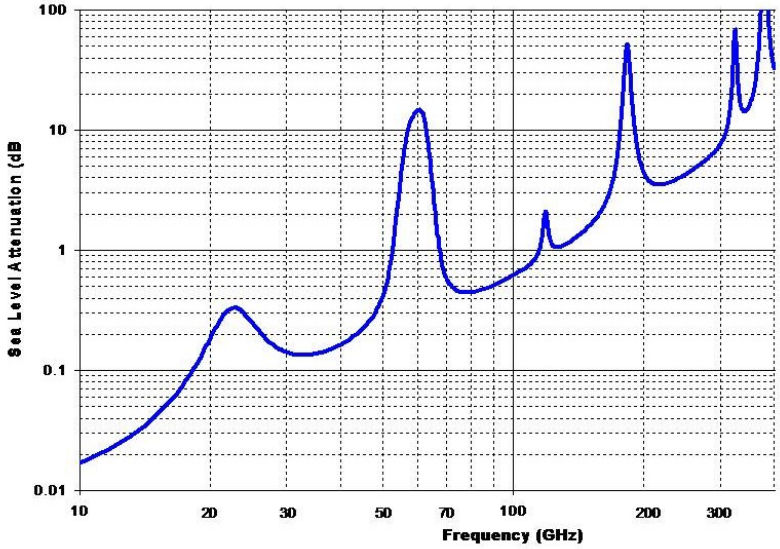

Figure 2.1: Atmospheric and molecular absorption of mmWave signals [15]

From these two figures, we can see that the rain attenuation and atmospheric absorption do not add significant path loss for the signal propagation distance on the order of 300 m [16]. Therefore, mmWave communications are mainly used for indoor scenarios, and small cell access and backhaul with cell sizes on the order of 300 m.

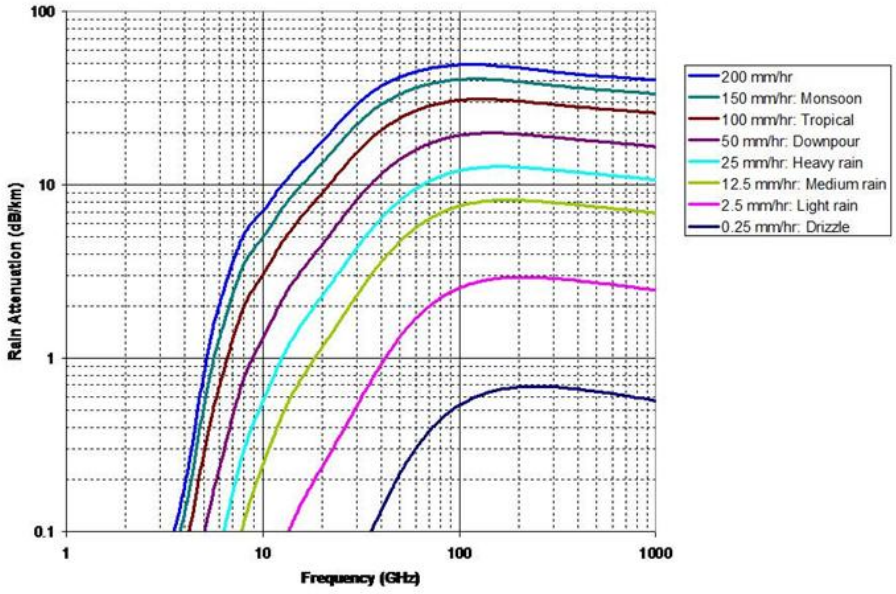

Figure 2.2: Rain attenuation of mmWave signals[15]

mmWave channel models and path loss calculation

3GPP has proposed TR 38.900 and TR 38.901 channel models for above 6GHz frequency, which provide details on the path gain, spatial and delay characteristics of the channel [17]. A lot of research work also focus on the measurement of mmWave channels, and here we go through some related work aiming at the outdoor scenario. Based on the measurement, it is found that the transmission range of mmWave signals can reach even above 200m in outdoor environments [18, 16, 19], which matches the conclusion above. Many researchers conducted research on the outdoor statistical channel characterization and modeling. In [20], propagation measurements are performed on the 73 GHz band in New York City. A preliminary 3GPP-style 3D mmWave channel model was proposed which utilizes the ray tracer to determine elevation model parameters. Moreover, the authors of [21] develop spatial statisitical channel models for both 28 and 73 GHz mmWave bands based on the extensive real-world measurements at 28 and 73 GHz in New York. It is found that in dense urban environments, thanks to the multi-path effect, mmWave signals strong enough for the cellular communication can be detected even 100-200m away from mmWave base

stations. [22] shows the results of 71-76 and 81-86 GHz in a street canyon scenario, which aims at the wide band channel modeling. As an important parameter for broadband wireless channels, the mean values of root mean square delay is ranging from 0.089 ns to 0.125 ns. Besides, Haneda et al. [23] build mmWave channels for frequencies ranging from 6 GHz to 100 GHz. It takes many factors into account, such as path loss, shadowing, LOS probability, penetration, and blockage models. Experimental results show that different materials in building construction introduce different penetration loss. For instance, normal transparent glass only introduces a small increase of loss; while energy-efficient glass can add as large as 40 dB additional loss even at a relatively low mmWave frequency band. Materials such as concrete or brick have losses that increase rapidly with frequency. Two types of blockages are considered, one is the dynamic blockage such as cars and humans, and the other is the geometry-induced blockage such as buildings. The effect of dynamic blockage is equal to transient additional loss on the paths that intercept the moving object. However, the impact of geometry-induced blockage on propagation channels highly depends on diffraction and sometimes by diffuse scattering. Note that, most the above channel measurement and modeling focus on the access tier, which means they characterize the communication channel between user ends and base stations.

Our work focuses on the backhaul tier of the cellular system, which is quite different from the access tier. In the backhaul network, the transmit power is relatively large, more powerful devices can be used, the backhaul links are usually line-of-sight, and the network topology is stable in most of the time. Therefore, to simplify the analysis, we make the standard assumption of additive white Gaussian noise (AWGN) channels instead of those complicated access channel models [1]. Link capacities are assumed to follow Shannon's Theorem with an upper limit, i.e.,

$$C = B \log_2(1 + \min\{\mathrm{SINR}, T_{max}\}) \ , \tag{2.1}$$

[1] In fact, we can substitute the AWGN channel using any of the "new" mmWave channel models, as the channel model in use only affects the channel capacity estimation in our research.

where B is channel bandwidth, SINR is signal to interference plus noise ratio, and T_{max} is the SINR that produces the network's maximum rate. In real networks, capacity cannot be increased without limit and this is captured by T_{max}. Since the LoS link is relatively short and the SINR at the receiver end is required to be high to support backhaul usage, it is assumed that the small scale fading is mild, thus the channel estimation penalty is negligible, and the maximum achievable rate of the channel can be closely approximated by eq. 2.1.

SINR is defined by the following relationship,

$$\text{SINR} = \frac{P_r}{N_T + I} \quad , \tag{2.2}$$

where P_r is the power of the intended transmitter's signal when it reaches the receiver, N_T is the power of thermal noise, and I is the combined power of signals from any interfering transmitters.

For the calculation of both P_r and I, the Friis transmission equation is used:

$$P_r(d) = P_t \times G_t \times G_r \times (\frac{\lambda}{4\pi d})^{\eta} \times e^{-\alpha d} \tag{2.3}$$

where P_t is the transmit power, G_t and G_r are antenna gains at transmit and receive ends, respectively, λ is the wavelength of the signal, d is the propagation distance, α is the attenuation factor due to the atmospheric absorption, and η is the path loss exponent. Because of the short LoS link used in the backhaul and the high SINR at the receiver, ignoring the relatively small random attenuation due to the shadowing effect does not hurt the effectiveness of our analysis. However, due to the implementation loss (5 dB), noise figure (5 dB), and the heavy rain attenuation (10 dB/km), an additional link margin $L_m = 10\text{dB} + 10\text{dB/km} \times d$ should be deducted when calculating the receive power.

2.1.2 Directional transmission and antenna model

In the sub-6 GHz wireless communication systems, antennas are usually omni-directional or sectored with relatively large sector range. In contrary, mmWave wireless links are considered inherently directional. Due to the small wavelength of mmWave signals, it is feasible to integrate a large number of antenna elements into electronically steerable antenna arrays with very high antenna gain and very narrow beam width [24, 25, 26]. Different from adjusting the beam direction mechanically, the beam steering functionality of the electronically steerable antenna arrays is realized through controlling the phase of the signal transmitted by each antenna element, which is very efficient. Nowadays, 20-30 dBi antenna gain within the main beam of a directional antenna is quite normal; while the separation of the antenna gains between the main beam and the side lobes can reach more than 20 dBi, because of the development on side lobe compression technology. This helps alleviate signal propagation problems and reduces the interference footprint. A hot research area related to the directional transmission is the fast beam training or beam alignment technology, as it is expected that the transmitter and receiver direct their beams towards each other, so that the communication link between them can enjoy the very high antenna gain at both ends. Several beam training algorithms have been proposed to reduce the required beam training time [27, 28, 29].

In the research above the physical layer, usually simplified antenna models are used. Different from the 2D antenna model used in the previous related work, such as [30], the antenna model used in 3D scenarios is also 3D in our research. With directional antennas, the antenna gain is not the same for all azimuth and elevation angle values. In this thesis, we employ an ideal 3D-flat-top antenna model, which has a constant high gain G_{high} within the beam and a constant low gain G_{low} outside the beam.

In fact, more sophisticated antenna models can be used in our research freely, because the choice of antenna models mainly affects the mutual interference relationship between different physical links in the backhaul network, which is usually pre-computed based on

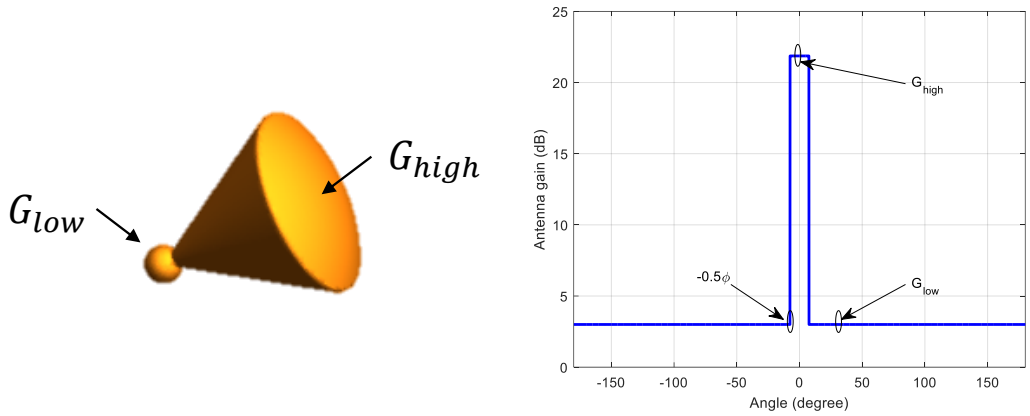

Figure 2.3: 3D flat-top antenna. (a) 3D model. (b) Antenna gain (azimuth cut-line)

the position of nodes, the direction of links, and the antenna model in use. Choosing more complicated antenna models will increase the calculation complexity of this procedure; while it does not affect the design of all the algorithms proposed in this thesis.

2.1.3 Blockage effect of mmWave wireless signals

It is known that the wireless signals cannot diffract easily around obstacles with a size significantly larger than their wavelength. Therefore, due to the small wavelength, wireless links in the 60 GHz band are sensitive to blockage by obstacles in both outdoor and indoor environments. For example, there are large numbers of buildings, trees, and billboards in the outdoor dense urban area; while human bodies and furniture are considered as obstacles usually for the indoor case. In [31], the authors showed that the blockage by the human body introduces a penalty to the link budget by 20–30 dB. Moreover, the authors of [32] measured the propagation characteristics of mmWave wireless signals in an indoor environment in the presence of human activity, where they found that taking human mobility into consideration, mmWave links are intermittent.

2.2 Small-cell backhauling at the mmWave band

As a large number of small-cell BSs will be deployed in the dense urban area to provide 5G services to mobile users, it leads to a severe backhaul challenge, where a huge amount of aggregated backhaul traffic needs to be transferred between small-cell BSs and the macro-cell BS. Note that, the terminology "backhaul" is referred to as the set of connections between BSs, which has been widely used by the academic community. On the other hand, as the cellular network becomes more complicated, where new network entities have been introduced, the set of connections between remote radio heads (which can be regarded as small-cell BSs without baseband processing units) and baseband processing units (which are usually available on macro-cell BSs) are often called "fronthaul" by some industrial companies, especially in the research related to C-RAN. However, in this dissertation, we use the word "backhaul" to refer to the connections between BSs, which is compliant with the usage in academia.

2.2.1 An overview of solutions to small-cell backhauling

In the backhaul network within a single macro-cell region, the macro-cell BS is considered to be connected with the core network through a wired fiber connection, and it will serve as the gateway node to core network for a set of small-cell BSs. Figure 2.4 depicts the conceptual idea of small-cell backhauling.

To implement these backhaul links, the ultimate solution is to use wired fiber to connect all BSs, as it is the most robust solution which can provide the highest link capacity. However, in many places, such as in North America, due to the construction limits and cost issue, fiber connections may not be available immediately to meet the approaching small-cell backhauling demand. Therefore, wireless backhauling becomes a strong candidate before fiber is everywhere. However, wireless backhauling working at the sub-6 GHz band cannot support the huge traffic demand as expected due to the limited available bandwidth.

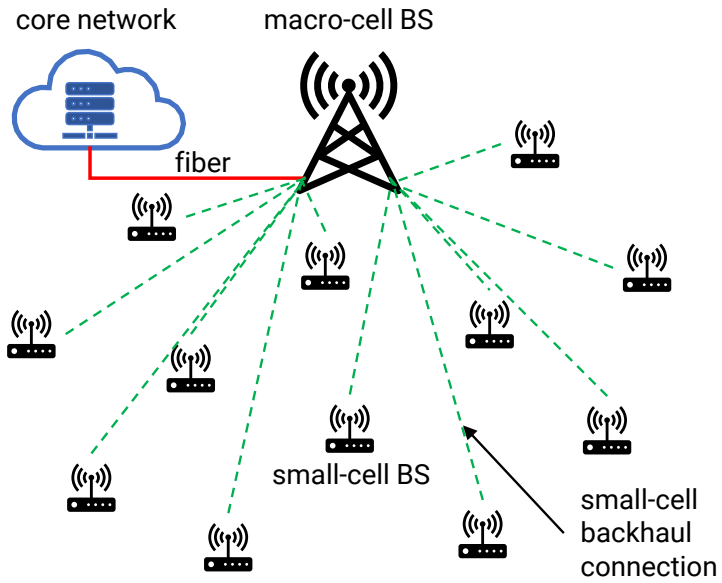

Figure 2.4: The conceptual idea of small-cell backhauling

To address this issue, mmWave backhauling is proposed as a promising solution, because it can utilize more than 1 GHz available bandwidth for the backhaul usage. Nowadays, 10−25 Gbps peak link capacity is feasible for mmWave backhaul links [33].

2.2.2 Point-to-multipoint mmWave backhaul networks in urban environments

Different kinds of network architectures have been investigated for mmWave backhaul in typical urban scenarios. Due to its flexibility and cost-effectiveness, the point-to-multipoint (P2MP) mmWave backhaul has been widely discussed, where a single macro-cell BS (M-BS) serves as the gateway node for a number of small-cell BSs (S-BSs) to the backbone Internet, and the inter-BS communications are supported by mmWave wireless links.

In 2015, Samsung proposed a P2MP "in band" mmWave backhaul for 5G networks [34], where backhaul and access transmissions are multiplexed on the same frequency band in a star topology. Meanwhile, [35] investigates a massive-MIMO based mmWave P2MP backhaul scheme which can guarantee the M-BS to simultaneously support multiple S-BSs with multiple streams for each S-BS. Similarly, the solution proposed in [36] concerns that the M-BS in the mmWave backhaul consists three sectors with each sector serving multiple

S-BSs in a TDM manner. Different from the above single-hop star-like backhaul, [37, 38, 39, 40] deal with the multi-hop tree/mesh-like P2MP backhaul, where S-BSs can cooperate with one another and communicate with the M-BS via mmWave radios.

Few work has been done to address the site deployment in outdoor mmWave backhaul networks. An approach for optimizing the joint deployment of S-BSs and wireless backhaul links is discussed in [41]. This joint deployment scenario is cast as a multi-objective optimization problem under the constraints of limited backhaul capacity and outage probability. As for the specific street canyon scenario in urban environments, a P2MP backhaul network with a linear topology is concerned in [42], where both star and mesh topologies can be formed with mmWave S-BSs mounted on top of lampposts.

The existing works prefer using the line-of-sight (LoS) mmWave links to achieve every high data rate; however, the feasibility of NLoS mmWave backhaul is explored in [43]. It claims that with good reflectors (e.g., metal surface), the NLoS backhaul link is feasible at 60 GHz with medium/short link length for moderate rate requirement. Moreover, despite that half-duplex (HD) transceivers are applied in most of the related works, the developing full-duplex (FD) technique is considered in [44, 45] to further enhance the performance of mmWave self-backhaul networks.

The aforementioned related works are different from our research, since they are "self-backhaul" solutions, while dedicated mmWave decode-and-forward (DF) relays for backhaul usage are deployed in our settings. Though in [46], a relaying architecture is proposed for mmWave backhaul, the research focuses on the end-to-end performance analysis of a restricted three-hop topology with both DF and amplify-and-forward (AF) relays in rain fading channels, without considering any scheduling or networking related issues, which are heavily concerned in the proposed research. Additionally, most of the related works adopt an "in-band" solution [47, 48, 49, 50], while in our research, we adopt the "out-of-band" scheme [51, 52, 53] such that the dedicated frequency band for backhaul usage can further enhance the network performance. Moreover, for the specific roadside scenarios,

the topology design issue (i.e., the placement of BSs and relays) has not been addressed yet to control the mutual interference in the related works either.

2.2.3 Relay-assisted mmWave backhaul network architecture

Future 5G cellular system deployments will be based on small cells to provide better user access experience, such as higher data rates, in-building coverage, etc. A large number of small cell base stations (BSs) will be deployed in urban areas, which makes the traditional wired backhaul almost impossible considering the prohibitive cost and installation constraints. On the other hand, wireless, especially mmWave, backhaul networks are an ideal candidate for small cells. We propose a relay assisted mmWave mesh network architecture for backhaul in urban areas [54, 55, 56, 57, 58], in which mmWave relay nodes are used to assist in connecting BSs of the wireless mesh network. Although the idea of relaying appeared in the literature for a long time in both legacy cellular systems [59, 60] and the general mmWave networks [61, 62, 63, 64], we are the first to introduce dedicated mmWave relays to help build mmWave backhaul networks with the ultra-high throughput requirement.

As shown in Fig. 2.5, in a typical urban area, there exist small cell BSs, macro cell BSs, and mmWave relays. It is assumed that all three types of entities can communicate in the mmWave band and they all have directional antennas with steerable beams to help compensate for high mmWave path loss. We assume that macro-cell BSs and a small portion of small-cell BSs will have wired connections, and we refer to these as anchored BSs (A-BSs), while the rest of the small-cell BSs are non-anchored ones (i.e., no wired connections). The backhaul transfers data between non-anchored BSs and anchored BSs.

To achieve the required very high data rate of mmWave links (around 10 Gbps) in the backhaul network, LoS paths have to be utilized. Though some work tries to make use of NLoS paths to achieve a better coverage in mmWave cellular network, the propagation measurement at mmWave bands conducted in the urban environment has shown that typ-

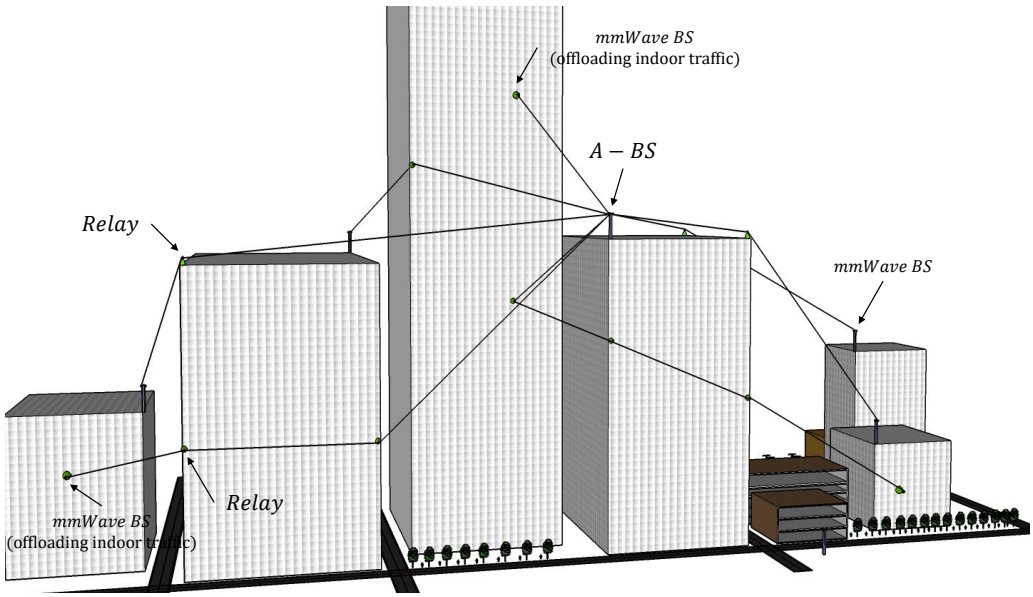

Figure 2.5: Relay assisted mmWave backhaul network architecture.

ically every reflection would introduce more than 15dB signal attenuation [65], which is unacceptable in the backhaul use case, where very high signal to interference and noise ratio (SINR) must be achieved. However, due to the existence of buildings, walls, trees, and other obstacles, the LoS path between two BSs is usually blocked, even when they have a distance shorter than 100m. For example, small cell BSs deployed within buildings cannot connect with the outdoor BSs directly, due to the poor penetration property of mmWave signals. In fact, connecting indoor and outdoor BSs is a key feature in mmWave backhaul, because wireless operators prefer not to use wired Internet to offload their indoor wireless data traffic due to the high service cost. Thus, indoor mmWave BSs need an outdoor mmWave BS mounted on the surface of the building to act as the gateway connecting the indoor and outdoor scenarios in urban backhaul.

Above all, it is not always possible to build a self-backhaul network which only relies on the direct communications between BSs [66], or a centralized mmWave backhaul structure where single-hop connections are built between small cell BSs and macro cell BSs [49]. Thus, a relay assisted network architecture becomes a more favorable choice for mmWave backhaul in 5G era. The relay-assisted mmWave backhaul architecture we propose has the

following characteristics:

- Any obstacles between two BSs are bypassed by a relay path. Every individual link along a relay path is LoS.
- The lengths of individual links are shortened, which increases the capacity of individual links along the path.
- The relays are dedicated devices in mmWave backhaul, which operate on a frequency different from the access frequency. The out-of-band backhaul solution further increases both the backhaul and access network capacities as compared with an in-band solution.
- With steerable beams and redundancy in the relay deployment, temporary blockage and link failure can be recovered locally, which reduces the burden of network layer rerouting and load balancing. This part is not covered in this thesis, but in our published work [67, 68, 69].
- The complexity of relays is much smaller than that of BSs, as discussed in the next subsection.

Relay use and deployment issues

As mentioned in the previous subsection, relays might be required in mmWave backhaul networks to connect two BSs that do not have a LoS path between them in urban areas. However, even if there are some situations where LoS paths exist, e.g. traversing a distance over a straight-line street, relays are still useful to improve performance. This is due to the poor mmWave signal propagation characteristics, which mean that achieving very high capacity with link lengths of more than a few hundred meters is not possible.

Fig. 2.6 shows the capacity of an individual mmWave link as the link length changes in an interference-free/minimal case. The channel model and the parameter choices used to generate this figure can be found in section 2.1.1 and Tab. 3.1, respectively.

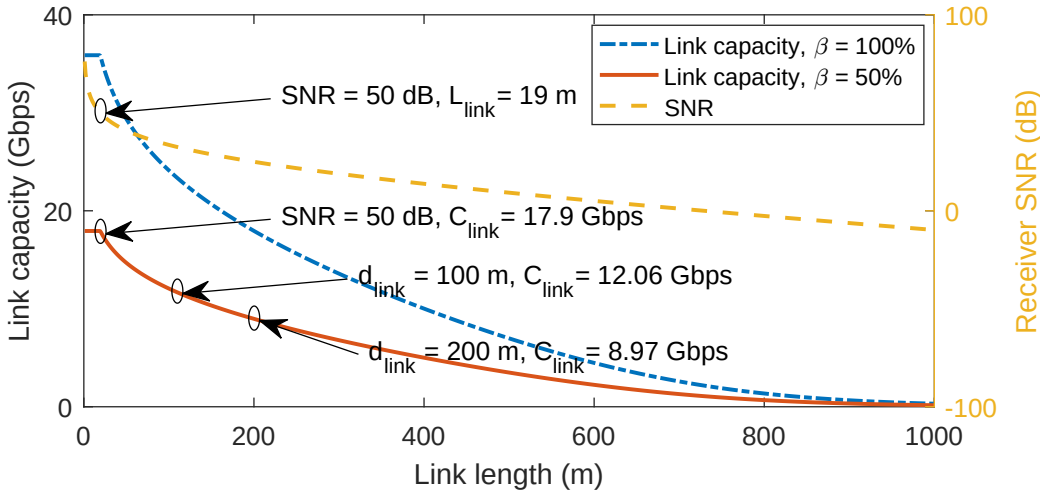

Figure 2.6: LoS Link capacity vs. link length at 60 GHz

Note that as the link length decreases, the link capacity increases, which indicates that deploying more relays and keeping link lengths short might yield higher end-to-end throughput. In an extreme case, all hops along the path reach a maximum link capacity if the length of each hop is very short (in this setting, $C_{\max}$ is around 36 Gbps, when $L_{link} \leq 19$m). In this case, the maximum end-to-end throughput across a relay-assisted path is βC_{max}. The value β is called the link utility ratio, which represents the portion of a node's transmit time in the overall schedule. If paths are subject to primary interference, $\beta \leq 0.5$ and the maximum throughput in this setting is about 18 Gbps. Note that with a very long mmWave link, say around 600 meters, link capacity is significantly less (5 Gbps or less) even if $\beta = 1.0$. Fig. 2.6 shows the trend of βC_{link} when $\beta = 0.5$. The value of β greatly impacts the end-to-end throughput and, as mentioned, it is determined by the schedule of links along the path. Construction of an optimal schedule within a virtual long link will be addressed later.

The preceding discussion seems to indicate that deploying a very large number of relays with very short inter-relay distance is an optimal choice. However, since deploying more relays increases the cost, consumes more power, and increases end-to-end delay, in practice, it is necessary to limit the number of hops in a relay path.

Even if the hop count is limited, the total number of relays deployed across an urban area can become quite large. Thus, it is important to keep the cost of deploying and maintaining each relay low. Our architecture addresses this in several ways. First, contrary to prior work that proposed using relays in non-mmWave wireless backhaul, our relays are dedicated to the relay function and do not serve as access points for the user tier. We assume with small cells and the suitability of NLOS paths for the access tier, that good coverage can be achieved by the BSs alone. Second, each relay is part of only one path, which simplifies scheduling and other MAC aspects, compared again to more general ad hoc network relay structures used in non-mmWave wireless backhaul. Resources (e.g., time, frequency, memory, and CPU) need to be shared to satisfy the sharing of a relay on multiple paths, which will either drop the performance or increase the complexity and cost of each relay. Finally, we assume that relays are constrained by primary interference. Primary interference could possibly be avoided with multiple external antennas for each relay node that are mounted in a well separated fashion. However, this would signicantly increase the cost and complexity of deploying and maintaining relays and also limit the possible relay locations.

2.2.4 3D modeling of urban area

In this section, we discuss the 3D modeling of urban area for analyzing the relay-assisted mmWave backhaul network. In most previous work, the modeling of the deployment area is two-dimensional (2D) for simplicity. It is reasonable for 2D models to be used in analyzing the performance of previous generations of cellular system, such as 3G or 4G, since the signal at lower frequency band has better penetration and diffraction properties, and the cell size is much larger than the size of buildings. However, in mmWave band, the blockage effect is very significant, thus the height of a building and the height at which mmWave BSs and relays are deployed will largely determine whether possible paths can bypass the building. Skyscrapers may reach several hundred meters in a typical urban area. For example, there are 38 buildings taller than 122m (i.e., 400 feet) in downtown Atlanta, GA

(see Fig. 2.7). As shown in Fig. 2.6, the maximum length of mmWave links in urban areas is considered around 100m–150m to achieve very high data rate (around 10 Gbps). Due to the similar scale of both building height and mmWave link length, the third dimension can have a big impact on the coverage of mmWave signals.

As mentioned above, the backhaul scenario discussed in our work is a mmWave backhaul network constructed by LoS paths. Thus, 3D modeling of the environment is more suitable than 2D, as it gives us a more practical view of the transmission environment, and the process of finding LoS paths can be more accurate and reliable. On the other hand, 2D modeling may still be useful in the research on the cellular access tier, where NLoS path and multi-path effects will be considered. In addition, our 3D modeling uses the real building information. In a typical downtown area, buildings are arranged in blocks, and they have similar orientations, which is totally different from the assumption in previous stochastic 2D modeling, where Poisson Point Process is used to model the location of buildings and the orientations of buildings are assumed to follow a uniform distribution on $[0, 2\pi]$. For example, as we can see in Fig. 2.7, among the recorded 227 buildings in downtown Atlanta, most of them have an azimuth angle close to 0^o or 49^o, while only 7.9% have other orientations. In fact, the distribution of building orientations in Atlanta already appears more random than in other metropolitan areas such as Chicago or New York.

Building model

Considering the abundant existence of trees, moving vehicles, and other obstacles located at relatively low heights, it is a wise choice to deploy outdoor mmWave BSs and relays at a height higher than 5m. Otherwise, the blockage attenuation is high and temporary blockages can happen frequently. Thus, all possible LoS paths between mmWave nodes (i.e., BSs and relays) are above the level of 5m as well. Therefore, only buildings higher than 5m are modeled in our simulations. The blank areas in Fig. 2.7 are parks and ground parking lots.

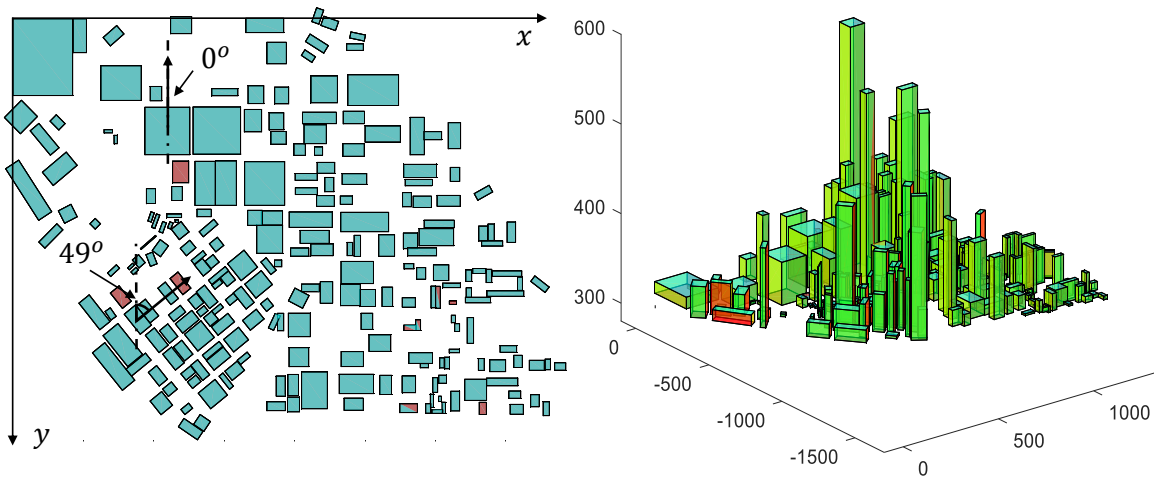

Figure 2.7: Building topology in downtown Atlanta. (a) Top view. (b) 3D view.

As for a rectangular area to be modeled such as in Fig. 2.7, at the top-left corner, there is a reference point with a coordinate $(0, 0, 0)$. The horizontal and vertical lines are x-axis and y-axis, respectively, while the z-axis follows a left-hand coordinate system with x-axis and y-axis. There are 227 buildings higher than 5m in the area. The location of building $i, (1 \leq i \leq 227)$ is recorded as the coordinate (x_i, y_i, z_{gi}) of its center point from the top view, where z_{gi} is the height of its ground level. All buildings are modeled as cuboids, which is a common method used to reduce the complexity of modeling buildings. The orientation of building i is defined as the angle $\Theta_i \in [0^o, 90^o]$ between the normal direction of a building surface perpendicular to the XY plane and the Y^- direction.

Comparison among different small-cell backhauling solutions

In the following table, we summarize the key features in terms of performance and cost of several possible solutions to the small-cell backhauling. As we can see in the table, the relay-assisted mmWave backhaul costs more than the mmWave self-backhaul, due to the introduction of extra mmWave relay devices. As the relays are much simpler and cheap than the small-cell BSs, the extra cost can be controlled to an acceptable level if not too many

Table 2.1: Comparison among different small-cell backhauling solutions

Solution	Cost	Performance
fiber backhaul	high	very high
mmWave relay-assisted backhaul	medium	high
mmWave self-backhaul	low	low

relays need to be deployed. However, the throughput performance of the relay-assisted mmWave backhaul is much higher than that of the mmWave self-backhaul, which will be shown in Chapter 4. Thus, the proposed relay-assisted mmWave backhaul network is a promising candidate to provide small-cell backhauling services to roll-out the 5G before fiber connections are everywhere.

2.2.5 Scheduling in mmWave backhaul networks

Adopting the P2MP backhaul network architecture, a number of mmWave links are established between BSs, thus the scheduling of transmissions among all backhaul links becomes a critical issue, which essentially affects the over system performance.

A time-division-multiplex (TDM) based scheduling for inter-BS mmWave backhaul links is proposed in [34]. TDM based scheduling is flexible and well fits the feature of asymmetric traffic pattern in the mmWave backhual in urban areas. The idea of TDM-based and beam-division-multiplex-based (BDM) hybrid scheduling is mentioned in [35], where different numbers of beams can be formed and selected on the M-BS to serve one S-BS according to the dynamic traffic demand. In [36], a TDM-based statistic scheduling and multiplexing among S-BSs supported by each sector of M-BS, presents a significant scalability and cost advantage over wired or point-to-point (P2P) backhaul solutions. A joint dynamic time-domain duplexing (DTDD) and orthogonal-frequency-division-multiple-access (OFDMA) scheme is proposed in [40], where the sub-frames or slots are synchronized network-wide, but the transmit/receive selections in each slot can be made on a link-by-link basis. This flexibility enables the duplexing pattern being dynamically optimized according to traffic loads, channel conditions and local topology constraints. [38] proposes the max-

imum QoS-aware independent set based scheduling algorithm for the mesh-like mmWave backhaul network to maximize the number of flows with their QoS requirements satisfied. In the algorithm, concurrent transmissions and the QoS aware priority are exploited to achieve more successfully scheduled flows and higher network throughput. Niu, et al., propose a joint transmission scheduling scheme for the radio access and backhaul of small cells in the mmWave band, termed D2DMAC, where a path selection criterion is designed to enable device-to-device transmissions for performance improvement [70]. Through formulating the problem of minimizing the energy consumption via concurrent transmission scheduling and power control into a mixed integer nonlinear program (MINLP), an energy-efficient mmWave backhaul solution consists of a maximum independent set based scheduling algorithm and a power control algorithm is proposed in [71]. The problem of joint scheduling and congestion control in a multihop mmWave cellular network using a network utility maximization framework is considered in [72]. Throughput and utility optimal policies are derived for different interference models with different heuristic scheduling algorithms, jointly with decentralized dual congestion control.

Different from the above TDM based scheduling algorithms, in [42, 39], the frequency-division-multiplex (FDM) based scheduling schemes are proposed aiming to alleviate the potential co-channel interference when concurrent transmissions happen on different links. However, the FDM based scheduling limits the efficiency of frequency reuse which in turn limits the achievable network throughput as well. A multi-layer dynamic transmission scheme is proposed in [73], which enables cooperation between different service-based network slices through dynamic time-frequency resource allocation among them. Several dynamic resource allocation algorithms are proposed in [74] aiming to mitigate the interference among pico stations, so that the network capacity and the fairness among stations can be maximized. In [75], the idea of exploiting topology control to enhance the efficiency of the spatial-time-division-multiple-access (STDMA) scheme is discussed.

However, these related works are different from our research, beacuse 1) due to the

self-backhaul architecture used in these works, the scheduling algorithm can not be directly applied to the relay-assisted mmWave backhaul network investigated in the proposed research; 2) the scheduling algorithms proposed in related works usually handle the multiplexing between access and backhaul transmissions because of the use of in-band backhaul; while in the proposed research, that can be ignored due to the out-of-band concept in use, and the scheduling problem aims to organize the transmission of backhaul links between BSs and relays.

2.3 Chapter summary

In this chapter, the basic background information and preliminary knowledge related to mmWave wireless communications and backhaul networking are provided. The first half focuses on the unique characteristics of mmWave wireless communications, which are different from the sub-6 GHz wireless communications. The propagation features, measurement results, channel modeling, directional transmission, and blockage effect are discussed. Besides the channel model and antenna model used in this thesis are also introduced. The second half aims to survey the current research status of mmWave backhauling, where the point-to-multi-point mmWave backhaul architecture and the scheduling in mmWave backhaul networks are explained and surveyed. Moreover, the novel relay-assisted mmWave backhaul network architecture is proposed and elaborated to the readers, which is the backhaul architecture used throughout this thesis. Additionally, the 3D modeling of urban environments is also mentioned, which provides a much accurate framework of evaluating the backhaul system performance in the dense urban area.

CHAPTER 3
RELAY SELECTION AND SCHEDULING FOR SINGLE MMWAVE BACKHAUL LOGICAL LINK IN DENSE URBAN AREAS

3.1 Introduction

mmWave communication has the potential to provide ultra high speed wireless communication and it is being heavily researched for use in 5G cellular systems. Due to the limited communication range of very high rate mmWave links, applications where high rate is desired over several hundreds of meters will likely require the use of relay nodes. It is anticipated that a sequence of relatively short but very high rate mmWave links combining to produce a long-distance high-rate mmWave path, which emulates a single long-range mmWave link. In this chapter, we investigate the use of such relay paths to extend the range of wireless backhaul communications in an urban area. mmWave relay paths could also be useful in other applications that need long-range and high rate wireless communications, e.g., to deploy 5G service along highways or deliver high speed Internet to rural areas.

The specific problems addressed in this paper are relay selection and scheduling to maintain high end-to-end throughput between a pair of BSs in relay-assisted mmWave backhaul networks in dense urban areas. A novel relay selection algorithm is proposed that can be applied in 3D urban scenarios to find available interference-minimal multi-hop relay paths that connect a pair of source and destination BSs and can sustain very high throughput. It is shown that the available paths are determined by several control parameters, such as the maximum number of hops, the link length range of individual relay links, the beamwidth of directional antennas, the locations of the source and destination pair, the density and height variation of buildings sitting between source and destination, and the density of candidate relay locations to be selected. Simulations incorporating the

3D urban area model built from a real urban scenario (i.e., downtown Atlanta, Georgia) are used to demonstrate the efficacy of our proposed algorithm for relay path selection. We also show that, over a range of settings, our path selection algorithm produces from 23% to 49% higher throughput than average interference-minimal paths satisfying the given criteria.

3.2 Optimal scheduling algorithm for an interference-minimal multi-hop path

We first consider the problem of maximizing throughput on a single mmWave relay path. As mentioned in Section 2.2.3, the end-to-end throughput is determined not only by the capacity of each individual link, but also by the link schedule. Due to the use of narrow beam directional antennas in the mmWave backhaul network, secondary interference-minimal multi-hop paths can be formed in urban areas through the relay selection method covered in section 3.3. In this section, we present an algorithm to find the optimal schedule that has the maximum available throughput for a given multi-hop path subject to primary interference only, which is quite different from the related scheduling research in traditional wireless networks where secondary interference must be considered due to the use of omni-directional antennas. In the next section, we use the algorithm to find an overall best path given a set of candidate relay locations and a source, destination BS pair.

3.2.1 Formal problem statement

The scheduling problem in the proposed multi-hop interference-minimal path (virtual long link) for mmWave backhaul networks can be formally described as follows. A finite set of mmWave nodes is represented by $V = \{N_1, N_2, ..., N_{|V|}\}$. Due to the linearity of the multi-hop path, the nodes in V are ordered in space (see the abstract model in Fig. 3.1(a)). A link e_i is an ordered pair (N_i, N_{i+1}), where $1 \leq i \leq |V| - 1$ and N_i, N_{i+1} are the transmitter and receiver of the link, respectively. The $|V| - 1$ links form a set E, and the pair (V, E) forms a graph consisting of a single path from N_1 to $N_{|V|}$.

We say that a link is active if its transmitter is transmitting data to its receiver. A set

of links $M \in E$ satisfies the primary interference constraint if no two links in M have a node in common. Such a set M is called a matching and allows all links in M to be simultaneously active. A schedule $\mathcal{S}$ is an indexed family $\mathcal{S} = (M_\alpha, \tau_\alpha : \alpha \in \mathcal{A})$, where the index set $\mathcal{A}$ is an arbitrary finite set, $\tau_\alpha \geq 0$ for each α and M_α is a matching for each α. The indicator vector $I(F)$, for any $F \subseteq E$, is the vector in R^E defined by

$$I_e(F) = \begin{cases} 1 & \text{if } e \in F \\ 0 & \text{if } e \in E - F \end{cases} \tag{3.1}$$

Using the above notations, the length t and the demand vector $f \in R^E$ of the schedule $\mathcal{S}$ can be defined by

$$t = \sum_\alpha \tau_\alpha \tag{3.2}$$

$$f = \sum_\alpha \tau_\alpha I(\mathcal{M}_\alpha) \tag{3.3}$$

where each element f_e in vector f is the total amount of time link e is active over the entire schedule. Thus, the optimal scheduling problem is equivalent to finding a schedule S for graph (V, E) with the minimum schedule length $t_{min}(f)$, where each element f_e satisfies the demand of the link e.

In [76], an algorithm is provided that computes the optimal schedule in polynomial time for any network that is subject to primary interference only through linear programming. However, [76] considers more general network structures, and the algorithm is relatively complicated. The time complexity for computing $t_{\min}(f)$ is $O(|V|^5)$ and the computation of the corresponding schedule requires $O(|E| \cdot |V|^5)$. Here, we provide a much simpler $O(|V|)$ algorithm to compute the optimal schedule for the single path case.

3.2.2 Optimal scheduling algorithm

In a relay path, all traffic is originated at the first node in the path and all traffic is consumed by the last node in the path.[1] Thus, the demand in bits, D, is the same for every link. Since different link lengths result in different link capacities, the time demand f_{e_i} of link e_i is determined by D and the capacity of e_i, which we denote by C_i. Considering a linear network, we use f_i in place of f_{e_i} to refer to the demand of link e_i for simplicity. Then,

$$f_i = D/C_i; \tag{3.4}$$

The following theorem shows how the minimum schedule length can be calculated in single path networks with only primary interference. While this theorem can be proved by adapting some of the analysis in [76] to the single-path case, we instead prove it in a simpler way using induction.

Theorem 1. *The minimum schedule length in a multi-hop interference-minimal relay path is equal to the maximum demand sum of two consecutive links, i.e.,*

$$t_{\min} = \max_{1 \le i \le |V|-1} f_i + f_{i+1} \tag{3.5}$$

Proof. Due to the path's secondary-interference-minimal nature, the scheduling on the two sides of a pair of consecutive links are independent. Let the two consecutive links with maximum demand sum be e_j and e_{j+1}. We must prove that $t_{\min} = f_j + f_{j+1}$. It is clear that e_j and e_{j+1} cannot transmit at the same time due to the primary interference constraint and, therefore $t_{\min} \ge f_j + f_{j+1}$. It remains to show that $t_{\min} \le f_j + f_{j+1}$, i.e. that all links' demands can be scheduled within $f_j + f_{j+1}$. We use induction to prove this.

1) *Basis*: It is clear that e_j and e_{j+1} can be scheduled within $f_j + f_{j+1}$. Without loss of generality, let e_j's transmission time be $[0, f_j)$, and e_{j+1}'s transmission time be $[f_j, f_j +$

[1] In line with our virtual long link concept, we assume that traffic flows in only one direction along the path at a time.

$f_{j+1})$. Also, denote $f_j + f_{j+1}$ by t_{end}.

2) *Forward inductive step*: Assume e_i is scheduled during $[0, f_i)$ and e_{i+1} is scheduled during $[t_{end} - f_{i+1}, t_{end})$. (Note that this holds for e_j and e_{j+1} from the base case.) Now, consider links e_{i+2} and e_{i+3}. e_{i+2} can be scheduled during $[0, f_{i+2})$. Note that e_{i+2} will be done transmitting before e_{i+1} starts transmitting, because $f_{i+1} + f_{i+2} \leq f_j + f_{j+1} = t_{end}$. Now, e_{i+3} can be scheduled during $[t_{end} - f_{i+3}, t_{end})$. Since, it is again true that $t_{end} = f_j + f_{j+1} \geq f_{i+2} + f_{i+3}$, then $t_{end} - f_{i+3} \geq f_{i+2}$ and the transmissions of e_{i+2} and e_{i+3} do not overlap and are completed within the total scheduling length of $f_j + f_{j+1}$.

The inductive step continues until the last link in the path, $e_{|M|}$. If $e_{|M|}$ is the 1st link in an inductive pair, i.e. $|M| = j + 2k$ for some integer k, then we must add an imaginary link $e_{|M|+1}$ with zero demand and schedule $e_{|M|}$ and $e_{|M|+1}$ according to the inductive rule in order to complete the induction.

3) *Backward inductive step*: Here, we must start from e_j and e_{j+1} and go down to e_1. The scheduling is the same as in the forward step and the logic is the same to show the scheduling does not violate the primary interference constraint. Here, if $e_1 = e_{j+1} - 2k$ for some integer k, then we must add an imaginary edge e_0 with demand zero and schedule it with e_1 to complete the induction.

Thus, all links along the linear network can be scheduled within $[0, f_j + f_{j+1} = t_{\min})$, and the proof is completed. □

Following the idea of the scheduling scheme outlined in the proof, once $t_{\min}$ has been calculated, the schedule for each link e_i in the network can be specified as:

$$\begin{cases} t = [0, f_i) & \text{if } i \text{ is } odd \\ t = [t_{min} - f_i, t_{min}) & \text{if } i \text{ is } even \end{cases} \tag{3.6}$$

The scheduling algorithm goes through the link demands one by one to find the largest consecutive pair and then assigns time slots to each link according to (3.6). The time complexity is thus $O(R)$, where R is the number of relays in the path.

An example network is shown in Fig. 3.1 with $C_2 > C_4 > C_3 > C_1$, and $\frac{1}{C_3} + \frac{1}{C_4} > \frac{1}{C_1} + \frac{1}{C_2} > \frac{1}{C_2} + \frac{1}{C_3}$. From Theorem 1, the minimum schedule length is $t_{min} = D(\frac{1}{C_3} + \frac{1}{C_4})$, and one possible link schedule is shown in Figure 3.1(b) following the scheme used in the proof.

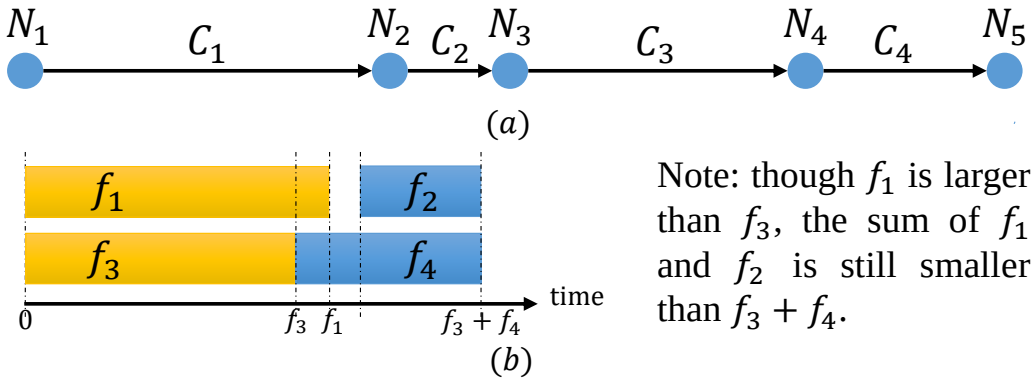

Figure 3.1: (a) Abstract model of a multi-hop interference-minimal virtual long link. $|\mathcal{N}| = 5$. (b) Minimum schedule example.

3.3 Relay Selection for Connecting Two Base Stations in Urban Area

As in the previous section, we focus on optimal path selection from one BS to the other. As long as channels are symmetric, which should be the case particularly since only LoS paths are used in our approach, the optimal path in the reverse direction will be the same. There are several ways that traffic in both directions could be handled. The simplest would simply be to alternate traffic flows in the two directions according to some schedule. This would obviously cut the overall throughput in each direction roughly in half. If that result is not satisfactory and relay cost is not a limiting factor, a network provider could choose to create separate paths in the two directions and achieve full duplex operation across the virtual long link. This would be possible as long as the endpoint BSs can create a reasonable separation between antennas for the two paths. Since our focus is solely on constructing optimal relay paths, we assume all traffic flows in the same direction in the remainder of the discussion.

3.3.1 Interference avoidance along the multi-hop relaying path

Considering a multi-hop relaying path connecting two BSs in the urban area, it is intuitive to think that the directions of all transmitters along the path are correlated with the direction from the source to the destination. Additionally, side/back lobes always exist in practice. Thus, mutual interference may exist due to the concurrent transmissions along the path.

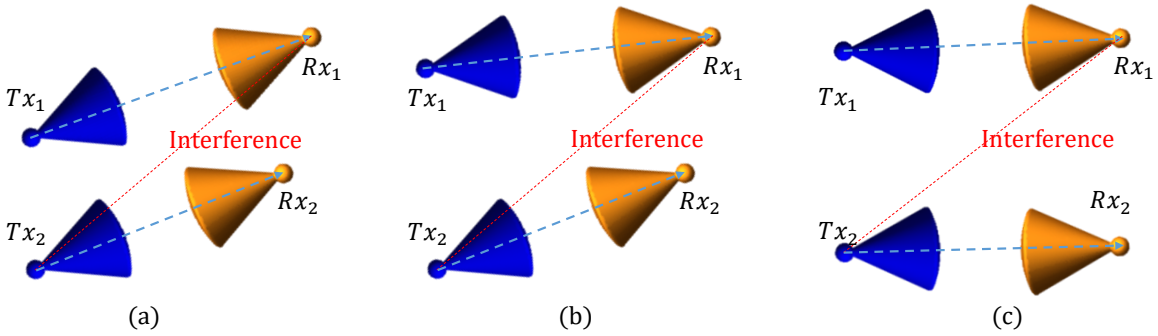

Figure 3.2: Three different interference scenarios. (a) Most interference. (b) Medium interference. (c) Least interference.

Fig. 3.2 shows three different interference cases: (a) depicts the most interference case where the interference signal experiences G_{high} at both Tx_2 and Rx_1. In (b), the antenna gains on interference signal are G_{high} and G_{low}, while in (c), both gains are G_{low}.

If we assume the intended link length is 100 m, an interferer is 300 m away from the intended receiver, and $\beta = 50\%$, the achieved link rate is 1.3 Gbps, 7.2 Gbps, and 12.6 Gbps in case (a-c) respectively. Since in case (c), the amount of interference is smaller than the noise level, it is regarded as *interference-minimal*. Note that the reflected signal is ignored in the interference analysis due to its low power and its very low possibility of reaching the intended receiver in a 3D scenario; however, the interference detection of one-time reflection signal can be easily incorporated into our algorithm if needed.

Mutual interference will significantly reduce the link capacity and the network throughput. Thus interference has to be avoided when selecting relays to form a multi-hop path in mmWave backhaul, due to its high throughput demand.

3.3.2 Finding the interference-minimal path with the optimal throughput

Algorithm 1 shows the pseudocode for our optimal path selection algorithm, which does a search of possible paths subject to several constraints, which are discussed below.

Algorithm 1 Finding the path with maximum throughput

Input: src, dst, $relays$, $numHop$, bW
Output: $maxPath$

1: $nodes$.add($relays, src, dst$); // $nodes$ stores all nodes
2: **for** $node$ in $nodes$ **do**
3: $iNbs$.add(findAllLoSNbs(node, nodes));
4: $iNbsList$.add($iNbs$); // store indices of neighbors
5: Initialize $allPaths$ as an empty list of paths;
6: $minSL =$ Inf; // minimum schedule length;
7: **for** $maxHop = 1 : numHop$ **do**
8: Initialize $path$ as an empty list of nodes' indices;
9: $path$.add($iSrc$); // $iSrc$ is the index of src in $nodes$
10: $iHop = 1$; // the index of current hop;
11: searchNextNode($path, iHop, maxHop$);
12: $maxPath = allPaths$.get(end);
Function: void searchNextNode($path, iHop, maxHop$)
13: **if** $iHop \leq maxHop$ **then**
14: $iPreNode = path.get(iHop - 1)$;
15: $iCurNbs = iNbsList.get(iPreNode)$;
16: **for** iNb in $iCurNbs$ **do**
17: Calculate the sum of demand of the current link and the previous link as $sumDemand$.
18: **if** ($sumDemand \geq minSL$) **then**
19: **return**
20: **if** (!intfTest($iNb, path, iHop, bW$)) **then**
21: $path$.add(iNb);
22: **if** ($nodes.get(iNb) == dst$) **then**
23: $allPaths$.add($path$);
24: $minSL =$ calMinSL($path, iHop$);
25: **if** ($nodes.get(iNb)! = dst$) **then**
26: searchNextRelay($path, iHop + 1, maxHop$);
27: **return**

First, only the LoS neighbors of each $node$ (Lines 2–4) are considered as candidate nodes to be selected in one step. The start of a path is the given source node (Line 9). The main loop of the algorithm does a depth-first search for a maximum throughput path using

a progressively larger maximum number of hops, $maxHop$, at each iteration (Lines 7–11). This is done because the paths found at one iteration can be very helpful in bounding the search done at the next iteration.

In the depth-first search (Line 13–27), when the index of current hop does not exceed $maxHop$ (Line 13), the selection of a candidate node makes the current path invalid in the following cases: (1) the sum of link demand of two consecutive links, the current link (i.e., from the previous node to the selected node) and the previous link in the path, exceeds the current minimum schedule length (Lines 18–19); (2) the candidate node will be interfered by previously selected nodes in the path, which means the relationship between two concurrent transmitting links is the most or medium interference case shown in Fig. 3.2 (Line 20). If neither of the above cases occurs, the node is added to the current path (Line 21). If the selected node is the destination, the path is added to the path list and the minimum schedule length is updated (Lines 22–24). Otherwise, the search continues to the next hop (Line 25–26). At the end, the last path added to the list is the maximum throughput path, as discussed next.

Note that condition (1) above comes from Theorem 1 in section 3.2.2. When the first path to the destination is found, the minimum schedule length of that path is recorded. From that point forward, each partial path is tested against the minimum schedule length at each step. If at any point, its schedule length would become greater than the minimum already found, the path is abandoned. Thus, when a new path actually reaches the destination, it means that its schedule length is better than the best previously found. Therefore, at the end of the algorithm, the last path added to the path list is the optimal path. The minimum schedule length value is propagated from one iteration of the main loop to the next and, as just discussed, this helps eliminate many possible paths in performing the depth-first search to a given maximum number of hops.

The time complexity of Algorithm 1 is $O(D^M)$, where D is the maximum degree of the connectivity graph of candidate relay locations and M is the maximum hop count for a

path. Two relay locations are neighbors in the connectivity graph if they have a LoS path between them. In the worst case, the time complexity is $O(N^M)$, where N is the total number of candidate relay locations but, due to the large number of obstacles in the urban environment, the maximum degree will typically be much smaller than N. As long as M is constant, the algorithm runs in polynomial time in either case, although the polynomial degree can be fairly large. In practice, it runs much faster than this bound in most cases due to the constraints that limit the number of paths searched.

3.4 Numerical results and simulations

In this section, simulation results are provided to evaluate our relay path selection algorithms. The fixed parameters used throughout this section are shown in Tab. 3.1. These parameter choices represent typical values taken from a survey of the mmWave literature. The topology of buildings in downtown Atlanta (see Fig. 2.7) is used. In our model, a large number of candidate relay locations are uniformly distributed on the surfaces of each building in the topology. The density δ_r is defined as the number of candidate relay locations per m^2. This topology contains 227 buildings higher than 5 meters, and for each building with a height between 20 and 200 meters, one of its rooftop corners is randomly picked as a candidate BS position (130 positions in total). BSs are expected to be deployed at positions with a good coverage of other relays mounted on the surfaces of surrounding buildings.

Table 3.1: Parameters of simulation environment

BW	2.16 GHz	P_t	1 W	$G_{tx,rx}$	21.87 dBi
f_c	60 GHz	ϕ	16^o	η	2.0
L_m	10 dB	α	16 dB/km	T_{max}	50 dB

3.4.1 End-to-end throughput of mmWave virtual long links

We randomly chose BS pairs separated by a distance in the range of $[20, 200)$, $[200, 400)$, $[400, 600)$, $[600, 800)$, and $[800, 1000)$. 100 BS pairs were picked for each distance range.

The maximum end-to-end throughput and minimum scheduling length of available interference minimal paths with a limited number of hops was computed using our relay selection algorithm. One candidate relay location was placed randomly on every building surface plus an additional $0.002/m^2$ candidate relay locations were uniformly distributed over all surfaces.

Table 3.2: Minimum number of hops for each BS pair ($\delta_r = 0.0020/m^2$)

BS distance (m)	Min number of hops (percentile)
$[20, 200)$	1 (48%), 2 (51%), 3 (1%)
$[200, 400)$	1 (13%), 2 (83%), 3 (14%)
$[400, 600)$	2 (30%), 3 (61%), 4 (9%)
$[600, 800)$	3 (35%), 4 (62%), 5 (3%)
$[800, 1000)$	4 (43%), 5 (49%), 6 (6%), 7 (2%)

Since deploying more relays along a path increases both cost and end-to-end delay, we are interested in performance at or near the minimum number of hops. Tab. 3.2 shows the distribution of the minimum number of hops for BS pairs over different distances, which is quite consistent for different BS pairs in the same range. In all cases, a difference of one in the minimum number of hops covers more than 90% of all BS pairs. One interesting note from this table is that, even for short mesh links ($< 200m$), more than half of the BS pairs do not have a LoS path connecting them due to blockages (minimum number of hops ≥ 2), which means that relays are absolutely necessary even across these short distances.

Fig. 3.3 shows the averages of the maximum throughput and minimum schedule length (for transferring 100 Gb data) over the BS pairs within each distance range, for the best paths both of minimum length and of minimum length plus one. These simulations were carried out with high candidate relay location density, meaning that a large number of choices exist for each link along the relay path. Note that for short mesh links ($< 200m$), the maximum throughput is around 15–18 Gbps, which exceeds the capacity of a 100 meter link with 50% utility rate (see Fig. 2.6). Here, shortening the individual link distances increases throughput compared to a longer 50% utility link due to the propagation loss of mmWave signals. When the distance increases, the end-to-end throughput of the optimal

path decreases. However, throughput is maintained close to 10 Gbps, which is the typical requirement for backhaul links, for BS separations up to 600 meters. Above 600 meters, optimal throughput drops to around 8 or 9 Gbps, which is still quite good. Note that, in these cases, single-hop paths do not exist between any BS pairs, but if they did exist, even their 100% utility rates would be well below what is achieved by the best relay paths due to the mmWave propagation effects.

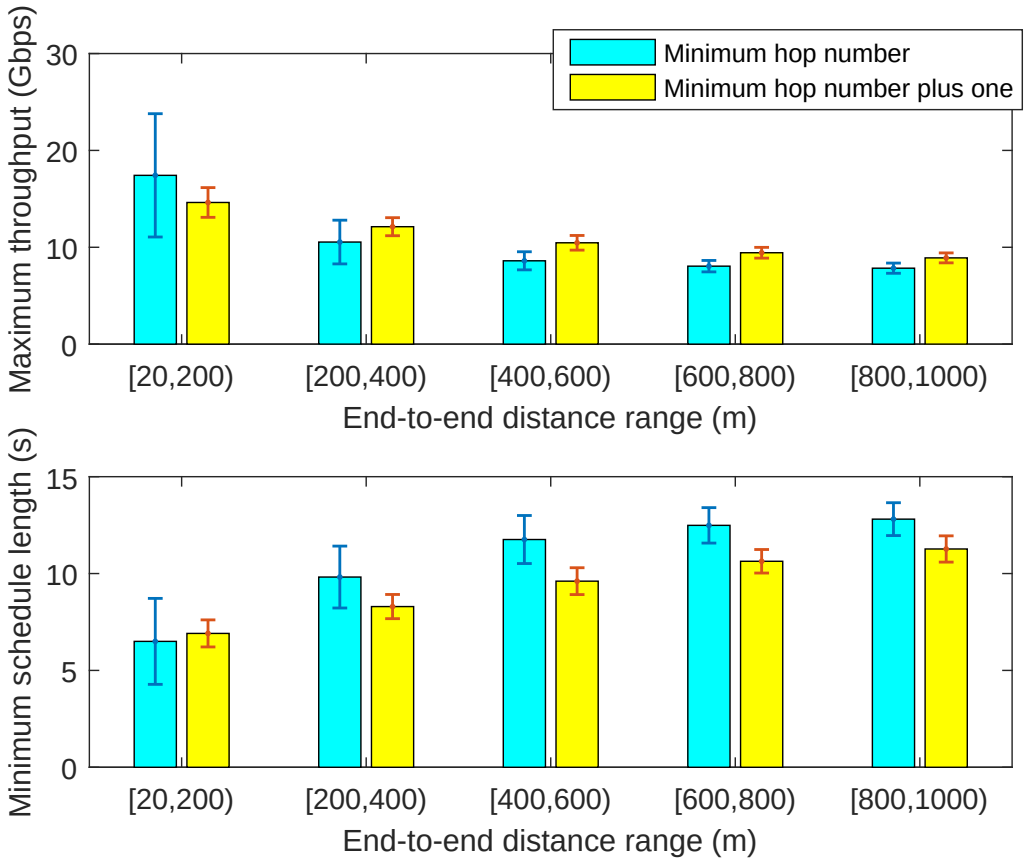

Figure 3.3: Maximum end-to-end throughput and minimum scheduling length (SL) among all available interference-minimal paths. ($\delta_r = 0.0020/m^2$)

We are also interested in how throughput and delay change when more hops are allowed in a path. We simulated a scenario where the distance range between two BSs is $[400, 600)$ meters with the same relay density as above. 50 random pairs of BSs were chosen and up to 9 more hops were allowed beyond the minimum number required to connect each pair. We make a simple assumption that each relay adds 0.5 ms delay. We first note that, if a

network provider can afford a few extra relays (+3) and the additional delay is tolerable to the applications using the network, throughput can be improved to almost 12 Gbps within this range, which is about a 20% improvement compared to Fig. 3.3. Beyond 3 additional relays, however, throughput does not improve due to bottleneck effects, while delay continues to increase. Thus, we expect that using a number of relays close to the minimum number needed for connectivity will be the best choice in practice.

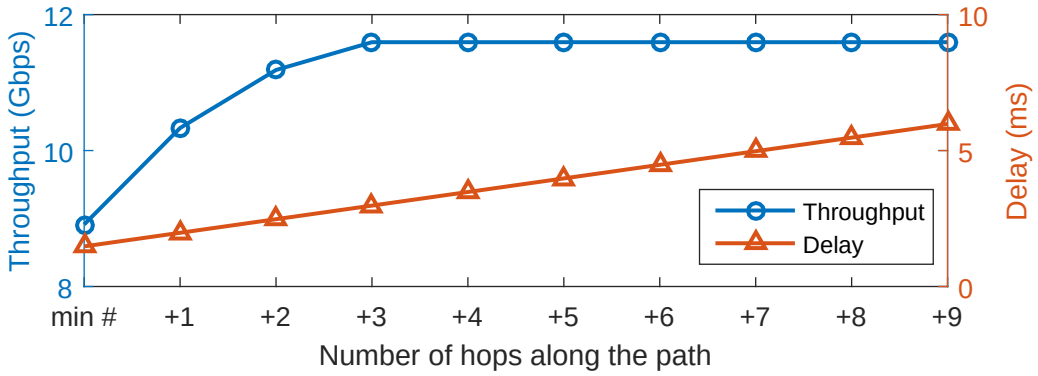

Figure 3.4: Average throughput and estimated delay as hop number increases.

We also investigated the impact of the density of candidate relay locations on the results. Surprisingly, we found that the maximum throughput and minimum number of hops hardly varied over a fairly wide range of candidate relay location densities and, hence, we do not show the results herein. The distance of links connecting different relays on the same two buildings are similar. Thus, the results seem to show that as long as different paths use the same sequence of buildings, the throughputs will be similar. Due to the large number of buildings in the simulated urban area, one relay per building surface already produces good results. In the simulated area, one relay per surface corresponds to 1100 candidate relay locations, which is already a large number.

3.4.2 Impact of optimal scheduling

To investigate the benefit of finding the path with maximum throughput among all available paths using our optimal scheduling algorithm, we ran a brute-force version of the relay

selection algorithm to obtain all possible interference-minimal paths. Only ten pairs of BSs were simulated in each distance category, due to the high complexity of finding all possible paths. Since the number of available paths in the minimum number of hops case is relatively small, to have a better sample size, we studied the minimum number plus one hop case, where thousands to millions of paths can be found in the scenarios that we simulated. The results are shown in Fig. 3.5. Note that the error bars in this figure represent the minimum gain and maximum gain, whereas the error bars in other figures of this paper represent the standard deviation.

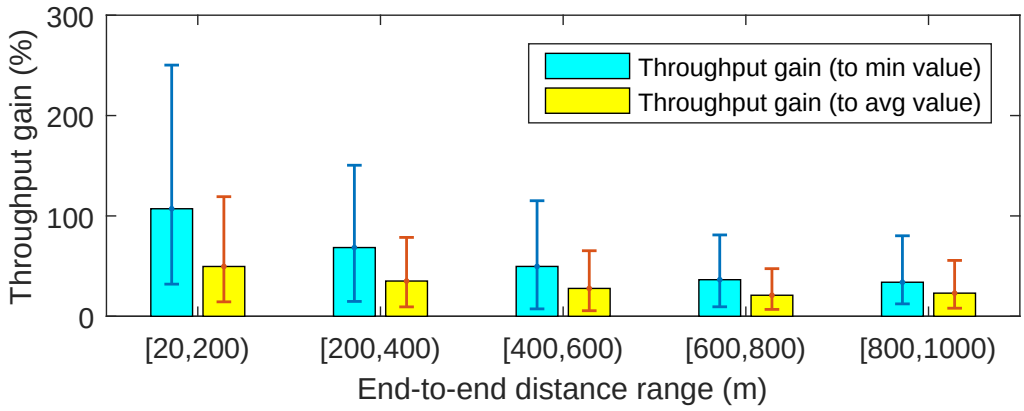

Figure 3.5: Throughput gain due to optimal scheduling. ($\delta_r = 0.001/m^2$)

Fig. 3.5 shows that the throughput gain from our optimal scheduling algorithm can exceed 200% when the BS separation is less than 200 meters, which reflects the large dynamics of link length in this case. On average, the throughput gain compared to the maximum throughput of the worst path ranges from 33% to 107%, and the gain compared to the maximum throughput of an average path ranges from 23% to 49%. Clearly, the use of optimal scheduling to guide path selection can provide large improvements compared to random paths satisfying the maximum hop and link length constraints.

3.4.3 Comparison between 3D and 2D deployments

To investigate whether consideration of all 3 dimensions of the urban environment are really necessary, we also simulated a 2D scenario. To do this, we maintained the same height for

all BS locations and all candidate relay positions. In order to provide a fair comparison, we kept the total number of candidate relay positions the same for each building surface in the 3D and 2D cases. Note that this effectively produces a higher density of possible relay positions for the 2D scenario since the relay positions are confined to a smaller area. For both 3D and 2D scenarios, we simulated 100 sets of BS pairs with separations in the same 5 ranges as in the earlier simulations. The throughput and minimum number of hops required in both scenarios are shown in Fig. 3.6.

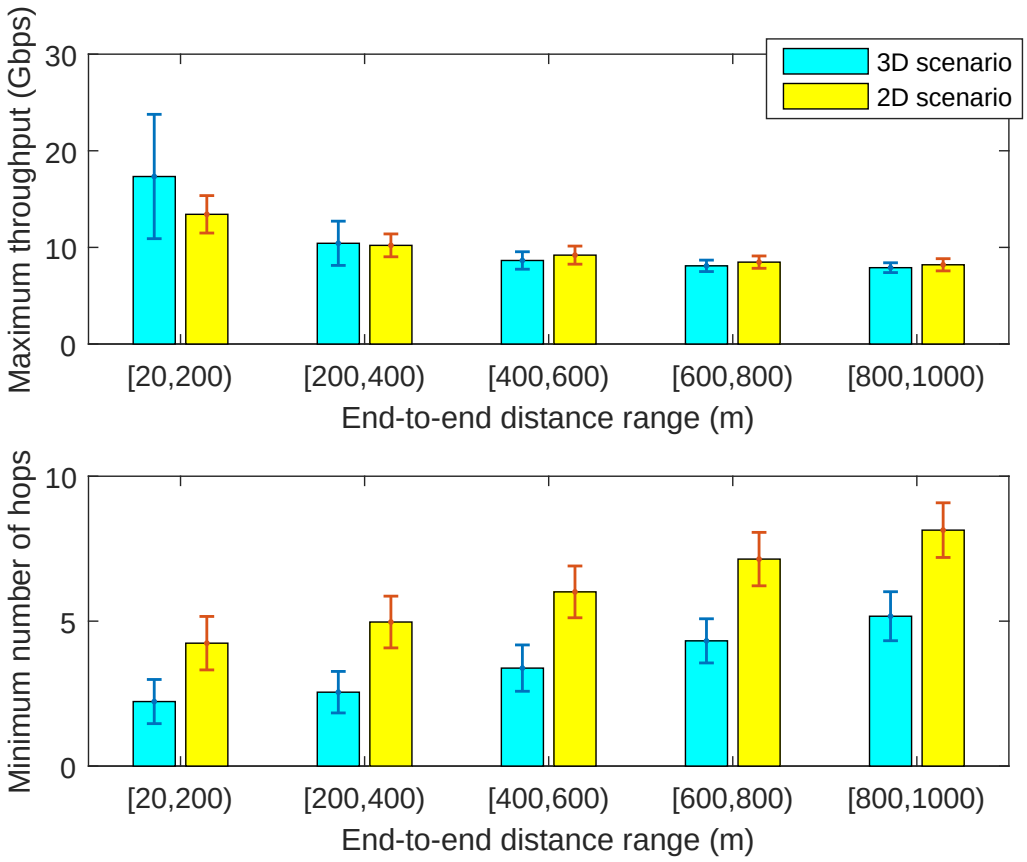

Figure 3.6: Minimum number of hops required and the corresponding maximum end-to-end throughput in 3D and 2D scenarios. ($\delta_r = 0.0010/m^2$)

Fig. 3.6 shows that when BS separation is small ($< 400m$), the throughput in the 3D scenario is better than that in 2D. This is because, in 3D, height diversity can be exploited to bypass some buildings, whereas in 2D, the same buildings have to be bypassed through multi-hop connections. This provides both more LoS paths between BS pairs and more

direct relay hops along multi-hop paths. The latter tends to shorten individual links, which brings a significant throughput improvement when the BS separation is short and the number of hops is small. When the distance between BSs becomes longer, the difference between average end-to-end throughput in 3D and 2D scenarios becomes smaller, and the throughput in 2D can even be slightly larger than that in 3D. The price of this slight throughput increase, however, is a significant increase in the number of hops required in the 2D case as seen in Fig.3.6. While this reduces average link length, the throughput improvement is minimal due to the bottleneck link effect. Deploying relays in 2D will therefore increase cost and delay significantly while providing little to no throughput benefit. Moreover, the fact that more relays are required in 2D scenario will greatly increase the running time of the relay path selection algorithm, which is definitely undesired.

3.4.4 Running time of relay path selection algorithm

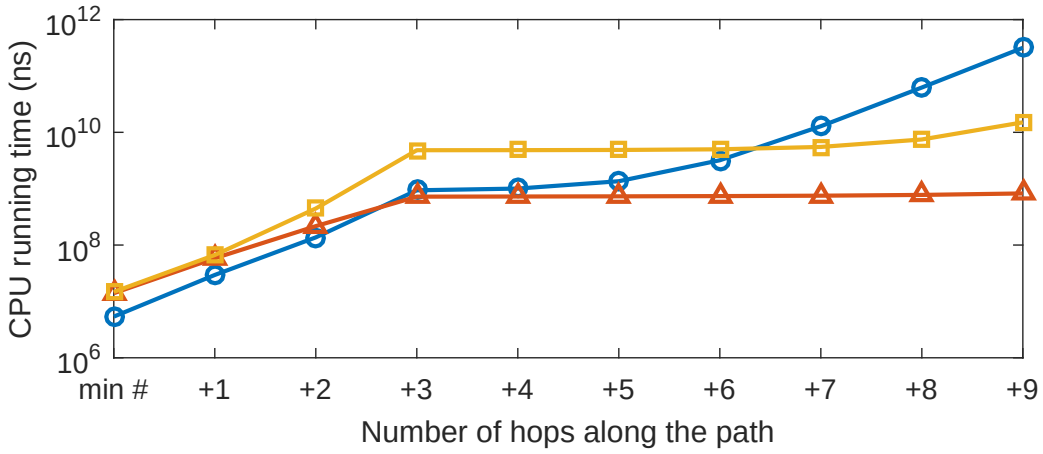

Figure 3.7: Running time of path selection alg. vs. max. no. of hops

Fig. 3.7 shows the CPU time taken by our path selection algorithm on an Intel 3.5 GHz i-7 processor with 16 GB of RAM on a single core for 3 representative source, destination BS pairs with separation in the range of 400 to 600 meters. Recall that the time complexity is $O(D^M)$, where D is the maximum degree of the candidate relay location graph and M is the maximum number of hops. Although, in theory, the polynomial degree increases with

M, we see that in some cases, the running time does not increase significantly with M. Here, the minimum number of hops is either 2 or 3, so M can be as large as 12. In spite of this large M, the running time for the red triangle plot is less than 1 second for all cases and the running time for the yellow square plot peaks at around 10 seconds. As discussed in Section 3.3.2, this is because, in many cases, the minimum schedule length determined with a smaller maximum number of hops can eliminate a very large number of paths from consideration when doing the depth-first search with the maximum number of hops equal to $|M|$. There are some BS pairs, however, where the running time does increase substantially with M, e.g. the blue circle plot. Even for this case, however, the running time is only a few minutes with the largest M. Since the relay path selection algorithm will be run in the network planning stage, a few minutes running time is acceptable.

3.5 Chapter summary

In this chapter, the relay selection and scheduling problem is investigated to maintain high end- to-end throughput in mmWave relay-assisted backhaul networks in urban environments. A major challenge in urban environments is the prevalence of large obstacles (buildings) that block long LoS paths that are necessary for very high capacity mmWave links. Using a 3D model for buildings targeted at urban environments, we provide optimal and efficient algorithms both for scheduling communications along a single mmWave relay-assisted path and for choosing the relay-assisted path with maximum throughput among all candidate paths connecting a given base station pair. In addition to proving optimality of these algorithms, we evaluate their performance through simulations based on a real urban topology. Simulation results show that our algorithms can produce short relay paths with end-to-end throughputs of around 10 Gbps and higher that are capable of providing virtual mmWave links for a wireless backhaul use case. Our algorithms improve throughput from 23% to 49% over a range of settings, as compared to an average relay path, and throughput can be more than doubled compared to some relay path choices with similar numbers of

relays.

CHAPTER 4
HIGH THROUGHPUT RELAY-ASSISTED MMWAVE OUT-OF-BAND BACKHAUL NETWORKS

4.1 Introduction

As the single mmWave relay path problem has been addressed in the chapter 3, in this chapter, we move a step further and focus on the whole backhaul network connecting the small-cell BSs within a single macro-cell region. Most related work on mmWave backhaul in the dense urban environment adopts a *self-backhaul* architecture, where BSs connect to each other directly through mmWave wireless links. However, due to the well-known *blockage effect* of mmWave signals, when LoS connections between BSs do not exist, NLoS signaling paths cannot support the high data rates required for backhaul traffic. Since the deployment of BSs typically focuses on maximizing cellular coverage, mmWave small-cell BSs will likely be mounted at lower heights. This will make it even more difficult to find LoS connections between small-cell BSs due to the abundant obstacles in dense urban areas. As an example, through simulations on the 3-D topology of downtown Atlanta shown in Fig. 4.1, we found that only 42% of base station pairs had LoS connections.

To address the above issues, as discussed in the previous chapter, we propose to deploy simple and cheap dedicated mmWave relays on the surfaces of buildings to build a relay-assisted mmWave backhaul in dense urban areas as shown in Fig. 4.1. With the deployment of relays, high throughput multi-hop paths, where every mmWave physical link is LoS, can be formed between BSs where LoS paths are not available. Furthermore, the introduction of relays brings the benefit of better utilizing the space diversity, which plays an important role in minimizing mutual interference. In the chapter 3 and [54], we present an optimal relay selection and scheduling scheme for a single backhaul link. However, if relays for

multiple backhaul links are chosen without coordination, several links may "share" some relays, which is not allowed as we assume each mmWave relay is dedicated to a single backhaul link. Moreover, the issue of "inter-path" mutual interference arises when multiple relaying paths co-exist in the same area. Mutual interference must be carefully dealt with, otherwise the performance of the whole system could degrade severely.

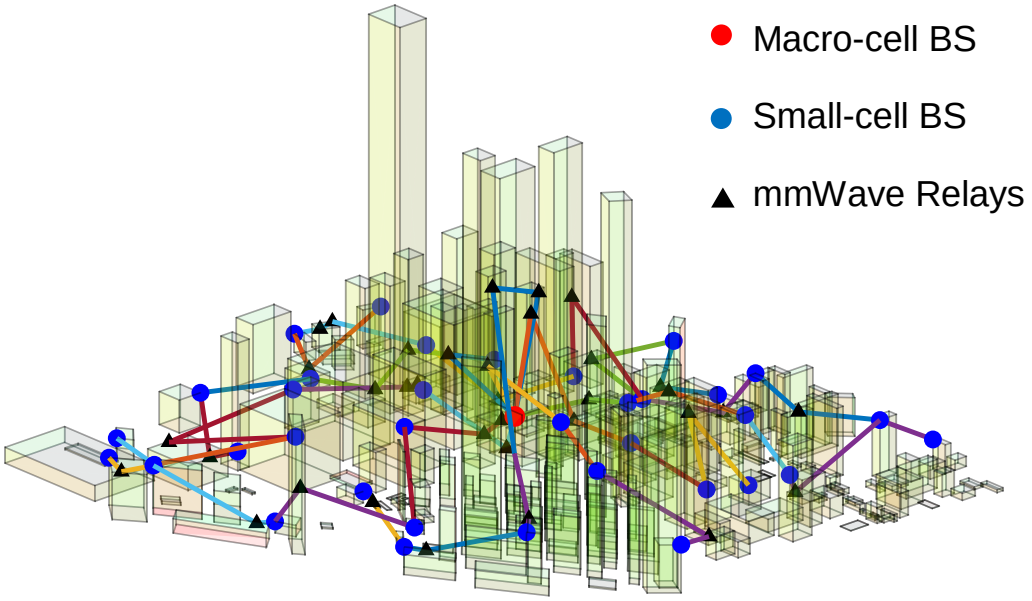

Figure 4.1: A relay assisted mmWave backhaul network in downtown Atlanta.

In the following sections, we present the first algorithm for relay selection across an entire mmWave backhaul network containing multiple logical links and accounting for interference between different physical links. Through extensive simulation results based on a 3-D model of a section of downtown Atlanta, we demonstrate that our algorithm can find interference-minimal high-throughput paths for all logical links comprising a backhaul network topology. Moreover, we propose two topology modification methods and show that they increase the probability of finding interference-minimal paths to above 95% even in certain problematic scenarios, and we demonstrate, through simulations, that the use of relays at least quadruples the aggregate traffic demand that can be met with our approach as compared to a self-backhaul network without relays.

4.2 System model

Point-to-multipoint mmWave backhaul in 3-D urban areas: To capture more practical features of the dense urban outdoor environment, we build a three-dimensional (3-D) model of downtown Atlanta, GA and use it throughout the paper. Note that the following problem analysis and proposed algorithms are not subject to the specific city model in use. In the 3-D model, buildings are modeled as cuboids for simplicity. To form "small-cells", we partition the modeled urban area into square grids with side length l_g. Within each small cell (i.e., grid), only one small-cell BS is deployed on a randomly selected top vertex of a building, except that in the central small cell, a macro-cell BS with wired backhaul connection is deployed. We denote the set of BSs as $\mathcal{B}$. When $l_g = 200$ m, about 40 small-cell BSs are deployed in our modeled area. In our problem, a single macro-cell BS serves as the gateway node of a number of small-cell BSs to the backbone Internet. The *backhaul topology* defines a set of *logical links* between BSs, so that each small-cell BS has a route, either single-hop or multi-hop, to the macro-cell BS. In section 4.3, we propose a simple tree-based backhaul topology to support the assumed backhaul traffic model, with each small cell having a total traffic demand of D Gbps. Moreover, as the downlink and uplink data traffic can be simply scheduled in a time-division way using the same backhaul network, we only focus on the downlink case in the rest of this paper.

Relay-assisted mmWave backhaul network: In the backhaul network, dedicated mmWave relays are used to form a multi-hop multi-Gbps path for a logical link whereever a LoS path between the end BSs is not available. Here "dedicated" means one relay can only be used to support one logical link. To lower the cost, we assume relays are simple devices that cannot support the sharing between different logical links. To deploy these relays, in our problem, a set of candidate locations $\mathcal{R}$ are uniformly randomly placed on the surfaces of buildings. Each surface has $(\rho + \sigma \times S)$ candidate relay locations, where ρ is the minimum number of relay locations per surface, σ is the density of extra relay locations, and S is the

area of the surface. Note that only a small number of these locations will be used for actual relays in the backhaul network.

Interference issues in mmWave backhaul networks: We assume *primary* interference does not allow a mmWave relay to transmit and receive simultaneously. However, as BSs are more powerful and complex devices, multiple logical links connected to the same BS can actively transmit data at the same time, as long as the *secondary mutual* interference among them is avoided. Mutual interference comes from the concurrent transmissions of different wireless *physical links* (i.e., relay-to-relay, relay-to-BS, and BS-to-BS) in the network. It is commonly assumed that LoS mutual interference is dominant in random mmWave ad-hoc networks with narrow-beam high-gain directional antennas and abundant obstacles in the environment, and the aggregated non LoS interference is negligible [77]. Thus, in this paper, we do not explicitly consider the mutual interference produced by the reflected signals, which experience much larger path loss due to the longer propagation distance and extra reflection attenuation against building surfaces. More importantly, as we deploy the backhaul network in a 3-D environment, usually the physical links are not in the horizontal plane, so that the reflected signals are likely pointing to either the sky or the ground, and it is therefore unlikely that they affect receivers with narrow beam directional antennas.[1] In our approach, when relays are selected to form different logical links, *space diversity* is exploited to minimize the (LoS) mutual interference among physical links in the network.

In this paper, we use a sectored antenna model, as shown in Fig. 4.2, which is also used in [77]. The antenna gain is G_h within the main beam with a beam width B; while the gain drops to G_l outside the main beam. Current directional antenna technology in the mmWave band is capable of achieving very narrow beam widths (e.g., $B \in [5^o, 15^o]$). Also, the use of advanced side lobe suppression techniques can maintain a very large isolation between G_h and G_l (e.g., 30 dB) [78].

[1] One-time reflection signals can be added to our model with some extra computation complexity, and we plan to investigate this aspect in future work.

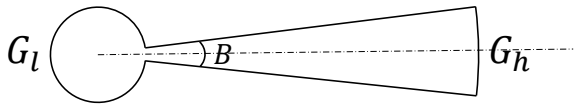

Figure 4.2: Sectored antenna model

4.3 Tree-based mmWave backhaul topology

In this section, we propose an algorithm to generate a tree-based backhaul topology, which defines a set of logical links $\mathcal{L}$ between BSs. For each logical link $l \in \mathcal{L}$, its required minimum end-to-end data transmission capacity, $l.th_m$, is also defined in the backhaul topology. The logical link between a parent BS and a child BS has to support the data traffic required by all nodes in the child BS's sub-tree.

To enable the mmWave backhaul network, each small-cell BS must have at least one route to the macro-cell BS; however, to cover a macro-cell, intuitively, establishing more logical links will make it harder to avoid the (LoS) mutual interference using space diversity; thus, a tree topology is preferred over a mesh topology, since the higher number of links in a mesh exacerbates the interference problem. Meanwhile, considering the hardware capability, it is preferred that each small-cell BS maintains fewer logical links (i.e., smaller degree) than the macro-cell BS does in the backhaul topology, as they are small devices with fewer radio chain resources and less capability to handle mutual interference among different logical links. This can be handled easily by a tree topology where the root has a large number of children and other nodes have smaller degree. We also assume that each BS only connects to the BSs in its neighboring cells, because it will be very difficult to find LoS paths to support very long logical links between BSs in non-neighboring cells. Furthermore, in our relay-assisted backhaul design, a long logical link will need a large number of hops, which means more hardware cost and increased interference.

In Algorithm 2, we first select the macro-cell BS b_m into the set of visited BSs $\mathcal{B}_v$. b_m is then used as a key to read out a list of b_m's neighboring BSs N_b from a 2-D list $\mathcal{N}_B$, which stores the lists of each BS's neighboring BSs. The first for-loop (line 2-5) constructs

$|N_b|$ logical links from b_m to each of its neighbors in N_b. The source (s), destination (d), and sequence number (seq) are updated for each new logical link l. Each neighboring BS is pushed into $\mathcal{B}_v$ after being visited. After b_m being used as the "root" node (i.e., source of a logical link), the next root node is the first node, indexed by i_r in the $\mathcal{B}_v$ which has not been used as root yet. The process of constructing new logical links continues till all BSs are visited. In every iteration, we first get the root node r, read its neighbors N_b; then we visit the first non-visited neighboring BS b to make a new logical link from r to b. i_r points to the next available root node in $\mathcal{B}_v$ (line 14). After all visited BSs in $\mathcal{B}_v$ have been used as root nodes once, if there still exists non-visited BSs in the network, we generate a new logical link between the first non-visited BS b and one of its visited neighboring BSs r. Note that this r has been used as root at least twice now. When all BSs have been visited, we go through each logical link l and sum all of the demands in the sub-tree rooted at $l.d$ to set the traffic demand $l.th_m$.

Fig. 4.3 shows an example of a mmWave backhaul topology with 1 macro-cell BS and 21 small-cell BSs in the downtown Atlanta area. Fig. 4.3 (a) is the abstract topology in grids ($l_g = 300$ m); while Fig. 4.3 (b) is the 2-D view of this topology in the 3-D modeled area. In this case, all small-cell BSs have one parent BS and one child BS, maintaining a degree of 2; however, in some cases, for example, when l_g shrinks to 200 m, several small-cell BSs may have a degree more than 2.

4.4 Multi-path selection for relay-assisted mmWave backhaul networks

As the backhaul topology only defines the set of logical links, we still need to determine how to establish these multi-Gbps logical links. In our relay-assisted approach, we select some candidate relay locations to deploy mmWave relays for each logical link in the topology. In this way, a logical link is constructed upon either a single-hop LoS path, or a multi-hop relaying path. In [54], a relay selection algorithm is proposed to find the optimal throughput logical link with a given number of hops between a pair of BSs. However, this

Algorithm 2 Generating mmWave backhaul topology

Require: $\mathcal{B}, b_m, \mathcal{N}_B, D$
Ensure: L
$seq \leftarrow 0$; $\mathcal{B}_v \leftarrow \{b_m\}$; $N_b \leftarrow \mathcal{N}_B[b_m]$;
for $b \in N_b$ **do**
  $l.s \leftarrow b_m$; $l.d \leftarrow b$; $l.seq \leftarrow seq$; $L.push(l)$;
  $\mathcal{B}_v.push(b)$; $seq \leftarrow seq + 1$;
$i_r \leftarrow 1$;
while $|\mathcal{B}_v| < |\mathcal{B}|$ **do**
  $r \leftarrow \mathcal{B}_v[i_r]$; $N_b \leftarrow \mathcal{N}_B[r]$;
  if $\exists b \in N_b \wedge b \notin \mathcal{B}_v$ **then**
    Pick first available b;
    $l.s \leftarrow r$; $l.d \leftarrow b$; $l.seq \leftarrow seq$; $L.push(l)$;
    $\mathcal{B}_v.push(b)$;
  $i_r \leftarrow i_r + 1$;
  if $i_r = |\mathcal{B}_v| \wedge |\mathcal{B}_v| < |\mathcal{B}|$ **then**
    Pick first $b \in \mathcal{B} \setminus \mathcal{B}_v$; $N_b \leftarrow \mathcal{N}_B[b]$;
    Pick first $r \in \mathcal{B}_v \bigcap N_b$;
    $l.s \leftarrow r$; $l.d \leftarrow b$; $L.push(l)$; $\mathcal{B}_v.push(b)$;
for $l \in L$ **do**
  get the number of nodes n_t in the sub-tree with root $l.d$;
  $l.th_m \leftarrow n_t D$;
return L;

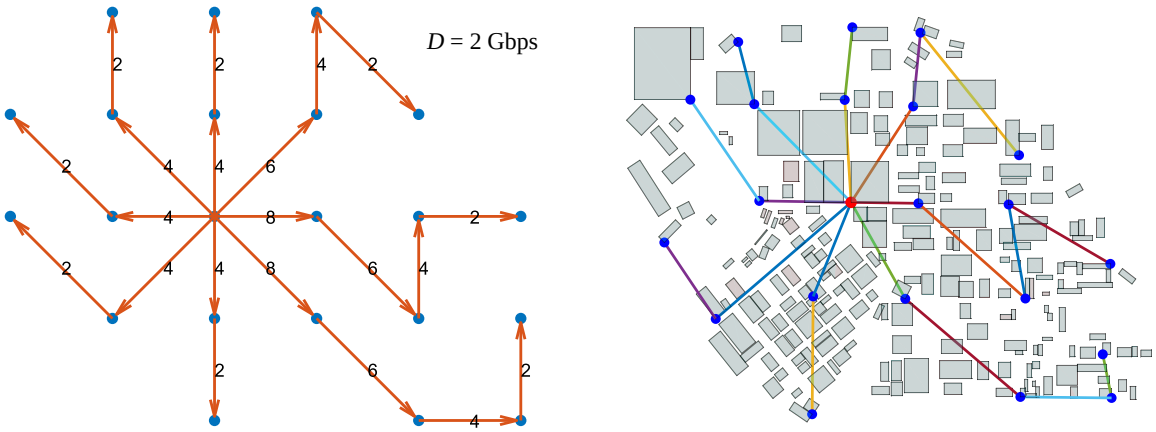

(a) (b)

Figure 4.3: An example of mmWave backhaul topology ($D = 2$ Gbps)

algorithm cannot be directly applied here, as in our problem, multiple logical links need to be constructed together, and the aim is to jointly optimize the relay selection within different logical links so that they can achieve their given throughput requirements. To maintain a high signal-to-interference-and-noise-ratio (SINR) value at each receiver, strong secondary mutual interference should not exist when concurrent transmissions among multiple physical links happen. However, the algorithm in [54] only considers controlling the intra-path interference; while in this work, we have to take both intra- and inter-path mutual interference into account. Besides the interference issue, if multiple paths are selected independently, it may result in relay sharing between different paths, which breaks the dedicated relay assumption mentioned earlier. Thus, we have to avoid the intersection between different relaying paths.

4.4.1 Simplified mutual interference model

Typically, upon the interference analysis in wireless networks, either physical or protocol interference model [79] is in use; however, physical model is hard to apply in the one-by-one relay selection process, as we cannot obtain the accurate amount of interference at each receiver until the whole process ends. Thus, in this work, upon the system assumption and the sectored antenna model in use, we adopt a simplified model to determine the inter-

ference relationship between different physical links in the network, which can be easily incorporated into our later proposed multi-path searching algorithm.

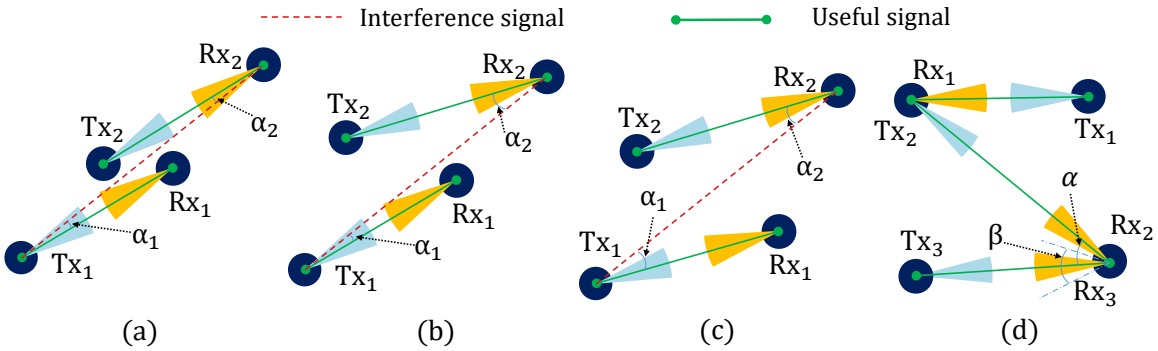

Figure 4.4: Interference conditions

The amount of mutual interference significantly varies according to the positioning relationship between different physical links. Fig. 4.4 (a-c) shows three different interfering cases between two disjoint physical links. When the angle between the directions of useful signal and interference signal (i.e., α_1 and α_2) is smaller than half of the beam width $\frac{B}{2}$, the interference is amplified by G_h; otherwise, it is amplified by G_l. (a) indicates the "*most-interfered*" case, where the interference signal from Tx_1 to Rx_2 is amplified by the high antenna G_h at both ends. The "*medium-interfered*" case is shown in (b), where the interference signal is only amplified by G_h once at either end. When the interference signal experiences G_l at both ends, as depicted in (c), the amount of interference becomes extremely low, and this case is considered as "*least interfered*". During the path selection process, we aim to form different physical links which have the least-interfered relationship between each other.

When two physical links share one end node (which can only be a BS in our architecture), the analysis of mutual interference involves two cases, as shown in Fig. 4.4 (d). First, when the two antennas on the BS are transmitting and receiving simultaneously (i.e., Tx_2 and Rx_1), this is actually a special case where interference is very high due to the receiver being so close to the transmitter. For simplicity, we assume that as long as their main beams do not overlap (i.e., $\alpha > B$), the isolation between antennas are large enough to handle the

mutual interference. Actually, this case can be avoided through scheduling also, which is not the focus of this paper. However, when two antennas on the BS are receiving at the same time, it is the "medium-interfered" case according to the analysis of case Fig. 4.4 (b). Nevertheless, considering BSs could have better antenna design and advanced antenna isolation technology, we assume that as long as the angle α between two physical links is larger than a threshold value β, the "medium-interfered" case at BSs are also acceptable during path searching. In fact, in the downlink, this case does not appear.

4.4.2 Interference controlled multi-path searching algorithm

Using the interference model just defined, we propose an interference-controlled multi-path searching algorithm for mmWave backhaul networks in dense urban areas, which is described by Algorithm 3.

Algorithm 3 Multi-path selection algorithm

Require: $\mathcal{L}, H, L_m, \mathcal{N}$
Ensure: $\mathcal{L}$
$ns \leftarrow$ **false**; $R_s \leftarrow \emptyset$; $P_s \leftarrow \emptyset$;
for $j \leftarrow 0$ to $|\mathcal{L}| - 1$ **do**
  if ns **then**
    return $\emptyset$;
  $h \leftarrow 1$; $\mathcal{L}[j].path \leftarrow \emptyset$; $\mathcal{L}[j].links \leftarrow \emptyset$;
  while $\mathcal{L}[j].path = \emptyset$ **do**
    if $h > H$ **then**
      find $\max_{k<j} k$, such that $\mathcal{L}[k].seq < \mathcal{L}[j].seq$;
      if $k \geq 0$ **then**
        switch $\mathcal{L}[k]$ and $\mathcal{L}[j]$ in $\mathcal{L}$;
        $R_s \leftarrow \emptyset$; $P_s \leftarrow \emptyset$; $i \leftarrow 0$;
      else
        $ns \leftarrow$ **true**;
      break;
    findNextNode($L[j], h, \mathcal{N}, L_m, 100, \{l.s\}, P_s, R_s$);
    if $L[j].path \neq \emptyset$ **then**
      $R_s \leftarrow R_s \bigcup L[j].path(1 : end - 1)$;
      $P_s \leftarrow P_s \bigcup L[j].links$
    $h \leftarrow h + 1$;
return $\mathcal{L}$;

We first initialize the binary indicator variable ns (i.e., no solution) as false, and empty the lists R_s and P_s which record the selected relays and physical links, respectively (line 1). The paths for logical links in the given set $\mathcal{L}$ are searched one by one sequentially, and this process ends when either all paths are found or there is "no solution" (line 4). Each logical link object has the following attributes: $\{s,\ d,\ th_m,\ seq,\ path,\ links\}$, which represent the source BS, destination BS, the minimum required throughput, the initial sequence number, the nodes along the path (i.e., BSs and relays), and the selected physical links, respectively. The process of single logical link searching corresponds to the function call of "*findNextNode*" (line 15), which is a depth-first searching algorithm summarized in Algorithm 4. The search of a logical link will not end until either a path has been found or its number of hops h exceeds H, the maximum hop number allowed within a logical link. When h exceeds H, we move $\mathcal{L}[j]$ forward through switching it with a logical link $\mathcal{L}[k]$ before it in $\mathcal{L}$. (line 8-11) In the algorithm, the previous link $\mathcal{L}[k]$ is the one closet to $\mathcal{L}[i]$, and to avoid infinite loop, $\mathcal{L}[k]$ has to have a smaller sequence number seq than $\mathcal{L}[i]$'s. When a switch occurs, $R_s, P_s,$ and i are reset, and the multi-path search restarts. However, if no previous path $\mathcal{L}[k]$ is available to switch with $\mathcal{L}[j]$, which means the heuristic algorithm cannot find a path for $\mathcal{L}[j]$, and ns is set as true (line 13). If a path is found, update R_s and P_s (line 16-18). When all paths are found, the updated $\mathcal{L}$ is returned (line 20).

Moving to Algorithm 4, the parameters of function "*findNextNode*" are the logical link object l, the maximum number of hops h_m, the current $path$ (i.e., a list of selected nodes) and the capacity cap_p of the last selected physical link. cap_p is initialized as 100 Gbps in the first call of this function. We define the maximum length of a physical link as L_m, since LoS mmWave links with ultra high speed tend to be relatively short in dense urban areas. $\mathcal{N}$ is a two dimensional list, in which each row records the LoS neighboring nodes of each wireless node in the network. The pre-computed $\mathcal{N}$ contains the necessary geographical information to solve the multi-path selection problem. P_s and R_s are the same as defined in Algorithm 3.

Algorithm 4 findNextNode() for single path selection

Require: $l, h_m, \mathcal{N}, L_m, cap_p, path, P_s, R_s$

1: $h_c \leftarrow |path|$;
2: **if** $h_c > h_m \vee l.path \neq \emptyset$ **then**
3: **return**
4: $n_p \leftarrow path.back()$; $N_c \leftarrow \mathcal{N}[n_p]$;
5: **for** n_c in N_c **do**
6: **if** n_c is a BS $\wedge$ $n_c \neq l.d$ **then**
7: **continue**;
8: **if** $n_c \in R_s \vee n_c \in path$ **then**
9: **continue**;
10: $dist_c \leftarrow \|n_c - n_p\|$; $dist_d \leftarrow \|l.d - n_c\|$;
11: **if** $dist_d > (h_m - h_c)L_m \vee dist_c > L_m$ **then**
12: **continue**;
13: $cap_c \leftarrow$ dist2cap$(dist_c)$;
14: $cap_{cp} \leftarrow cap_p cap_c (cap_p + cap_c)^{-1}$;
15: **if** $cap_{cp} < l.th_{min}$ **then**
16: **continue**;
17: $intra \leftarrow$ intraINFCheck$(n_c, n_p, path)$;
18: $inter \leftarrow$ interINFCheck(n_c, n_p, P_s)
19: **if** $intra \vee inter$ **then**
20: **continue**;
21: $path.push(n_c)$;
22: **if** $n_c = l.d$ **then**
23: $l.path \leftarrow path$;
24: **else**
25: findNextNode$(l, h_m, \mathcal{N}, dist_m, cap_c, path, P_s, R_s)$;

If the current hop h_c exceeds h_m or l has already found a path, the searching procedure ends (line 2-3); otherwise, the algorithm iterates through every node n_c in the neighbor list of the last selected node n_p in the $path$ to check whether it is a qualified node for the current hop. Since we do not allow other BSs to appear as "relays" in a logical link, thus they are filtered (line 7-9). Moreover, if n_c has been selected by other logical links or by the current $path$, it is discarded as no relay is shared. Line 13-16 restricts the scale of the depth-first search through discarding n_c when the physical link from n_p to n_c is too long or the distance from n_c to the destination $l.d$ cannot be covered by the remaining hops. If n_c is still "alive", the capacity of current hop cap_c is calculated through calling a function "dist2cap", which turns link length into capacity. As the bottleneck of a multi-hop logical

link is determined by the consecutive link pair with the minimum end-to-end throughput, thus it has to make sure that the end-to-end throughput of the current consecutive link pair cap_{cp} is larger than the throughput demand $l.th_m$. Next, the current candidate physical link has to pass both intra- and inter-path interference check before n_c is appended as a new node in $path$. Both interference checking functions are designed based on our proposed simplified protocol interference model. If n_c is the destination, $path$ is officially assigned to l; otherwise, the procedure calls "findNextNode" again to continue searching the next node. The complexity of Algorithm 4 is $O(M^h)$, where M is the maximum degree of the connectivity graph of candidate relay locations and h is the number of hops in a logical link.

4.5 Simulation results and analysis

In this section, we explain the simulations conducted to evaluate the performance of our proposed algorithms. Table. 4.1 summarizes the system parameters used in our simulations.

Table 4.1: Simulation parameters

Symbol	Value	description
l_g	300, 200 m	grid/cell size (side length)
l_p	300 m	maximum physical link length
n_{rm}	1,2,3	minimum number of relays per surface
σ_r	$n_{rm}\times10^{-4}$/m^2	density of extra relays
h_t	50 m	maximum height for BSs
G_h	21.40 dBi	antenna gain of main lobe
$G_h - G_l$	20-40 dBi	antenna gain isolation
β	30^o	antenna isolation angle
B	$5^o - 15^o$	beam width
f_c	60 GHz	carrier frequency
BW	2.16 GHz	channel bandwidth
D	2 Gbps	traffic demand of each small cell BS
p_t	1 watt	transmit power
α	16 dB/km	atmosphere attenuation
η	2.0	path loss exponent
m_l	10 dB	link margin

227 buildings higher than 5m are modeled in the $1200 \times 1600\ m^2$ area, which is larger

than a typical 4G macro-cell in a dense urban environment (see Fig. 4.1 and Fig. 4.3). We set the traffic demand D at each small cell BS to be 2 Gbps when $l_g = 300$ m, which means the backhaul network will have to support about 44-46 Gbps of total traffic demand.

4.5.1 Feasibility of high-throughput mmWave backhaul

We first run the multi-path selection algorithm with different antenna beam widths (i.e., $5^o - 15^o$), candidate relay densities, and a grid size of 300m (i.e., $22 - 23$ small cells). For each parameter setting, the simulation runs 100 times. For each run, we generate a new mmWave backhaul topology on a new set of randomly selected BSs and with a new set of candidate relay locations in the modeled macro-cell region. As we modify the parameters n_{rm} and σ_r, the total number of candidate relay locations varies among $\{1152,\ 2384,\ 3644\}$.

Note that, without relays, the lack of LoS links between base station pairs makes it impossible to support the data rates necessary for backhaul scenarios. Fig. 4.5 shows that, in many cases, the use of relays enables a high-throughput backhaul network to be formed. To be specific, when the beam width is small (e.g., 5^o–9^o), more than 90% of the time, we find a set of paths with required capacity and physical links that only experience the "least-interfered" case to build a relay-assisted mmWave backhaul network. As more candidate relay locations are added, the feasibility of backhaul network construction increases, due to the extra available space diversity brought by the additional candidate relay locations. However, as the antenna beam width increases, the feasibility using Algorithm 4 decreases, because the wider beams produce larger interference regions.

To further investigate feasibility, we "shrink" the size of each small cell by setting $l_g = 200\ m$, which results in more small cells (i.e., $37 - 41$ BSs) and correspondingly more backhaul logical links. As the cell size is almost halved, we set the traffic demand of each small cell BS to $\frac{D}{2}$ Gbps. As shown in Fig. 4.5 (b), the percentage of feasible network scenarios drops substantially, and even when the beam width is 5^o, it is below 70%. The

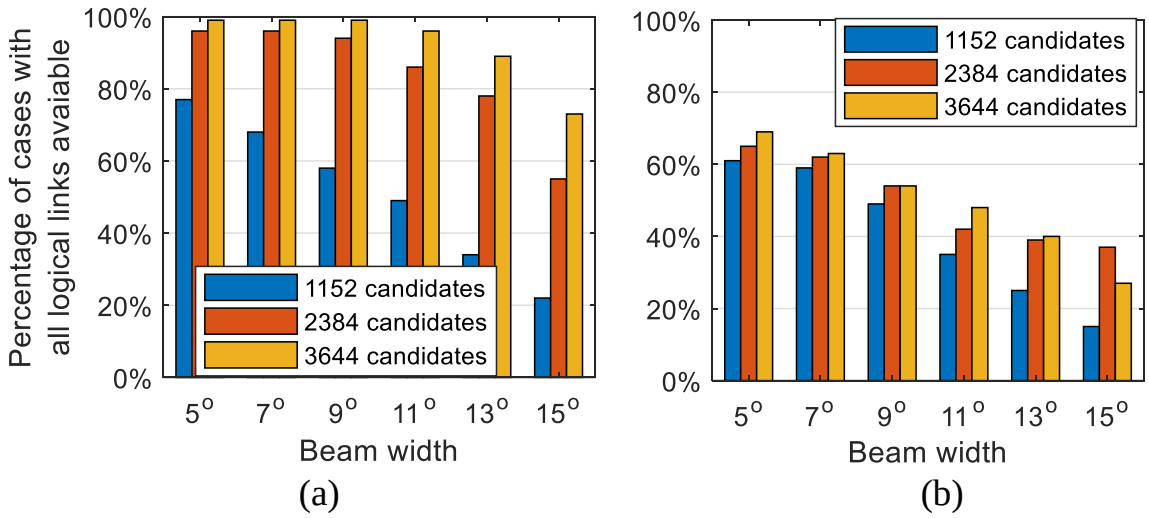

Figure 4.5: Probability of finding feasible paths for all logical links.

reasons for this drop are: 1) the space diversity at the macro-cell BS may be not enough to support 8 logical links connecting to it,[2] 2) too many logical links have to be constructed within the overall area, which produces large interference regions, limited space diversity, and more severe relay contention, and 3) the modeled macro-cell area is not symmetric, i.e. as more small cell BSs appear, the generated backhaul topology becomes even more unbalanced leading to some "hot" logical links with much higher throughput requirement than others near the macro-cell BS. To address these issues, we consider modifying the topology generating process by either macro-cell BS splitting or macro-cell shrinking, which are described next.

1) *Macro-cell BS splitting*: To address the insufficient space diversity issue, we propose to "split" the macro-cell BS by adding another radio head (see Fig. 4.6 (a)) to the BS. The extra radio head is mounted at a higher level, and connected to the BS through a wired connection. Each radio head handles half of the logical links at the macro-cell BS, which reduces the space diversity requirement on each radio head.

2) *Macro-cell shrinking*: In fact, the modeled area is much larger than the typical size of

[2]We tested the maximum number of physical links from the macro-cell BS that will not interfere with each other using the Bron-Kerbosch algorithm [80] and found that in more than 30% of the total simulated cases, the space diversity at the macro-cell BS cannot support 8 links

a 4G macro-cell in a dense urban environment. Thus, we re-size the interested macro-cell to a $1000 \times 1000\ m^2$ area, where the macro-cell is located at the center (see Fig. 4.6 (b)). In this way, the number of logical links within a macro-cell is reduced to around 23, and the traffic requirement of logical links is also reduced.

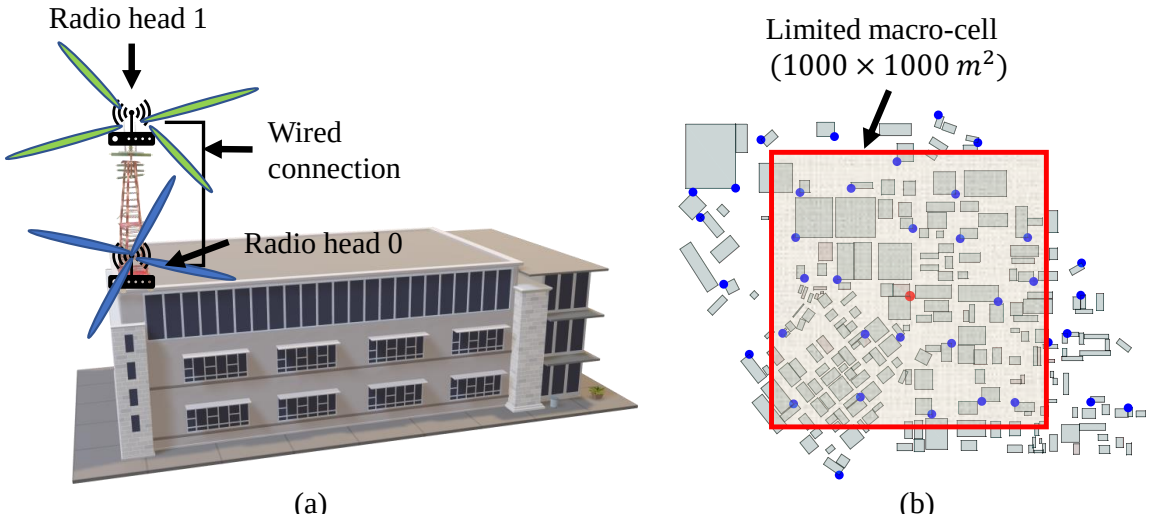

Figure 4.6: Methods to improve the backhaul topology

We apply method 1) to the simulations with $l_g = 300\ m$, and apply both method 1) and 2) to the simulations with $l_g = 200\ m$. Fig. 4.7 shows that mmWave backhaul feasibility with $l_g = 200\ m$ is greatly improved using a combination of the two proposed methods, and the likelihood of finding feasible paths for all logical links in the topology is above 90% when the antenna beam width is not larger than 11^o. The "macro-cell BS splitting" method works fairly well in narrow beam cases; however, when the beam width is large (i.e., 15^o), to achieve favorable performance, we need to control the size of a macro-cell. It is also noticed that, when the first method is applied in the $l_g = 300\ m$ case, as long as the beam width is not larger than 13^o, the likelihood of finding a feasible solution using our algorithm is above 95%.

The above discussion indicates that if the density of small cell BSs is high, to increase the feasibility of a mmWave backhaul in dense urban areas, the size of a macro-cell has to be controlled so that single macro-cell BS does not have to support too many small cell

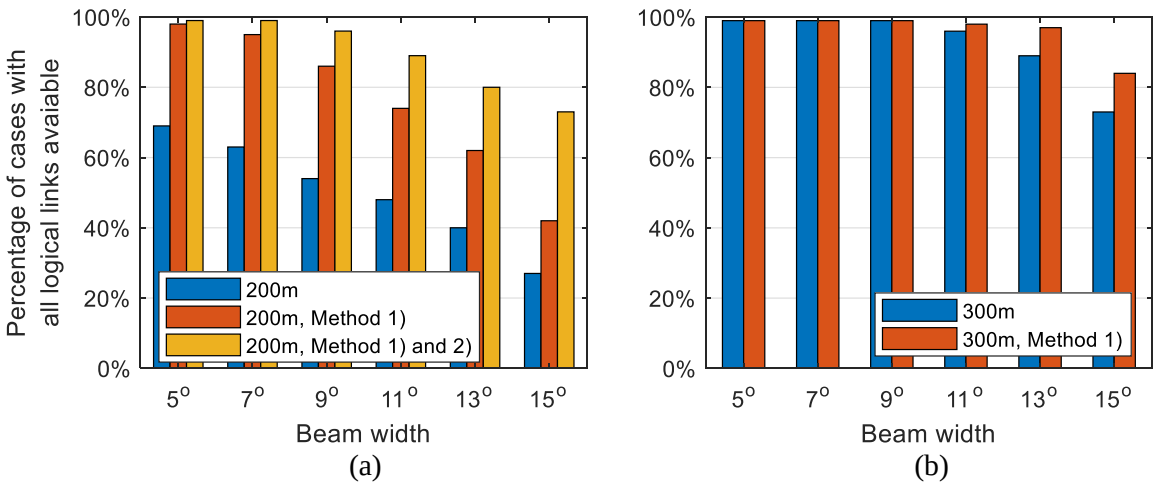

Figure 4.7: Updated probability of finding feasible paths for all logical links.

BSs. Moreover, the backhaul topology is expected to be balanced, so that the number of hops from a edge BS to the macro-cell BS is not too large.

4.5.2 The number of relays used in the mmWave backhaul

While feasibility of the network is our primary concern, we are also interested in how efficient the constructed networks are in terms of the number of relays that need to be deployed. Note that a lower bound on the total number of relays required can be found by running the optimal single path selection algorithm from [54] for each path independently.

As shown in Fig. 4.8, on average, about 27-33 relays are used by 21-23 paths in our algorithm. As the beam width increases, a few more relays are needed to help control the mutual interference in the network. We can reduce the number of relays needed by increasing the number of candidate relay locations in the backhaul area. The number of relays deployed is fairly close to the calculated lower bound, especially when the beam width is no larger than 11^o.

4.5.3 Accuracy of the simplified interference model

As mentioned earlier, it is hard to incorporate an accurate interference calculation into the path searching algorithm; thus, we use a simplified interference model during path search.

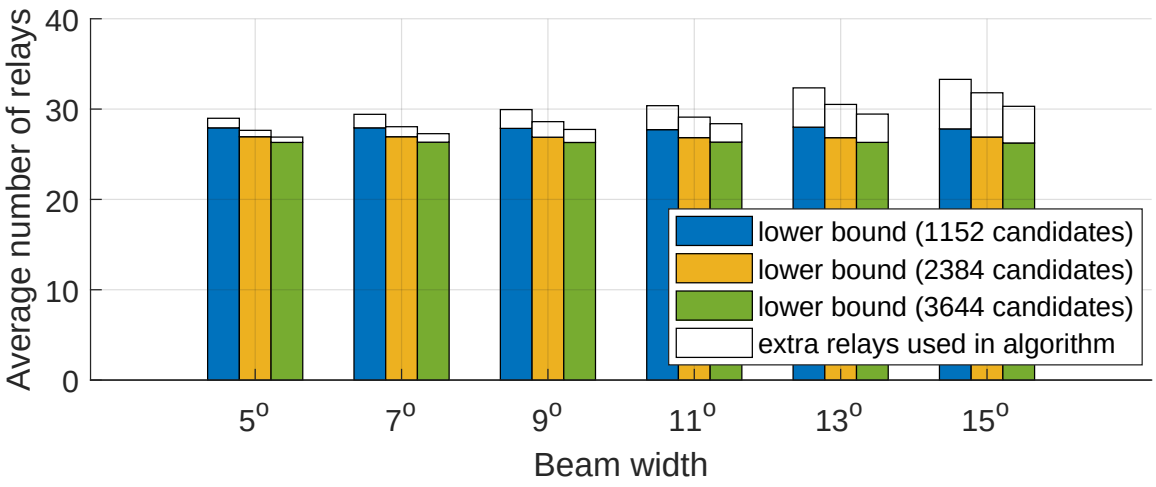

Figure 4.8: The number of relays used ($l_g = 300$ m).

To evaluate the accuracy of our simplified model, we took the final topologies and calculated the mutual interference at the receiver of each physical link using the physical interference model. The worst case is considered in the calculation, where a receiver receives a certain amount of interference signal from any feasible LoS wireless interferer in the network. Fig. 8.4 shows the cumulative distribution functions (CDF) of the path throughput degradation when the more accurate physical interference model is used and for different antenna main-beam-to-side-lobe-ratio. In fact, with our interference model and algorithm, we consistently select relays and paths so that any pair of disjoint physical links are "least-interfered" with each other (see Section 4.4). However, in case multiple physical links share a BS, there could be significant interference, and the amount of interference is determined by the *link scheduling*, the *antenna isolation* on the same BS and the *antenna main-beam-to-side-lobe-ratio*.

In all figures, a larger antenna main-beam-to-side-lobe-ratio means smaller throughput degradation. Fig. 8.4(a) shows the throughput degradation when the transmissions on multiple links at a BS are intelligently scheduled, and no two links on the same BS are simultaneously receiving, or simultaneously transmitting and receiving. In this case, we see that the simplified interference model is very accurate for main beam to side beam ratios of 25 dB and higher, which are typical with state-of-the-art antennas. Fig. 8.4(b) shows the

situation when multiple links on the same BS are used simultaneously but there is near-perfect isolation (i.e., > 120 dB) between antennas. Although the throughput performance is still good in this case, it drops somewhat because the large antenna isolation only eliminates the interference due to two antennas transmitting and receiving simultaneously while the interference due to two antennas receiving at the same time still hurts the throughput. The largest performance drop occurs in Fig. 8.4(c), where we assume leakage of -80 dBm between every pair of antennas transmitting and receiving simultaneously on the same BS, and we can see that there is additional throughput degradation that cannot be eliminated by increasing the antenna main-beam-side-lobe-ratio.

Fig. 8.4 indicates that antenna isolation is the most crucial factor in maintaining the throughput required for backhaul networks. Absent good antenna isolation, intelligent scheduling can maintain high performance on individual paths but its impact on overall network throughput requires further study.

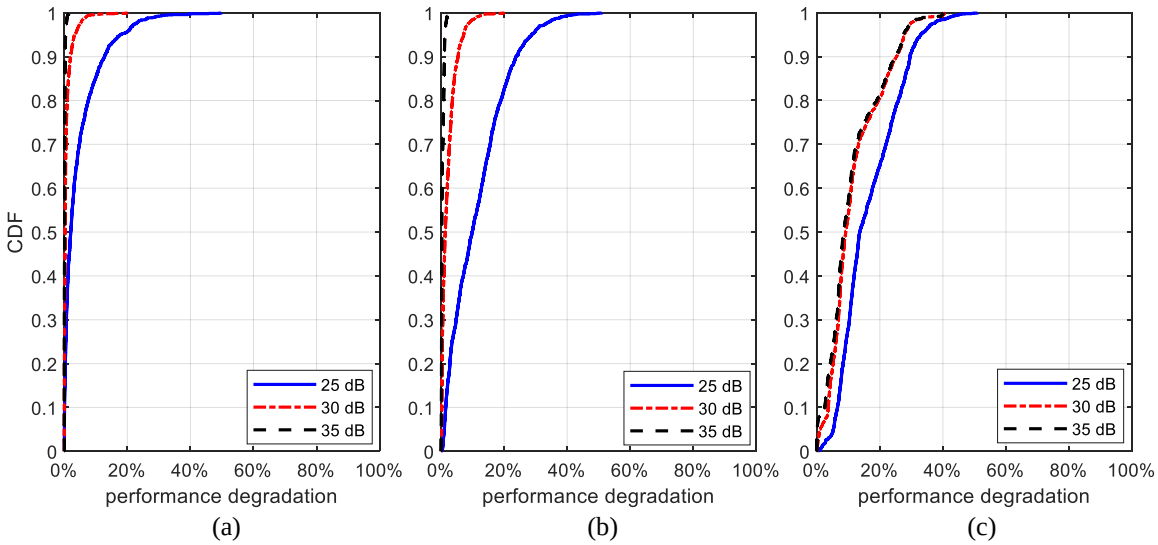

Figure 4.9: Throughput performance degradation with more accurate interference model for different main beam to side lobe ratios ($l_g = 300$ m, $B = 15^o$)

4.6 Chapter summary

In this chapter, we investigate the design of high throughput relay-assisted mmWave backhaul networks in urban areas. Different from most related works, we consider the deployment of dedicated simple mmWave relay devices to help enhance the LoS connectivity of the backhaul network in urban areas with abundant obstacles. Given a set of logical links between base stations in the network, we propose an algorithm to find high-throughput LoS (relaying) paths for all logical links by minimizing interference within and between paths. We also propose methods to modify the backhaul topology to increase the probability of finding high-throughput paths using our algorithm. Extensive simulations, based on a 3-D model of a section of downtown Atlanta, are conducted to show the effectiveness of our algorithms and models. Some insights on the network design problem are also provided.

CHAPTER 5
ANALYZE THE MAXIMUM TRAFFIC DEMAND SUPPORTED BY RELAY-ASSISTED MMWAVE BACKHAUL NETWORKS

5.1 Introduction

In chapter 4, we have explored the methods to select mmWave relays from a set of candidate relay locations, so that interference-minimal logical links between BSs can be constructed to support the targeting high volume backhaul traffic in the urban area. However, our previous work mainly focuses on addressing the feasibility issue of constructing the relay-assisted mmWave backhaul network, while few detail has been provided from the perspective of performance. After the relay-assisted mmWave backhaul network has been built (i.e., all logical links have been constructed), to find out the maximum traffic demand of small-cell BSs that could be supported by the backhaul network is of interest to us.

Specifically, there are two critical constraints that affect the analysis on the throughput performance of a mmWave backhaul network. The first one is the number of radio chains available on each BS. It is assumed that one radio chain cannot transmit and receive at the same time, which is referred to as the primary interference. One radio chain can only serve the transmission on one logical link at a time. If there are not "enough" radio chains available, the BS may not be able to simultaneously transmit data on all its attached logical links. In fact, in a multi-hop mmWave backhaul network, most of the BSs have more than one logical links attached; thus, it is meaningful to investigate the impact of limited radio chain resources on the throughput performance of the backhaul network. The other constraint is rooted in the possible existence of secondary mutual interference among different logical links in the backhaul network. In chapter 4, we try to construct a secondary mutual interference-minimal network topology; however, the simulation results show that it may

not be always possible to form such a backhaul network with the interference-minimal property through relay selection. In the case where mutual interference exists, to maintain the high throughput of logical links, we have to schedule the transmissions of those interfering logical links into different time periods, so that they do not affect each other. Therefore, it is interesting to investigate the throughput performance of a relay-assisted mmWave backhaul network where limited secondary mutual interference exists between a few pairs of logical links.

In this chapter, we formulate several optimization problems to explore the throughput performance of a relay-assisted mmWave backhaul network considering two different traffic models. First, we assume each small-cell BS maintains the same traffic demand, and linear programming is used to maximize that traffic demand. Second, if small-cell BSs have different traffic demand, instead, the aggregated traffic demand at the macro-cell BS in the network is maximized. Each problem is categorized into four individual cases according to the two factors discussed above, i.e., whether there are enough radio chain resources on BSs and whether limited secondary mutual interference exists between logical links. Moreover, we propose a simple scheduling algorithm that can be used to implement a schedule where each logical link can achieve its schedule length obtained through solving the optimization problems. Simulation results are provided to show the throughput performance of our proposed relay-assisted mmWave backhaul networks in different cases.

5.2 System model

We consider that a relay-assisted mmWave backhaul network has already been constructed and given to us. The backhaul network contains a single macro-cell BS M, a set of small-cell BSs $\mathcal{B} = \{B_1, B_2, ...\}$, and a set of mmWave relays. The backhaul network has a tree topology that defines a set of backhaul logical links $\mathcal{L} = \{L_1, L_2, ...\}$ which connect all BSs. In the tree topology, we define the single "inbound" logical link between B_i's parent BS and BS B_i as L_i. In Figure 5.1, an example of a relay-assisted mmWave backhaul

network with a tree topology containing 17 logical links is shown.

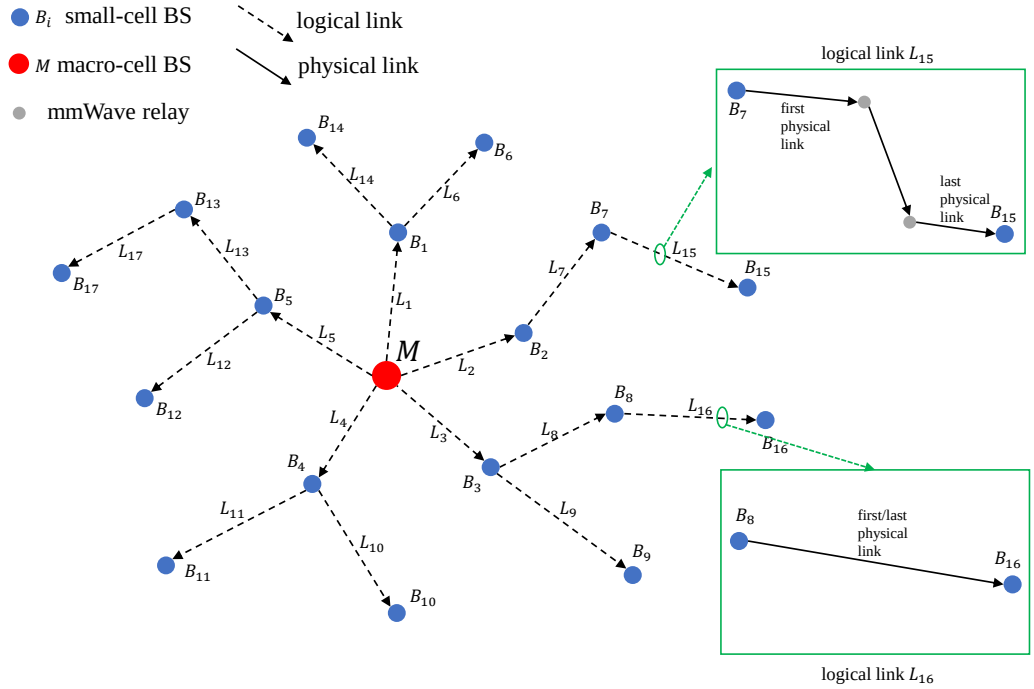

Figure 5.1: An example of a relay-assisted mmWave backhaul network with tree topology (arrows indicate the traffic direction of links in the downlink case)

Note that since the downlink (i.e., from macro-cell BS to small-cell BSs) and uplink (i.e., from small-cell BSs to macro-cell BS) traffic in the backhaul network can be easily duplex-ed in the time domain or frequency domain (e.g., the Time Division Duplex (TDD) and the Frequency Division Duplex (FDD) used in 4G-LTE systems [81, 82, 83]), we optimize the traffic demand of small-cell BSs in either the downlink or the uplink case for simplicity. Note that, to obtain the optimal traffic demand of small-cell BSs in the downlink and uplink hybrid case is closely related to the general scheduling problem in the wireless network, which is usually considered as NP-complete depending on the specific mutual interference model in use, and we leave it as future work. The optimization process described in this chapter uses the downlink case as an example, despite that the same optimization formulation can be applied to the uplink case as well. Therefore, all logical links and physical links defined in the backhaul network are directional. A logical link is either a single-hop LoS physical link or a multi-hop path going through several relays sequen-

tially from the source BS to the destination BS. In the downlink backhaul scenario, as the macro-cell BS serves as the gateway node to the backbone Internet for all small-cell BSs, all the data traffic requested from each small-cell BSs comes from the macro-cell BS, and the mmWave backhual network disseminates data traffic from the macro-cell BS to every small-cell BS.

To maintain the high throughput capability of a logical link, we assume that all physical links within a logical link are mutual interference-minimal, which is referred to as the "intra-path" interference-minimal. Note that, "interference-minimal" here means that the amount of mutual interference has been controlled to a minimal level which is even smaller than the noise level, so that in the latter analysis, that minimal interference can be neglected. For each intra-path interference-minimal logical link, we can obtain its optimal schedule for all its physical links according to Theorem 2 in the chapter 3. Therefore, we can further get the corresponding maximum end-to-end capacity C_i of a logical link $L_i \in \mathcal{L}$. To achieve C_i of L_i, the first physical link of L_i is scheduled to transmit for a portion $P_i^f \in (0, 1]$ of the total schedule length, while the portion of the scheduled transmission for its last physical link in the total schedule length is denoted as $P_i^l \in (0, 1]$.

As mentioned before, the number of radio chains N_i^R on a small-cell BS B_i (N_M^R on the macro-cell BS M) is a key factor that affects the scheduling of all logical links attached to the same BS. According to the definition in [84], "a radio chain is defined as a single radio and all of its supporting architecture, including mixers, amplifiers, and analog/digital converters." We assume that radio chains considered in this work are half-duplex, which means a radio chain will not transmit and receive at the same time. As for the multiple logical links attached to a BS with single radio chain, they cannot be active, either transmitting or receiving, simultaneously. This is usually referred to as the primary interference. However, when multiple radio chains are available on a BS, if the mutual interference between logical links does not exist (i.e., interference-minimal), some of them could be active at the same time. Note that, since mmWave relays are devices much simpler and cheaper than

BSs, each relay only has one radio chain; thus relays are always constrained by the primary interference.

New model of mutual interference between logical links

TDMA-based scheduling in wireless networks has been researched a lot in the literature. If any two backhaul logical links are possible to interfere with each other, depending on the exact interference model in use, the general scheduling problem is often NP-complete [85, 86, 87]. Sometimes it is even hard to find polynomial approximate algorithm to address the scheduling problem [88, 89, 90, 91].

However, due to the specific propagation features of mmWave signals, such as the well-known blockage effect and directional transmissions, the interference relationship is not that "general" in a relay-assisted mmWave backhaul network in the dense urban environment. Based on the simulation results in chapter 4, in the cases where the interference-minimal backhaul network is not feasible through using our proposed relay selection algorithm, we find that the path searching for those problematic logical links usually "fails" due to the searched path of a problematic logical link is interfering with some already constructed logical links which intersect with the problematic logical link.

Based on the above observation, for the relay-assisted mmWave backhaul network, we propose a new mutual interference model that only logical links connecting to the same BS would interfere with each other and a logical link can at most interfere with one other logical link at a BS. In the worst case, a logical link may interfere with two logical links in total, one at each end. This model is reasonable because the ultra high throughput requirement of a mmWave backhaul network requires the mutual interference to be controlled to a minimal or close-to minimal level, and if too many logical links interfere with each other, the throughput performance will be very bad. Moreover, we also observe that after modifying the relay selection algorithm in the chapter 4 which allows limited mutual interference exists between logical links as described in the new interference model, the

feasibility of finding high throughput relay-assisted mmWave backhaul network increases a lot. The further optimization problem formulations in this chapter are using the new mutual interference model.

5.3 Maximizing the backhaul throughput performance

In this section, we are going to address the issue of finding both the maximum traffic demand of small-cell BSs and the maximum backhaul throughput at the macro-cell BS of a given relay-assisted mmWave backhaul network. To answer these two questions, we have to find out the corresponding optimal schedule of each logical link in the network with two different traffic models, respectively. Therefore, we formulate the scheduling problem using linear programming, which can be solved efficiently, under different backhaul network configurations.

The traffic demand of a small-cell BS B_i is defined as D_i and the overall backhaul throughput at the macro-cell BS M is denoted as D_M. Thus, the relationship between D_i and D_M is

$$D_M = \sum_{i=1}^{N_B} D_i \tag{5.1}$$

where N_B is total number of small-cell BSs in the backhaul network.

5.3.1 Maximizing the traffic demand of small-cell BSs

We first address the problem of maximizing the traffic demand of small-cell BSs in the backhaul network. In this problem, we assume each small-cell BS maintains the same traffic demand D_B, i.e., $D_i = D_B, \forall\, i \in \{1, 2, ..., N_B\}$. In practice, the traffic demand of a small-cell BS is determined by the actual amount of data requested from all user ends that access to it, which is quite relevant to the location, time, and other environmental factors. Despite that the traffic demand may be different among different small-cell BSs, it is still reasonable to make the above assumption, as we aim to maximizing the traffic demand of

each small-cell BS without taking the specific environmental factors into consideration.

We categorize the optimization problem into four different cases according to the different conditions on the existence of mutual interference between logical links and the number of available radio chains on BSs. Each case will be discussed in detail later.

Case 1: interference-minimal, enough-radio-chain

In this case, the backhaul network is interference-minimal, which means that any two logical links scheduled to be active concurrently will not experience end-to-end throughput decrease due to the factor of mutual interference. Moreover, the meaning of "enough radio chains" is that the numbers of radio chains N_i^R on a small-cell BS B_i as well as N_M^R on the macro-cell BS M are no fewer than the number of logical links attached to B_i and M, respectively. In this scenario, different logical links can be scheduled to transmit data simultaneously without being constrained by the primary interference, because each logical link has its own radio chain.

Therefore, we only need to make sure that the single "inbound" logical link L_i at the BS B_i has enough link capacity to support the total traffic demand of all small-cell BSs in the sub-tree rooted at B_i. This is called the *logical link capacity constraint*. The optimization problem of this case can be written as,

$$\begin{aligned} \max \quad & D_B \\ \text{s.t.} \quad & C_i \geq \sum_{B_j \in \mathcal{B}_i} D_j = |\mathcal{B}_i| D_B, \ \forall\, i \in \{1, 2, ..., N_B\} \end{aligned} \tag{5.2}$$

where $\mathcal{B}_i$ is the set of small-cell BSs in the sub-tree rooted at B_i, and $|\cdot|$ is the operation which returns the number of elements in a set.

Case 2: interference-minimal, limited-radio-chain

In this case, we move a step forward, and consider that there are not "enough" radio chains available on BSs. It means that multiple logical links connecting to a BS have to compete for the use of available radio chains, because one radio chain can only serve one active logical link at a time. Note that one logical link cannot use multiple radio chains to transmit or receive data simultaneously due to the interference issue. Meanwhile, the mutual interference is still controlled to the minimal level in the backhaul network, which is the same as that in the case 1.

Therefore, it is found that the total active time of all physical links attached to a small-cell (macro-cell) BS B_i (M) should not exceed N_i^R (N_M^R) times the total schedule length, because every radio chain on a BS could be actively working for the entire schedule length if the transmissions on the logical links are properly scheduled in the ideal case. This is referred to as the *limited radio chain constraint*.

As for a physical link attached to a BS, it is either the first physical link of a logical link starting at the BS or the last physical link of a logical link ending at the BS. Since every physical links within a logical link follows the optimal schedule of that logical link, the scheduled active time for the first and last physical link of the logical link L_i is no longer than P_i^f and P_i^l of the total schedule length, respectively. It is because that P_i^f or P_i^l is the maximum schedule length for the first or last physical link in L_i, which can only be achieved when the logical link L_i is scheduled to be active during the entire schedule length. We called it the *physical link scheduling constraint*.

Figure 5.2 gives an example of the optimal schedule of a logical L_i. We denote p_i^f and p_i^l as the portion of the total time resource when the first and last physical links of L_i are scheduled to be active, respectively. Therefore, the average logical link rate c_i of L_i over

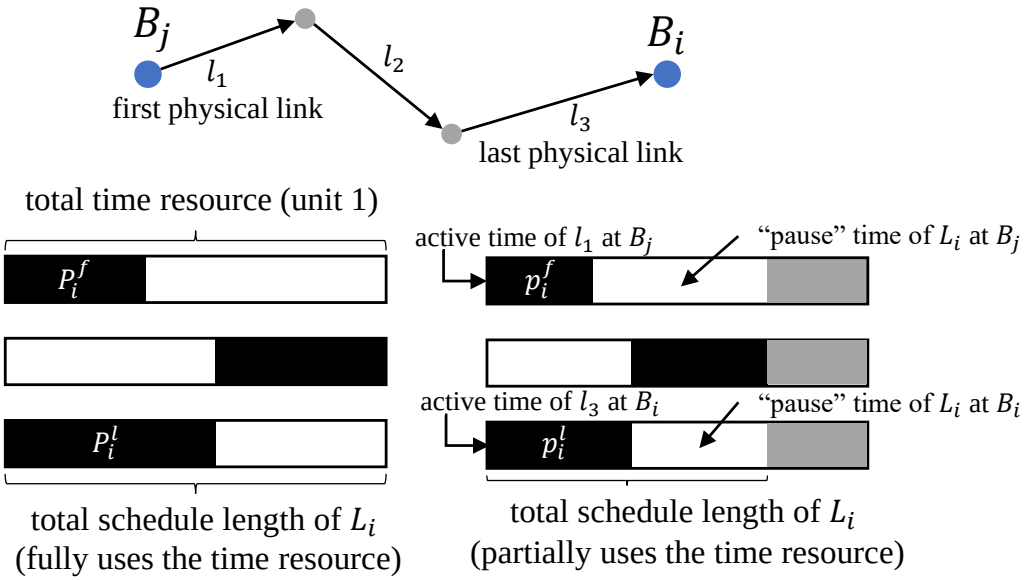

Figure 5.2: An example of the optimal schedule of a logical link L_i

the entire time resource can be calculated as,

$$c_i = \min\{\frac{p_i^f}{P_i^f}, \frac{p_i^l}{P_i^l}\} \cdot C_i \tag{5.3}$$

Thus, the optimization problem can be written as,

$$\begin{aligned}
\max \quad & D_B \\
\text{s.t.} \quad & \min\{\frac{p_i^f}{P_i^f}, \frac{p_i^l}{P_i^l}\} \cdot C_i \geq \sum_{B_j \in \mathcal{B}_i} D_j = |\mathcal{B}_i| D_B, \ \forall\, i \in \{1, 2, ..., N_B\} \\
& 0 \leq p_i^f \leq P_i^f, \ \forall\, i \in \{1, 2, ..., N_B\} \\
& 0 \leq p_i^l \leq P_i^l, , \ \forall\, i \in \{1, 2, ..., N_B\} \\
& p_i^l + \sum_{L_j \in \mathcal{L}_i \setminus L_i} p_j^f \leq N_i^R, , \ \forall\, i \in \{1, 2, ..., N_B\} \\
& \sum_{L_i \in \mathcal{L}_M} p_i^f \leq N_M^R
\end{aligned} \tag{5.4}$$

where $\mathcal{L}_i$ is the set of logical links attached to the small-cell BS B_i; $\mathcal{L}_M$ is the set of logical links attached to the macro-cell BS M.

As shown in Equation 5.4, the logical link capacity constraint is different from that in the case 1, because when logical links compete for the radio chains, it is possible that a logical link L_i cannot achieve its optimal capacity C_i due to less time would be scheduled for the transmission on its first or last physical link. In fact, since the schedule of the physical links within a logical link follows the logical link's optimal schedule, we can get

$$\frac{p_i^f}{P_i^f} = \frac{p_i^l}{P_i^l}$$

because when the bottleneck of a logical link's capacity is determined by either its first physical link or its last physical link in Equation 5.3, allocating more active time for the physical link at the other end is meaningless.

Therefore, we can use p_i^f to represent p_i^l, and update the formation of the optimization problem as,

$$\begin{aligned}
\max \quad & D_B \\
\text{s.t.} \quad & \frac{p_i^f}{P_i^f} \cdot C_i \geq \sum_{B_j \in \mathcal{B}_i} D_j = |\mathcal{B}_i| D_B, \ \forall\, i \in \{1, 2, ..., N_B\} \\
& 0 \leq p_i^f \leq P_i^f, \ \forall\, i \in \{1, 2, ..., N_B\} \\
& \frac{P_i^l}{P_i^f} \cdot p_i^f + \sum_{L_j \in \mathcal{L}_i \setminus L_i} p_j^f \leq N_i^R, \ \forall\, i \in \{1, 2, ..., N_B\} \\
& \sum_{L_i \in \mathcal{L}_M} p_i^f \leq N_M^R
\end{aligned} \tag{5.5}$$

Case 3: limited-interference, enough-radio-chain

Before moving to the problem formulation for this case, we have make it clear that the mutual interference between logical links is produced by the mutual interference between physical links within them. To eliminate the existing mutual interference between logical links, the straight-forward idea is to schedule the interfering physical links into different

time periods. However, a logical link may contain several physical links, and each physical link may have its individual interference relationship with different physical links of other logical links, which makes the physical link level interference-avoid scheduling complicated. Not to mention that it likely breaks the optimal scheduling assumption within each logical link. Therefore, when we deal with the mutual interference between logical links, we consider a multi-hop logical link as a "virtual link", and the schedule of the physical links within a logical link follows the optimal schedule of that logical link, which is the same assumption as used in case 2. Thus, we only need to make sure that the scheduled active time periods of any two interfering logical links do not overlap. This is referred to as the *logical link interference constraint*. Since only the logical link level interference-avoid scheduling is in use to maximize the traffic demand of small-cell BSs, the schedule found by solving the following optimization problem is sub-optimal in the original problem setting.

The maximize the traffic demand in this case, we have to solve the following linear programming problem.

$$\begin{aligned} \max \quad & D_B \\ \text{s.t.} \quad & \frac{p_i^f}{P_i^f} \cdot C_i \geq \sum_{B_j \in \mathcal{B}_i} D_j = |\mathcal{B}_i| D_B, \ \forall\, i \in \{1, 2, ..., N_B\} \\ & 0 \leq p_i^f \leq P_i^f, \ \forall\, i \in \{1, 2, ..., N_B\} \\ & \frac{p_i^f}{P_i^f} + I_{ij} \cdot \frac{p_j^f}{P_j^f} \leq 1, \ \forall\, i, j \in \{1, 2, ..., N_B\} \end{aligned} \tag{5.6}$$

where I_{ij} is a binary parameter identifying the interference relationship between logical link L_i and L_j. If L_i and L_j interfere with each other, $I_{ij} = 1$; otherwise, $I_{ij} = 0$. From the analysis on the interference relationship between physical links in the chapter 4, we can derive that L_i interferes L_j if and only if L_j interferes L_i, which means $I_{ij} = I_{ji}$.

Comparing Equation 5.5 and Equation 5.6, there is similarity between expressions of

the "radio chain constraint" and the "logical link interference constraint". It is intuitive to think that both of them reflect the idea of scheduling the link transmissions to avoid interference in the network, since the "radio chain constraint" can be regarded as the "primary interference constraint".

Case 4: limited-interference, limited-radio-chain

This case can be considered as the combination of case 2 and case 3, as both primary and secondary mutual interference have impact on the schedule of transmissions in the backhaul network.

We can formulate the optimization problem as,

$$
\begin{aligned}
\max \quad & D_B \\
\text{s.t.} \quad & \frac{p_i^f}{P_i^f} \cdot C_i \geq \sum_{B_j \in \mathcal{B}_i} D_j = |\mathcal{B}_i| D_B, \ \forall\, i \in \{1, 2, ..., N_B\} \\
& 0 \leq p_i^f \leq P_i^f, \ \forall\, i \in \{1, 2, ..., N_B\} \\
& \frac{p_i^f}{P_i^f} + I_{ij} \cdot \frac{p_j^f}{P_j^f} \leq 1, \ \forall\, i, j \in \{1, 2, ..., N_B\} \\
& \frac{P_i^l}{P_i^f} \cdot p_i^f + \sum_{L_j \in \mathcal{L}_i \setminus L_i} p_j^f \leq N_i^R, \ \forall\, i \in \{1, 2, ..., N_B\} \\
& \sum_{L_i \in \mathcal{L}_M} p_i^f \leq N_M^R
\end{aligned}
\tag{5.7}
$$

where all the variables and parameters are the same as defined in previous cases.

5.3.2 Maximizing the total backhaul traffic demand at the macro-cell BS

Based on the above analysis, we can easily adapt the problem formation in the section 5.3.1 to obtain the optimization problem of maximizing the total backhaul traffic demand at the macro-cell BS. In this problem, the traffic demand of each small-cell BS could be different. We first formulate the problem corresponding to the case 1 in the section 5.3.1.

Case 1: interference-minimal, enough-radio-chain

When neither "intra-path" nor "inter-path" mutual interference exists and there are enough radio chains to support the concurrent transmissions of multiple logical links at each BS, the maximum backhaul traffic demand at the macro-cell BS can be obtained through solving the following linear programming problem,

$$\begin{aligned} \max \quad & D_M = \sum_{i=1}^{N_B} D_i \\ \text{s.t.} \quad & C_i \geq \sum_{B_j \in \mathcal{B}_i} D_j, \ \forall \, i \in \{1, 2, ..., N_B\} \end{aligned} \tag{5.8}$$

where all the variables and parameters are the same as defined in the section 5.3.1.

As the case 4 is the combination of case 2 and 3 in the section 5.3.1, we will only provide the problem formation of the case where limited mutual interference exists and each BS has limited radio chain resources.

Case 2: limited-interference, limited-radio-chain

The optimization problem of this case can be formulated as follow,

$$\begin{aligned} \max \quad & D_M = \sum_{i=1}^{N_B} D_i \\ \text{s.t.} \quad & \frac{p_i^f}{P_i^f} \cdot C_i \geq \sum_{B_j \in \mathcal{B}_i} D_j, \ \forall \, i \in \{1, 2, ..., N_B\} \\ & 0 \leq p_i^f \leq P_i^f, \ \forall \, i \in \{1, 2, ..., N_B\} \\ & \frac{p_i^f}{P_i^f} + I_{ij} \cdot \frac{p_j^f}{P_j^f} \leq 1, \ \forall \, i, j \in \{1, 2, ..., N_B\} \\ & \frac{P_i^l}{P_i^f} \cdot p_i^f + \sum_{L_j \in \mathcal{L}_i \setminus L_i} p_j^f \leq N_i^R, \ \forall \, i \in \{1, 2, ..., N_B\} \\ & \sum_{L_i \in \mathcal{L}_M} p_i^f \leq N_M^R \end{aligned} \tag{5.9}$$

where all the variables and parameters are the same as defined in the section 5.3.1.

In the simulation section of this chapter, we focus on the performance evaluation of the cases where the traffic demand on each small-cell BS is the same; while leave the performance evaluation of the cases discussed in this section as our future work.

5.3.3 Maximizing the total backhaul throughput while considering fairness

As we can see from the numerical results in Figure 5.5, the traffic demand of each small-cell BS in the backhaul network is very unbalanced, when the aggregated traffic demand achieves the maximum at the macro-cell BS. In the cellular system, the resources have to be allocated in a way that fairness is considered to some extent, so that every cellular user who is paying their monthly bill can receive a service meeting the minimum quality of service requirement. From this perspective, we are interested in maximizing the total backhaul traffic demand aggregated at the macro-cell BS while considering the fairness issue across all the small-cell BSs in the backhaul network. Specifically, we complete the task through the following two steps.

First, we take advantage of the work in the section 5.3.1, to maximize the equal traffic demand of all small-cell BSs in the backhaul network. The maximum traffic demand value found using the linear programming formulation in Equation 5.7 will be served as the minimum traffic demand of each small-cell BS that is able to be supported by the given backhaul network. Then we try to utilize the available network resources to accommodate more traffic demand on some of the small-cell BSs. Here we only use the formulation of case 4 in section 5.3.1, because the other three cases can be regarded as special cases of case 4.

Second, we use the similar idea in section 5.3.2 to maximize the total aggregated backhaul demand at the macro-cell BS, while the minimum traffic demand of each small-cell BS obtained in the above first step can be satisfied. The objective can be achieved by solving

the following linear programming formulation,

$$
\begin{aligned}
\max \quad & D_M = \sum_{i=1}^{N_B} D_i \\
\text{s.t.} \quad & \frac{p_i^f}{P_i^f} \cdot C_i \geq \sum_{B_j \in \mathcal{B}_i} D_j, \ \forall\, i \in \{1, 2, ..., N_B\} \\
& D_i \geq \widehat{D_B}, \ \forall\, i \in \{1, 2, ..., N_B\} \\
& 0 \leq p_i^f \leq P_i^f, \ \forall\, i \in \{1, 2, ..., N_B\} \\
& \frac{p_i^f}{P_i^f} + I_{ij} \cdot \frac{p_j^f}{P_j^f} \leq 1, \ \forall\, i, j \in \{1, 2, ..., N_B\} \\
& \frac{P_i^l}{P_i^f} \cdot p_i^f + \sum_{L_j \in \mathcal{L}_i \setminus L_i} p_j^f \leq N_i^R, \ \forall\, i \in \{1, 2, ..., N_B\} \\
& \sum_{L_i \in \mathcal{L}_M} p_i^f \leq N_M^R
\end{aligned}
\tag{5.10}
$$

where $\widehat{D_B}$ is the maximum equal traffic demand obtained through the first step; while the other parameters and variables are the same as defined in the previous formulations.

5.4 Schedule the maximum traffic demand in the relay-assisted mmWave backhaul network

After solving the optimization problems described in the above section, we need to figure out how to schedule the transmission of each link in the backhaul network, so that the maximum traffic demand D_B at each small-cell BS or the maximum backhaul throughput D_M at the macro-cell BS can be achieved. As the by-product of maximizing traffic demand of BSs using linear programming, we can obtain a set of $\{p_i^f\}$ values, where each p_i^f represents the portion of the total time resource expected to be assigned to the first physical link of a logical link L_i. We propose a 'depth-first"-style algorithm to find a schedule accommodating all the values in $\{p_i^f\}$ for all logical links in the backhaul network.

The algorithm described using the pseudo code in the Algorithm 5 aims to address the scheduling issue in the case where limited mutual interference exists and there is limited radio chain resource on each BS in a tree-style relay-assisted mmWave backhaul network. Since other cases are special cases of this one, the algorithm can easily be modified to adapt to them. Since the optimization problem can deal with either downlink or uplink traffic scenario, the scheduling algorithm can handle either downlink or uplink traffic scenario as well, because the operations in the algorithm are not affected by the change of traffic directions in the network.

Basically, the scheduling process starts from the macro-cell BS M, runs in a "depth-first" way, and does not end until all non-leaf small-cell BSs have made their scheduling decisions. Every BS in the backhaul network only has to make scheduling decisions for all the logical links between the BS and its "child" BSs, because the schedule of the logical link between a BS and its "parent" BS has already been decided by the "parent" BS.

As shown in Algorithm 5, a stack $\mathcal{S}$ stores the set of BSs whose scheduling decisions need to be made. When one BS B_c is in turn to make its scheduling decision, a set $\mathcal{L}_c$ is used to store the to be scheduled logical links. If B_c is a small-cell BS, the schedule of the logical link L_c between B_c's parent BS and B_c has already been determined by B_c's parent BS. Therefore, B_c will first allocate time for L_c according to the determined schedule. If there exists one logical link to be scheduled interfering with L_c, B_c schedules the interfering logical link right after scheduling L_c. After that, B_c will schedule all non-interfering logical links, whose scheduled time periods do not overlap with each other, but can occupy the "pause" time of the previously scheduled logical links. Note that the schedule length of a logical link at a BS contains two parts: one is the scheduled time period for the physical link attached to the BS, and the other is the "pause" time which is used by other physical links within the logical link (see Figure 5.2). However, the logical link does not need to use the actual radio chain resource at the BS during the "pause" time, as the physical links being active at the "pause" time are not attached to that BS. In the end,

Algorithm 5 Optimal scheduling algorithm for tree-style mmWave backhaul networks

Require: $\{p_i^f\}$

$\mathcal{S}$.push(M);
while $\mathcal{S} \neq \emptyset$ **do**
  $B_c = \mathcal{S}$.pop();
  $\mathcal{L}_c \leftarrow \emptyset$;
  for each $B_i \in \mathcal{B} \wedge (B_i$ is a child of $B_c)$ **do**
    $\mathcal{S}$.push(B_i);
    $\mathcal{L}_c$.insert(L_i);
  if $B_c \neq M$ **then**
    assign the schedule length of $\frac{p_c^f}{P_c^f}$ on the 1^{st} radio chain according to the existing schedule of L_c;
    if L_c interferes with a single $L_i \in \mathcal{L}_c$ **then**
      assign the schedule length of $\frac{p_i^f}{P_i^f}$ on the 1^{st} radio chain for L_i, which does not overlap with the schedule of L_c;
      $\mathcal{L}_c$.remove(L_i);
    while there exists $L_i \in \mathcal{L}_c \wedge L_i$ does not interfere with any other logical link in $\mathcal{L}_c$ **do**
      assign the schedule length of p_i^f on the first available radio chain where blank time periods exist for L_i.
      if the first available radio chain does not have enough time available for L_i **then**
        assign the rest of the schedule length of L_i in the next available radio chain, and the assigned time period should not overlap with the already scheduled time period of L_i on the previous radio chain.
      $\mathcal{L}_c$.remove(L_i);
    while there exist $L_i,\ L_j \in \mathcal{L}_c \wedge L_i$ interferes with L_j **do**
      first assign the time periods p_i^f and p_j^f for the first physical links of L_i and L_j, respectively, on the first available radio chain where blank time periods exist.
      if the first available radio chain does not have enough time available **then**
        assign the rest of the schedule length of the first physical links of L_i and L_j in the next available radio chain, and the assigned time period should not overlap with the already scheduled time periods of them on the previous radio chain.
      assign the "pause" time periods $p_i^f \cdot (\frac{1-P_i^f}{P_i^f})$ and $p_j^f \cdot (\frac{1-P_j^f}{P_j^f})$ on the radio chains where the first physical links of L_i and L_j have been scheduled. These "pause" time periods should not overlap with each other or the scheduled periods of their corresponding first physical links, but they must reuse the time periods scheduled for other logical links, if there exist.
      $\mathcal{L}_c$.remove(L_i, L_j);

B_c schedule the remaining logical links interfering with each other in a pair-wise way. For a pair of interfering logical links, B_c first assign the "active" time for their physical links

attached to B_c, and then assign the "pause" time. Note that "pause" time of a logical link L_i can overlap with the schedule of any logical link that is not interfering with L_i.

5.5 Numerical results and analysis

This section aims to provide several sets of numerical results and simulation results, which will be analyzed to show the throughput performance of the relay-assisted mmWave backhaul network.

5.5.1 The maximum traffic demand of each small-cell BS

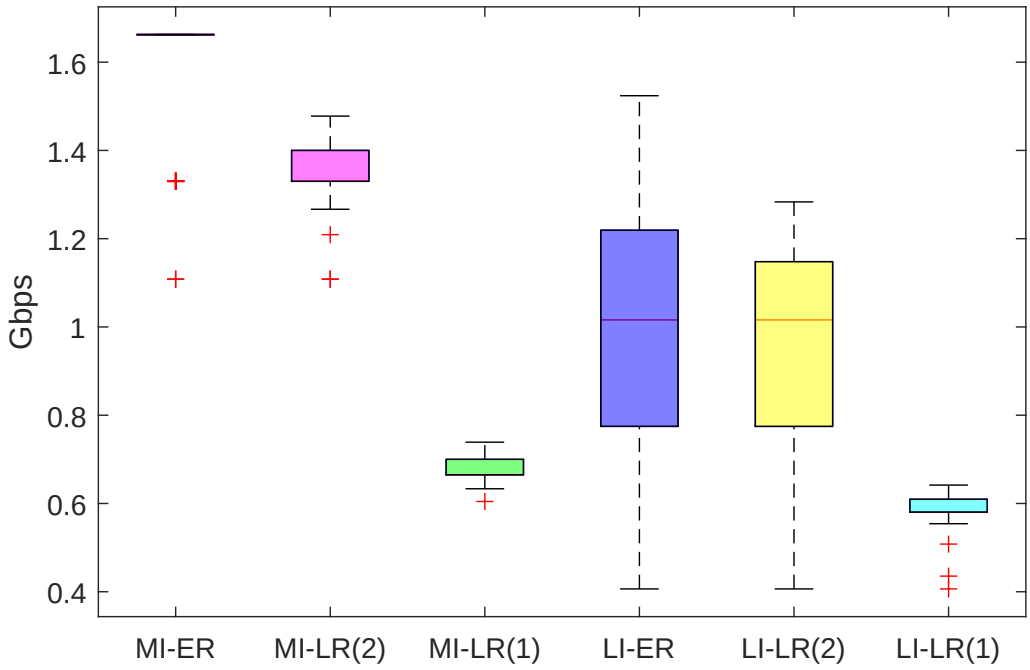

Figure 5.3: Maximum traffic demand of each small-cell BS in different network settings

First, the maximum traffic demand of each small-cell BS in a mmWave backhaul network is calculated in different network settings using the method introduced in section 5.3. Note that, in the calculation, only downlink traffic or uplink traffic is considered. Nowadays, the communication systems usually apply the OFDM and QAM modulation schemes. In our simulations, we consider a frame structure with the slot size 4.16 μs, a total band-

width 2 GHz, which contains 6912 sub-carriers, and the 256 QAM is in use. Therefore, the raw data rate [1] of each physical link is fixed at $6912 \times 8/4.16 = 13.3$ Gbps. Therefore, the data rate of a single-hop logical link equals to the physical link data rate, i.e., 13.3 Gbps; while the data rate of a multi-hop logical link equals to half of the physical link data rate, i.e., 6.65 Gbps. As shown in Figure 5.3, six different network settings are considered, in which "MI-ER" refers to the case where interference is minimal and enough radio chains are available, "MI-LR" refers to interference-minimal and limited radio chains, "LI-ER" refers to the case where interference exists between a few pairs of logical links and enough radio chains are available, while "LI-LR" refers to the case of limited interference and limited radio chains. In the cases of enough radio chains, the number of radio chains of each BS is set to the number of logical links attached to it; while in the cases of limited radio chains, each small-cell BS has only 1 radio chain, but the macro-cell BS has 2 or 1 radio chains identified by the number in the parenthesis at the end of the label. From Figure 5.3, we can see that the number of radio chains plays a crucial role in determine the maximum traffic demand of each small-cell BS, as the average values of the cases where enough radio chains are available are much higher than that of the cases where limited radio chains are available. One main reason is that in the considered topology, many logical links (e.g., 8) are attached to the macro-cell BS, and if only 1 radio chain is available, at any time, there is at most 1 logical link actively transmitting data, which is very inefficient. We also observe that when the number of radio chains at the macro-cell increases to 2, the obtained maximum traffic demand also increases a lot. Among the cases with limited radio chains, when interference exists between a few pairs of logical links, the maximum traffic demand drops slightly, because the primary interference only restricts the physical links attached to a BS of different logical links cannot be active simultaneously, while the mutual interference applies a even tighter constraint that the schedules of interfering logical links do not overlap with each other, and the schedule of a multi-hop logical link is much longer than that of a

[1] Here, we do not consider the channel coding efficiency.

physical link. Similarly, the maximum traffic demand in the "MI-ER" case is much better than that in the "LI-ER" case, as the mutual interference is minimal in the "MI-ER" case. In Figure 5.3, we can observe that the dynamic range of the values in the "LI-ER" case is very large. It is because that the maximum traffic demand is greatly affected by where the interference appears. If the most of the interfering pairs of logical links are attached to the macro-cell BS, the throughput will be very low; however, if the interference appears mostly at small-cell BSs, as the traffic demand around 2 Gbps can be easily handled when there is a few logical links (e.g., 2) attached to the small-cell BS, which is exactly the case in the considered topologies.

5.5.2 The lower bound of "enough" radio chains on each BS

As soon as the maximum traffic demand of each small-cell BS is calculated in the cases where enough radio chains are available on each BS, the portion p_i^f of the schedule of the first physical link within the logical link L_i attached to the parent BS of B_i can also be determined. Based on this set of values, the minimum number of radio chains needed at each BS can be updated.

Table 5.1: The numerical result on the minimum number of "enough" radio chains

BS type	interference-minimal	limited-interference
small-cell	1 (60%), 2 (40%)	1 (62%), 2 (38%)
macro-cell	2 (32%), 3 (68%)	1 (5%), 2 (69%), 3 (26%)

As shown in Table 5.1, in every tested case, only single radio chain is enough for the main portion of all small-cell BSs, no matter there is mutual interference or not. However, for the small-cell BSs close to the macro-cell BS, they may need two radio chains. This is because in most of cases, each small-cell BS may only have at most 2 logical links attached, and the BSs close to the macro-cell BS tend to have larger aggregated traffic demand. However, as for the macro-cell BS, since usually 8 logical links are attached to it, more radio chains are needed. But 2-3 radio chains are enough for the macro-cell BS in all test

cases, which is much smaller than the initial "enough" number of radio chains determined by the number of logical links attached (i.e., 8). This result is reasonable, because most of the logical links are multi-hop, and in their optimal schedule, each physical link can intuitively be thought as active for only half of the total schedule of the logical link. Thus, single radio chain can serve 2 logical links without any problem if they do not interfere with each other.

5.5.3 The maximum aggregated traffic demand at the macro-cell BS

Simulations are also conducted to show the aggregated traffic demand values at the macro-cell BS upon three different maximization objectives in two different network setting configurations. In Figure 5.4, the blue column represents the value corresponding to the case

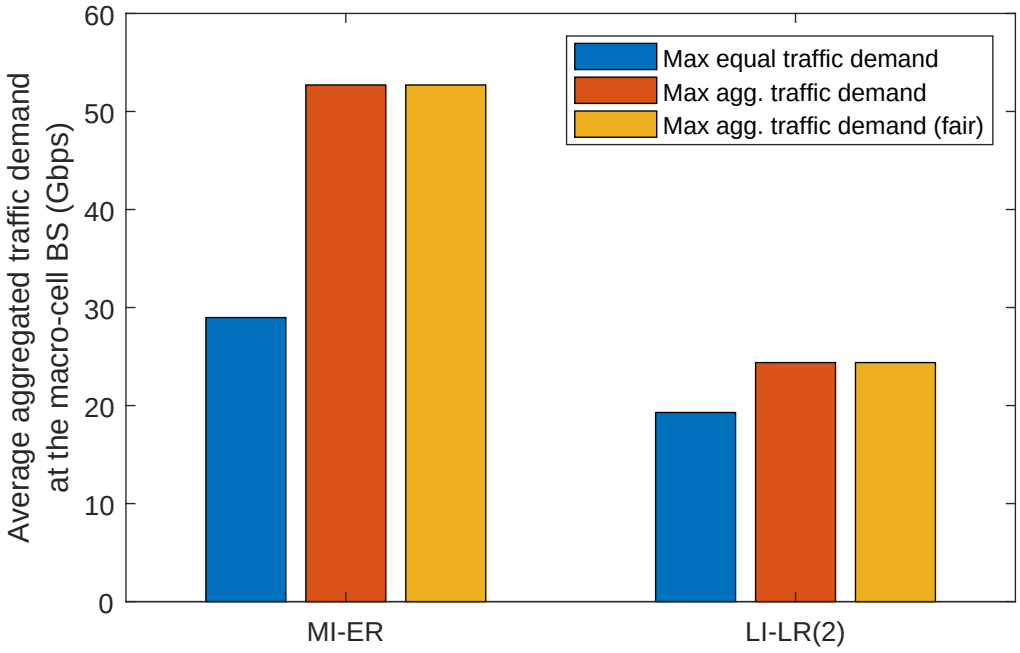

Figure 5.4: Maximum aggregated traffic demand at the macro-cell BS

where equal traffic demand of every small-cell BS is maximized; the red column represents the value corresponding to the case where the aggregated traffic demand at the macro-cell BS is maximized without considering fairness; while the yellow column represents the case where fairness is considered when the aggregated traffic demand is maximized. The left

three columns corresponds to the values in the interference-minimal backhaul networks with enough radio chain resources; while the right three columns shows the values in the backhaul networks where limited interference exists between a few pairs of logical links, and limited radios are available on BSs (i.e., 2 radio chains on the macro-cell BS, and 1 radio chain on each small-cell BS). Each value shown in the figure is an averaged value across 50 sets of individual simulations using the backhaul network data generated in Chapter 4.

As shown in Figure 5.4, maximizing the aggregated traffic demand at the macro-cell BS allows more traffic to flow into the mmWave backhual network than maximizing the equal traffic demand of each small-cell BS does, because in the later case, the equal traffic demand is limited by the traffic demand of BSs on the "bottleneck" routes. The bottleneck routes are the routes consisting the largest number of small-cell BSs in the backhual network. We can also see that the gap of aggregated traffic demand between the blue column and the yellow column shrinks from the MI-ER case to the LI-LR(2) case. This is because in the MI-ER case, plenty of radio chains are available on each BS, especially on the macro-cell BS, which means more extra resources are available after allocating the time resources to small-cell BSs to achieve the maximum equal traffic demand of each small-cell BS, and with more available extra resources, more additional traffic can flow into the backhaul network. It is also interesting to see that from the simulation result, considering the fairness factor in maximizing the aggregated traffic demand does not affect the achievable maximum value of aggregated traffic demand at the macro-cell BS, because in both MI-ER and LI-LR(2) cases, the logical links attached to the macro-cell BS can achieve the same utilization of the available radio chains on the macro-cell BS.

On the other hand, from the perspective of fairness, Figure 5.5 shows the comparison among different scenarios in terms of the Jain's fairness index [92]. It is obvious that when the equal traffic demand of each small-cell BS is maximized, the fairness index reaches its highest value of 1. Meanwhile, if fairness is not considered, purely maximizing the aggregated traffic demand at the macro-cell BS leads to poor fairness, which are shown by

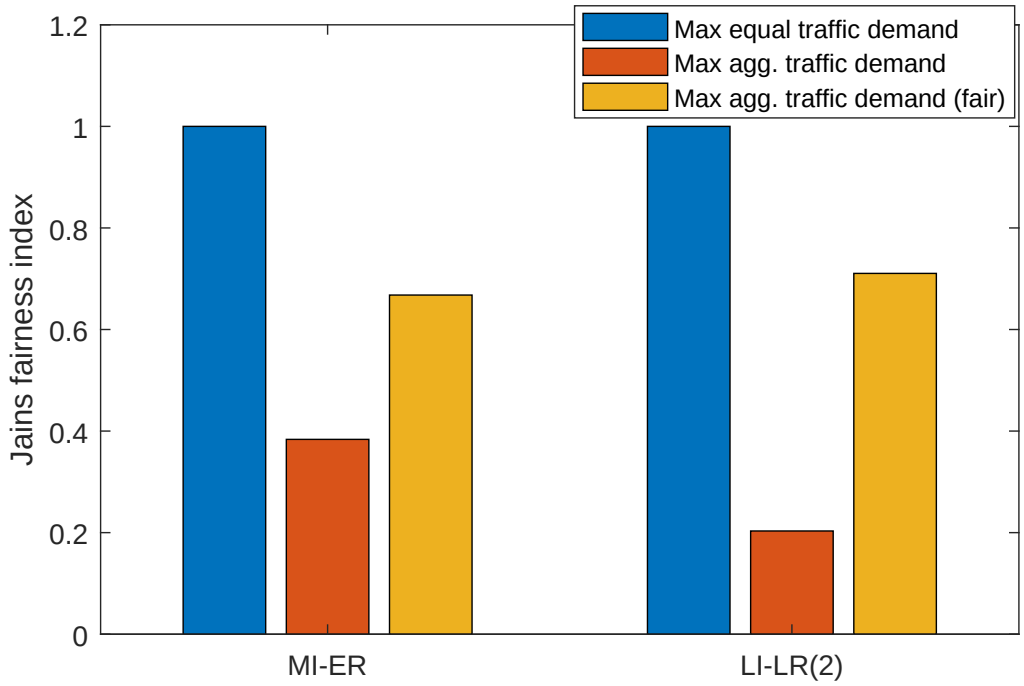

Figure 5.5: Jain's fairness index on the traffic demand of small-cell BSs

the red columns in the figure. However, as the fairness factor is considered as introduced in section 5.3.3, the fairness index value increases significantly, which is shown by the yellow columns.

5.6 Chapter summary

In this chapter, the throughput performance issue of the relay-assisted mmWave backhaul network is investigated. The maximum traffic demand of small-cell BSs and the maximum throughout at the macro-cell BS in the tree-style backhaul network have been found using linear programming under different network settings, which concern both the number of radio chains available on BSs and the interference relationship between logical links in the backhaul network. A new interference model for the relay-assisted mmWave backhaul network in the dense urban environment is proposed, which reflects the limited interference footprint of mmWave directional communications.

CHAPTER 6
AN EFFICIENT DISTRIBUTED SCHEDULING ALGORITHM FOR RELAY-ASSISTED MMWAVE BACKHAUL NETWORKS

6.1 Introduction

In the chapter 5, we focus on optimizing the throughput performance of the relay-assisted mmWave backhaul network with a tree topology in either the downlink or uplink case. However, the scheduling algorithm proposed in Chapter 5 only aims to show the feasibility of finding a schedule that is able to satisfy the set of schedule lengths of logical links obtained from solving the optimization problems. It is not an algorithm that can be directly deployed into the practical mmWave backhaul network system. Moreover, in the performance optimization, the link schedule length is a continuous value, but in the realistic system, time resource is partitioned into small slots with the same duration. Furthermore, in the practical cellular network, since the aggregated traffic load may be larger than the network capacity, the backhaul traffic has to be scheduled proportionally to the traffic demand of each small-cell BS, so that a certain level of fairness can be achieved. Besides, similar to the discussion in Chapter 5, network level intelligent scheduling has to come into play to handle the scenario where mutual interference exists between logical links and limited number of radio chains are available on BSs. Therefore, it is important to address the scheduling problem in the practical backhaul system.

In this chapter, we propose a novel distributed scheduling algorithm that can be deployed to efficiently schedule the data traffic in the practical relay-assisted mmWave backhaul network with a tree topology. Different from the work in the chapter 5, where either downlink or uplink traffic is considered, the proposed distributed algorithm is able to schedule both downlink and uplink traffic in every subframe. Since the mutual interference

relationship between a pair of logical links may vary according to different transmission directions of both links, we assume that two logical links are considered always interfering with each other if there exists at least one combination of transmission directions which leads to significant mutual interference when both logical links transmit concurrently. Although applying this assumption sacrifices a certain amount of throughput performance, it reduces the complexity of the algorithm design. In fact, since there are only a few pairs of logical links interfering with each other in the relay-assisted mmWave backhaul network in the dense urban area, the throughput performance loss is likely to be limited.

In the following sections, we first give an overview on the distributed scheduling algorithm, which describes the general idea of the algorithm design. Then, details on the system setting are provided. After that, three main components of the algorithm, i.e., the handshaking procedure for exchanging control information, the calculation of the local schedule of a small-cell BS, and the determination of the final valid schedule of a BS, are elaborated one after another. Simulation results show that the average throughput performance of the distributed scheduling algorithm can reach closely to the calculated maximum traffic demand of small-cell BSs (see chapter 5) in the tree-style mmWave backhaul network. Moreover, simulations are also conducted to show that the distributed algorithm is able to adapt to the dynamic traffic demand (with sharp changes) of BSs in the network as well.

6.2 Algorithm overview

The basic idea of the proposed algorithm is that in the relay-assisted mmWave backhaul network with a tree topology, every BS except the leaf small-cell BSs, makes scheduling decisions for all the logical links between the BS and its child BSs based on several types of information, including the traffic demand information, the queue length information, the final valid schedule received from its parent BS, and the set of local schedules received from its child BSs. All information is collected through monitoring the BS's own status and exchanging control messages between the BS and its one-hop neighbors via the handshaking

procedure introduced later.

The link scheduling happens on a per-subframe basis, and each subframe contains a fixed number of time slots with the same duration. Therefore, both the local schedule and the final valid schedule record the assignment of time slots to a set of logical links for each subframe. In the distributed scheduling algorithm, before a BS starts to calculate its final valid schedule for a subframe, it has to know its parent BS's final valid schedule for the same subframe in advance, because the schedule of the logical link between the BS and its parent BS is specified therein. This indicates a strong "happen-before" relationship in the calculation of final valid schedule. Since the calculation and propagation of the final valid schedules cannot complete instantly across the entire network, every BS calculates its final valid schedule for a specific subframe at least one subframe before the that subframe starts. Thus, in a tree topology, the BSs closer to the macro-cell BS will always make the scheduling decision for a future subframe earlier than those BSs farther away from the macro-cell BS. However, the calculation of local schedule does not need any information with a strict "happen-before" relationship. Therefore, a BS calculates its local schedule at the beginning of a subframe, and send it to its parent BS immediately after the calculation completes, so that the received local schedule can be used by the parent BS to calculate its final valid schedule within the same subframe. Details can be found in the section 6.4.1.

Moreover, in the calculation of both types of schedules, the local fairness is addressed, which means a BS assigns time resource to logical links proportionally to their traffic demand or queue lengths. This will be elaborated in later sections as well.

6.3 System settings

In a given relay-assisted mmWave backhaul network, there is one macro-cell BS M, a set of small-cell BSs $\mathcal{B} = \{B_1, B_2, ...\}$, and a set of mmWave relays. M, $\mathcal{B}$, and the set of logical links $\mathcal{L}$ between them together form a tree topology, where M is the root node of the tree.

A logical link $L_i \in \mathcal{L}$ ends at the BS B_i, and it is either a single-hop path or a multi-hop path going through several mmWave relays sequentially. Every physical link within a logical link is a LoS. Every logical link is "intra-path" interference-minimal, which means the mutual interference between the concurrent transmissions on the physical links within a logical link can be ignored. Based on our previous work, the optimal scheduling of a interference-minimal logical link can be computed. If a logical link L_j is attached to a BS B_i (i.e., L_j is between B_i and B_j), the physical link directly attached to B_i within L_j is named as l_{ji}. Therefore, the portion of time used by l_{ji} in the optimal schedule length of L_j is denoted as P_{ji}. The data rate of physical link l_{ji} is r_{ji}, which is a known system parameter.

It has to be clarified that the interference relationship between a pair of logical links in the backhaul network may vary according to the combination of their transmission directions in a downlink and uplink hybrid case. If there are x pairs of logical links that may interfere with each other, in total there could be 4^x different interference cases in the network, which introduces huge complexity to address them all. To address this issue, we assume that as long as two logical links with certain directions interfere with each other, they are considered always interfering with each other no matter which directions of their transmissions are. Under this assumption, despite that the throughput performance can not reach the optimal, we could first schedule both downlink and uplink traffic together, and then separate the traffic of different directions into different numbers of slots according to the traffic demand or queue length information.

The number of mmWave radio chains available on B_i or M is N_i^R or N_M^R, respectively. There are 2 control time slots followed by n_d data time slots in each subframe.

6.4 Main components of the distributed scheduling algorithm

In is section, we explain the distributed algorithm in details. The explanation focuses on three main components of the algorithm: the handshaking of control messages, the calcu-

lation of local schedule, and the determination of final valid schedule.

6.4.1 Handshaking of control messages

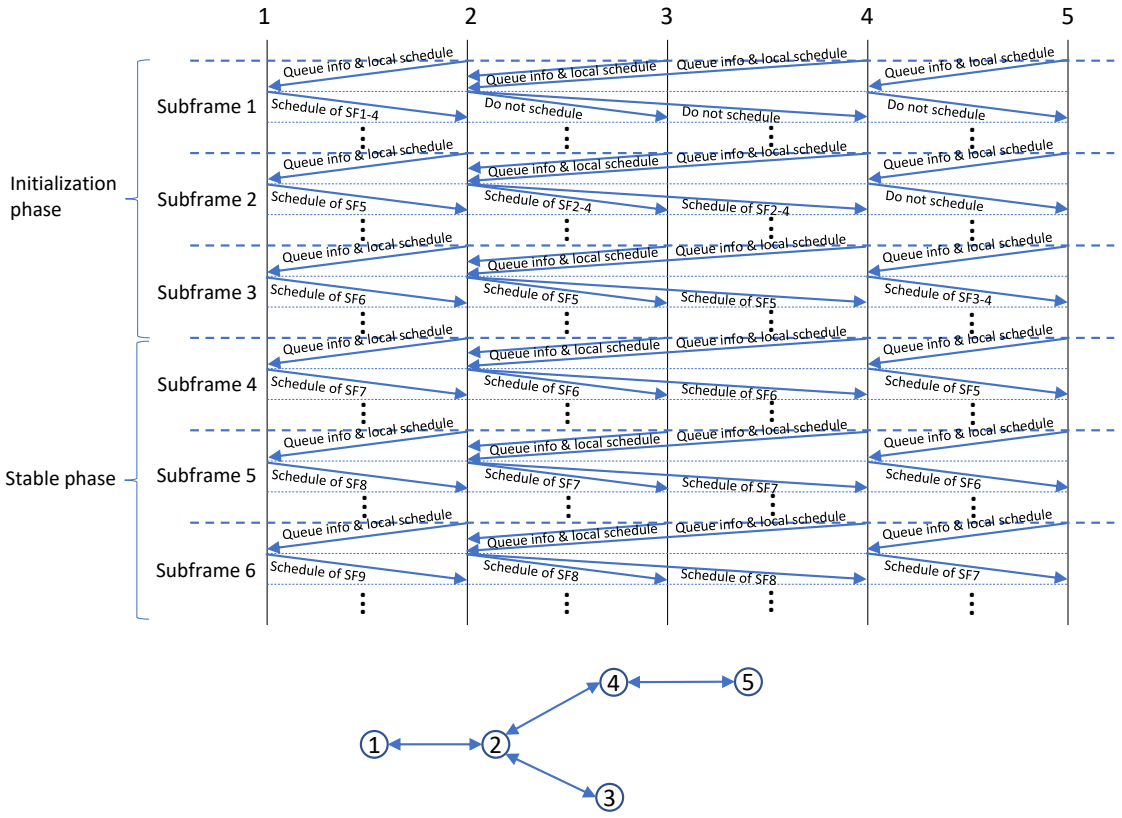

Figure 6.1: Hand-shaking procedure of the distributed scheduling algorithm

To elaborate the handshaking process, an example is provided in Figure 6.1. A small backhaul network with a tree topology is shown in the lower part of Figure 6.1, where BS 1 is the macro-cell BS, and BS 2-5 are all small-cell BSs.

It is noticed that some logical links between BSs are multi-hop relay paths. If control messages are sent through the multi-hop logical links, the delay of these control information will be too long. To address this issue, each BS is equipped with a communication module working at a lower frequency band (e.g., sub-6 Ghz band), which uses an omni-directional antenna. That communication module takes responsibility of transmitting and receiving control messages in the first two control slots of each subframe. To avoid the collision of

the control messages between a BS and its child BSs, each control slot is further partitioned into n_{sub} sub-slots, and each child BS is assigned a unique sub-slot to exchange control messages. The assignment of sub-slots between a BS and its child BSs happens in the initial configuration phase when the relay-assisted backhaul network is constructed. During the initial configuration phase, a child BS is associated with its parent BS to form the backhaul logical link.

As we can see in Figure 6.1, at the first slot of each subframe, each small-cell BS calculates its local schedule based on the traffic demand information, which will be explained in detail later. The calculated local schedule and updated queue and traffic demand information of a small-cell BS will be sent immediately to its parent BS. Note that, since there is no parent BS of the macro-cell BS, it will skip this step.

After a BS receives the control messages from its child BSs, before it starts the calculation of a final valid schedule for a specific future subframe, it checks whether the final valid schedule from its parent BS for the same future subframe has been received or not. If it has not been received, the BS will not schedule transmissions in that future subframe, because it does not know which slots are assigned to the logical link between itself and its parent BS. Any transmission from the BS may potentially conflict with the transmission from its parent BS. On the other hand, if the interested final valid schedule from the parent BS has been received, the BS will starts the calculation of its final valid schedule.

As shown in the example, each BS will start its scheduling in a specific subframe according to its height in the tree topology. If the topology has a depth of H, which is the height of the macro-cell BS and each small-cell BS B_i's height is denoted as h_i, the macro-cell BS will start its scheduling in subframe 1, while small-cell BS B_i will start its scheduling in subframe $(H - h_i + 1)$. Note that, because the schedule of leaf BSs is determined by their parent BSs, they do not calculate their final valid schedule.

Moreover, in the first scheduling subframe, each non-leaf BS will calculate its schedule of the next several subframes in advance (i.e., from subframe $H - h_i + 1$ to subframe H),

because when a child BS calculates its final valid schedule of a subframe, it has to know its parent BS's final valid schedule of the same subframe in advance; however, the schedule needs time to propagate to its child BSs. After the first scheduling subframe, each BS only needs to calculate the final valid schedule of the next unscheduled subframe. As depicted in Figure 6.1, the initialization phase lasts $H - 1$ subframe, and after that, the *stable phase* starts.

6.4.2 Calculate the local schedule of small-cell BSs

The purpose of calculating the local schedule on a small-cell BS B_i is to obtain the "desired" number of slots that B_i wants its parent BS B_i^p to assign for the data transmission on the logical link L_i between B_i and B_i^p. As a "desired" local optimal, it is calculated based on the local traffic demand information rather than the queue information.

Traffic demand information is an upper layer (i.e., application) statistics which is not typically used in the scheduling algorithm (i.e., MAC layer) in wireless ad hoc or mesh networks. However, in cellular networks starting from the 4G-LTE systems, the Quality-of-Service (QoS) has become a key performance metric. QoS related policies such as traffic classification and prioritization have already been installed in BSs. Application or service data rate of each user accessing to a BS, as a crucial QoS parameter, is constantly collected by the BS. In the 5G system, as a wider range of applications are going to be supported, even finer-grained management of QoS is expected to be implemented, which means more accurate traffic demand information is likely available at each BS [93]. In fact, the local schedule aims to provide a "desired" resource allocation requirement to the parent BS, the amount of which is usually much larger than the amount of resource that the parent BS can offer in a backhaul network with the heavy traffic load. From this point of view, a small estimation error on the traffic demand of each BS is acceptable. From the discussion in the above section 6.4.1, we know that each BS keeps updating its traffic demand information to its parent BS; thus, after a certain amount of time, BS B_i can obtain the accurate total

traffic demand D_j from its child BS $B_j \in \mathcal{B}_i^c$, where $\mathcal{B}_i^c$ is the set of child BSs of B_i. Note that, first, the traffic demand D_j of B_j is in fact the aggregated traffic demand of all small-cell BSs in the sub-tree rooted at B_j; second, as the proposed distributed algorithm schedules both uplink and downlink traffic, the traffic demand information contains both the downlink traffic demand and the uplink traffic demand information.

The local schedule of B_i indicates the number of slots assigned for the data transmissions (both uplink and downlink) on all physical links attached to B_i. We denote the number of slots assigned to the attached physical link within the logical link L_j as n_j. Note that, the demand may exceed the maximum throughput capacity of a BS; therefore, we use a local continuous scale variable S_i to indicate the fraction of traffic demand of each child BS actually being served at B_i in one subframe. From this perspective, our proposed distributed scheduling algorithm addresses the local fairness through proportionally schedule the data traffic according to the amount of the traffic demand of each child BS.

Based on the above system setting, we can formulate a mixed integer programming problem to address the calculation of the local scheduling on B_i, in which the local scale variable S_i is to be maximized. In Equation 6.1, continuous variable S_i is the optimization

objective, and integer variables $\{n_j |\ B_j \in B_i \bigcup \mathcal{B}_i^c\}$ are auxiliary variables.

$$
\begin{aligned}
\max \quad & S_i \\
\text{s.t.} \quad & n_i \cdot r_{ii} \geq S_i \cdot \sum_{B_j \in B_i \bigcup \mathcal{B}_i^c} D_j \\
& 0 \leq S_i \leq 1 \\
& n_j \cdot r_{ji} \geq S_i \cdot D_j,\ \forall\ B_j \in \mathcal{B}_i^c \\
& \frac{1}{P_{ji}} \leq \frac{n_j}{P_{ji}} \leq n_d,\ \text{if } D_j > 0,\ \forall\ B_j \in B_i \bigcup \mathcal{B}_i^c \\
& n_j = 0,\ \text{if } D_j = 0,\ \forall\ B_j \in B_i \bigcup \mathcal{B}_i^c \\
& \lceil \frac{n_j}{P_{ji}} \rceil + I_{jk} \cdot \lceil \frac{n_k}{P_{ki}} \rceil \leq n_d,\ \forall\ B_j, B_k \in B_i \bigcup \mathcal{B}_i^c \\
& \sum_{B_j \in B_i \bigcup \mathcal{B}_i^c} n_j \leq n_d \cdot N_i^R
\end{aligned}
\tag{6.1}
$$

As the distributed scheduling algorithm is expected to operate in the real relay-assisted mmWave backhaul system, in which every physical link has a length in the order of 200 m. Due to the use of high-gain highly-directional antennas, the data transmissions on these LoS physical links are likely to be able to use the highest level of modulation (e.g., 256 QAM) allowed in the system. Therefore, the physical link data rate is the same, and we denote the unified physical link data rate as r. Since the portion P_{ji} of the transmission on the physical link within the logical link L_j attached to B_i is either 1 (i.e., single-hop) or 0.5 (i.e., multi-hop), we define a new integer parameter $\alpha_{ji} = \frac{1}{P_{ji}}$, whose value is either 1 or 2. Therefore, we can update the above mixed integer programming problem into a mixed

integer linear programming problem.

$$
\begin{aligned}
\max \quad & S_i \\
\text{s.t.} \quad & n_i \cdot r \geq S_i \cdot \sum_{B_j \in B_i \bigcup \mathcal{B}_i^c} D_j \\
& 0 \leq S_i \leq 1 \\
& n_j \cdot r \geq S_i \cdot D_j, \ \forall \ B_j \in \mathcal{B}_i^c \\
& \alpha_{ji} \leq \alpha_{ji} \cdot n_j \leq n_d, \text{ if } D_j > 0, \ \forall \ B_j \in B_i \bigcup \mathcal{B}_i^c \\
& n_j = 0, \text{ if } D_j = 0, \ \forall \ B_j \in B_i \bigcup \mathcal{B}_i^c \\
& \alpha_{ji} \cdot n_j + I_{jk} \cdot \alpha_{ki} \cdot n_k \leq n_d, \ \forall \ B_j, B_k \in B_i \bigcup \mathcal{B}_i^c \\
& \sum_{B_j \in B_i \bigcup \mathcal{B}_i^c} n_j \leq n_d \cdot N_i^R
\end{aligned}
\tag{6.2}
$$

Since in the real system, $\mathcal{B}_i^c$ is a small set, n_d is a pre-set small integer, the known interference relationship matrix $\{I_{jk}\}$ is sparse, the computation time for solving this mixed integer linear programming problem is very short. After solving the problem, the maximum S_i is found, and correspondingly, we can calculate the minimum number of time slots $\widehat{n_i}$ to support the maximum achievable traffic demand for the physical link attached to B_i within L_i. $\widehat{n_i}$ is the key parameter of the local schedule, which will be transmitted to B_i's parent BS, as it indicates the maximum time slots that the parent BS shall allocate to the physical link within L_i. The parent BS could allocate more time slots to L_i; however, the extra traffic cannot be absorbed timely by B_i, as the total traffic on L_i exceeds the maximum achievable traffic demand of B_i.

In the real deployment of the distributed algorithm, since the traffic demand of each small-cell BS may be fluctuating within a small range in most of time or it changes gradually in a slow speed, the calculation of local schedule may fall into the trouble of tracking the demand change too sensitively, such that the final valid schedule may be changing too frequently as well. To address this issue, we modify the message exchange of local sched-

ule that the BS B_i only updates the value of $\widehat{n_i}$ to its parent BS when significant changes of $\widehat{n_i}$ happens. Specifically, B_i keeps recording the temporary $\widehat{n_i}$ value calculated in each subframe, and it applies a sliding window on the sequence of $\widehat{n_i}$ values to get the time-averaged value $\bar{\widehat{n_i}}$. When the difference between the current reporting $\widehat{n_i}$ value and the time-averaged value $\bar{\widehat{n_i}}$ is larger than a threshold of T percentage, the reporting $\widehat{n_i}$ value is updated to $\bar{\widehat{n_i}}$; otherwise the reporting value does not change. In our simulations, we choose a relatively large threshold (i.e., 50%), so that in a small backhaul network (e.g., 20 BSs), few small-cell BSs will experience sharp traffic demand change simultaneously.

6.4.3 Determine the final valid schedule of a BS

After a BS receives the queue, traffic and local schedule information from its child BSs, it will determine its schedule of a future subframe based on its height in the topology, as mentioned in the above section on hand-shaking. Different from the calculation of local schedule, the valid schedule is determined using not only the traffic demand information, but also the queue and local schedule information.

To realize the distributed algorithm, a non-leaf small-cell BS B_i has to maintain queues to store downlink and uplink packets, whose destinations are not B_i. We use $\mathcal{B}_i$ to denote the set of BSs located in the sub-tree rooted at B_i. For each small-cell BS $B_k \in \mathcal{B}_i$, B_i maintains a downlink queue and a uplink queue for it, which temporarily store all packets with the same destination BS as B_k and all packets to be routed to the macro-cell BS M with the same source BS as B_k, respectively. At the beginning of a subframe on B_i, the total number of packets to B_k in the corresponding downlink queue is $q_{i,k}^D$; while the total number of packets from B_k in the corresponding uplink queue is $q_{i,k}^U$.

However, the set of queue lengths actually used in the final valid schedule calculation are related to the routing, because we need to know the exact total number of uplink and downlink packets that wait to be transmitted on each logical link L_j between B_i and B_i's each child BS B_j. Therefore, at BS B_i, the total number of downlink packets waiting

to be transmitted on L_j is denoted as $Q^D_{i,j}$. Meanwhile, the uplink packets waiting to be transmitted on L_j are stored in the uplink queues at B_j, and the total number of them is denoted as Q^U_j.

$$\begin{aligned} Q^D_{i,j} &= \sum_{B_k \in \mathcal{B}_j} q^D_{i,k} \\ Q^U_j &= \sum_{B_k \in \mathcal{B}_j} q^U_{j,k} \end{aligned} \tag{6.3}$$

Based on Equation 6.3, the total number of uplink and downlink packet waiting to be transmitted on L_j is Q_j, and

$$Q_j = Q^D_{i,j} + Q^U_j \tag{6.4}$$

As mentioned in the "handshaking" procedure, at the first time slot of each subframe, the child BS B_j transmits the uplink queue information Q^U_j to its parent BS B_i, so that Q_j can be updated timely before the calculation of final schedule begins. Note that the queue maintenance on the macro-cell BS M and the leaf small-cell BS is similar to that on the small-cell BS, except that M does not have uplink queues and leaf small-cell BSs do not have downlink queues. There is no parent BS of the macro-cell BS and no child BS of the leaf small-cell BSs. The process of generating the valid schedule of a BS varies according to the type of that BS.

Macro-cell BS

To determine the final schedule at the macro-cell BS M, it has to first find out the maximum number of packets it can transmit to each child BS within a single subframe in the way local fairness is considered. Similar to the procedure of calculating the local schedule, we first

have to optimize the local scaling variable S_M,

$$
\begin{aligned}
\max \quad & S_M \\
\text{s.t.} \quad & n_j \cdot r \geq S_M \cdot \min\{Q_j, D_j\},\ \forall\ B_j \in \mathcal{B}_M^c \\
& 0 \leq S_M \leq 1 \\
& 1 \leq n_j \leq \widehat{n_j},\ \text{if } Q_j > 0,\ \forall\ B_j \in \mathcal{B}_M^c \\
& n_j = 0,\ \text{if } Q_j = 0,\ \forall\ B_j \in \mathcal{B}_M^c \\
& \alpha_j \cdot n_j + I_{jk} \cdot \alpha_k \cdot n_k \leq n_d,\ \forall\ B_j, B_k \in \mathcal{B}_M^c \\
& \sum_{B_j \in \mathcal{B}_M^c} n_j \leq n_d \cdot N_M^R
\end{aligned}
\tag{6.5}
$$

In Equation 6.5, the first constraint guarantees that a logical link L_j attached to the macro-cell BS will be allocated a certain number of slots so that $S_M \cdot Q_j$ packets in the queue of L_j can be transmitted in the scheduled subframe, where Q_j is the total number of packets in both uplink and downlink queues of L_j, while $\mathcal{B}_M^c$ is the set of child small-cell BSs of the macro-cell BS M. The third constraint indicates that for a logical link with non-empty queue, at least 1 time slot will be assigned to it, and the macro-cell BS will not assign more than $\widehat{n_j}$ to L_j, as this value is from the local schedule of B_j, which is considered as the maximum number of slots scheduled for L_j expected by B_j. The fourth constraint is the "logical link interference constraint" that is similar to the one discussed in section 5.3.1 case 3. The last constraint is the "radio chain constraint" explained in section 5.3.1 case 2.

Non-leaf small-cell BS

As for a non-leaf small-cell BS B_i, its valid schedule of a subframe is calculated upon the received valid schedule of its parent BS, the received local schedule and uplink queue information of its child BSs, and its own downlink queue information. Similar to the case of macro-cell BS, the non-leaf small-cell BS also has to first maximize the local variable

S_i as well,

$$
\begin{aligned}
\max \quad & S_i \\
\text{s.t.} \quad & n_j \cdot r \geq S_i \cdot \min\{Q_j, D_j\},\ \forall\ B_j \in \mathcal{B}_i^c \\
& 0 \leq S_i \leq 1 \\
& 1 \leq n_j \leq \widehat{n}_j,\ \text{if } Q_j > 0,\ \forall\ B_j \in \mathcal{B}_i^c \\
& n_j = 0,\ \text{if } Q_j = 0,\ \forall\ B_j \in \mathcal{B}_i^c \\
& I_{ik} \cdot \alpha_k \cdot n_k \leq n_d - \alpha_i \cdot \widetilde{n}_i,\ \forall\ B_k \in \mathcal{B}_i^c \\
& \alpha_j \cdot n_j + I_{jk} \cdot \alpha_k \cdot n_k \leq n_d,\ \forall\ B_j, B_k \in \mathcal{B}_i^c \\
& \sum_{B_j \in \mathcal{B}_i^c} n_j \leq n_d \cdot N_M^R - \widetilde{n}_i
\end{aligned}
\tag{6.6}
$$

where $\widetilde{n}_i$ is the number of slots scheduled for the physical link within L_i attached to B_i, which is a known information for B_i, because it is determined and sent to B_i by its parent BS before the calculation occurs. All the constraints are similar to the ones in the macro-cell BS case above, except that the total number of available time slots should subtract the ones (i.e., $\widetilde{n}_i$) already assigned to L_i.

Leaf small-cell BS

As leaf BSs do not have child BSs, their valid schedule is determined by their parent non-leaf BSs.

After obtaining the maximum S_i or S_M, the number of slots assigned to a logical link L_j attached to a BS B_i or M can be calculated. Based on the ratio between $Q_{i,j}^D$ and Q_j^U, we can determine the number of slots for downlink and uplink traffic transmissions on L_j, respectively. A similar scheduling procedure as the Algorithm 5 described in the section 5.4 can be used to actually schedule the set of slots assigned to each logical link within each subframe.

Moreover, we have to figure out how to fill packets into each slot when the schedule

is executed. Based on the slot allocation, B_i (i.e., the parent of B_j) can get the maximum numbers of downlink packets $N_j^{P,D}$ and B_j can get the maximum number of uplink packets $N_j^{P,U}$ allowed to be transmitted on L_i within a subframe. Then, B_i selects the downlink packets from different queues proportionally according to $\{q_{i,k}^D\}$, and B_j selects the uplink packets from different queues proportionally according to $\{q_{j,k}^U\}$.

6.5 Numerical results and analysis

6.5.1 The throughput performance of distributed scheduling algorithm

In this section, simulations are conducted to evaluate the throughput performance of the proposed distributed scheduling algorithm. In the simulations, the physical link data rate is set to 13.3 Gbps as discussed in section 6.4.2. There are in total 24 slots within a subframe which lasts for 0.1 ms, and the first two slots of each subframe is reserved to implement the operation of handshaking procedure described in section 6.4.1. The rest 22 slots are data slots which can be used to transmit both uplink and downlink data traffic. All backhaul topologies used in the simulations are generated using the spanning-tree algorithm introduced in the section 4.3.

Figure 6.2 shows the throughput performance of the distributed algorithm in different network settings (i.e., the interference condition and the number of radio chains available on each BS) under different traffic loads from 0.67 Gbps to 3.33 Gbps at each small-cell BS. Note that, all the simulated throughput values are averaged across 50 sets of individual simulations in each scenario. In each simulation, the ratio between the uplink and downlink input traffic demand of a small-cell BS is 1:2, and each small-cell BS has the same traffic demand. Each individual simulation runs for 1000 subframes. In Figure 6.2, we can see that the throughput performance of the "MI-ER" scenario (i.e., interference-minimal and enough radio chains available) is much better than that of the "LI-LR (2)" scenario (i.e., interference exists between a few pairs of logical links, and 2 radio chains on the macro-cell BS while 1 radio chain on each small-cell BS). This is because the maximum traffic

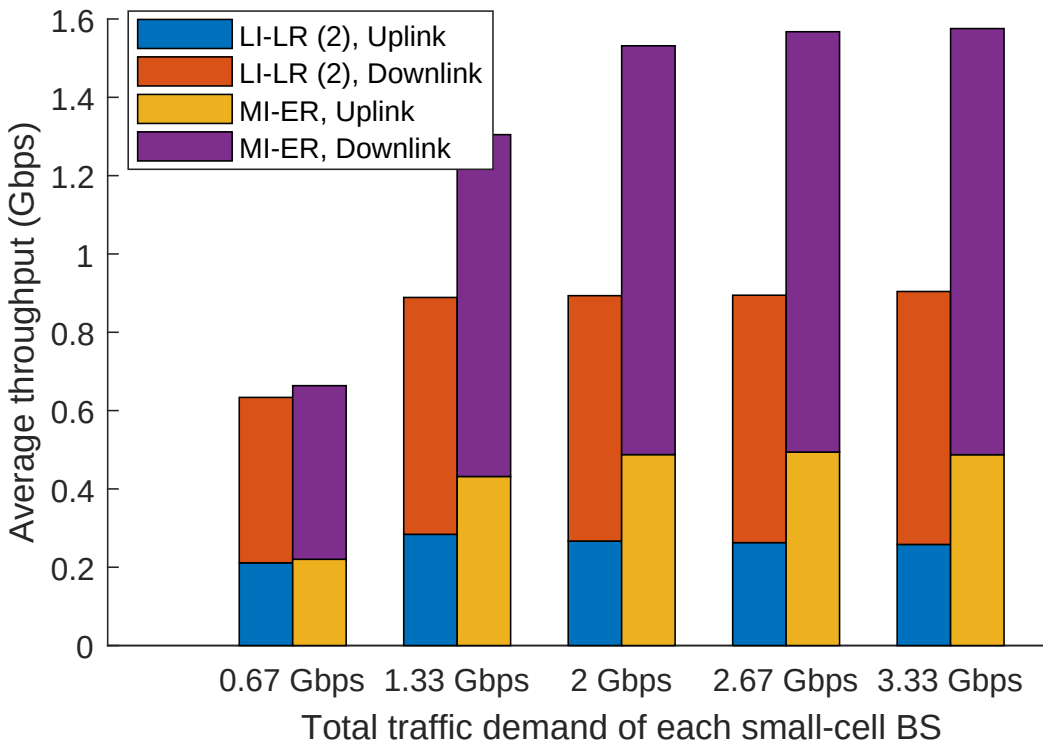

Figure 6.2: Throughput performance of distributed scheduling algorithm

demand achievable of each small-cell BS in the "MI-ER" case is much higher than that of the "LI-LR (2)" case. In fact, using the updated link capacity and $\{p_i^f\}$ values, we can get the updated maximum traffic demand of each small-cell BS in the "MI-ER" case as 1.64 Gbps in average; while the value of the "LI-LR (2)" case is 0.94 Gbps. Both of these two values are also depicted in Figure 5.3. As Figure 6.2 shows, the maximum throughput values in the simulation are close to the calculated maximum traffic demand values in both scenarios, which means the distributed algorithm can schedule the transmissions efficiently in the mmWave backhaul networks.

6.5.2 Enhance the aggregated throughput achieved using the distributed algorithm

It is noticed that the determination of the final valid schedule on BSs strictly follows the idea of scheduling the backhaul traffic proportionally according to the queue length of each flow bounded by the traffic demand of each corresponding small-cell BS. Although it addresses the fairness issue, the utilization of the network resource could be low when

there exist several bottleneck routes in the backhaul network. On those bottleneck routes, if the aggregated traffic demand is much larger than the network capacity of the routes, it leads to very small values of the optimized scaling variable S. As the local S_M value is applied to all routes in the network at the macro-cell BS, a very small S_M will limit the amount of traffic transferred on those non-bottleneck routes, where plenty unused network resource may exist.

To improve the low network resource utilization and increase the network aggregated throughput, we add a step in the determination of the final valid schedule after the optimization of S_M at the macro-cell BS. In this new step, the optimized $\widehat{S_M}$ is used to bound smallest amount of traffic demand of each small-cell BS that has to be serve in a subframe. In Equation 6.7, we can see that the new optimization objective is to maximize the number of data slots used in one subframe.

$$
\begin{aligned}
\max \quad & \sum_{B_j \in \mathcal{B}_M^c} n_j \\
\text{s.t.} \quad & n_j \cdot r \geq \widehat{S_M} \cdot \min\{Q_j, D_j\},\ \forall\ B_j \in \mathcal{B}_M^c \\
& 1 \leq n_j \leq \widehat{n_j},\ \text{if } Q_j > 0,\ \forall\ B_j \in \mathcal{B}_M^c \\
& n_j = 0,\ \text{if } Q_j = 0,\ \forall\ B_j \in \mathcal{B}_M^c \\
& \alpha_j \cdot n_j + I_{jk} \cdot \alpha_k \cdot n_k \leq n_d,\ \forall\ B_j, B_k \in \mathcal{B}_M^c \\
& \sum_{B_j \in \mathcal{B}_M^c} n_j \leq n_d \cdot N_M^R
\end{aligned}
\tag{6.7}
$$

We conduct simulations to compare the aggregated throughput achieved by using the modified distributed scheduling algorithm and the maximized aggregated traffic demand at the macro-cell BS that can be supported by the backhaul network, which is obtained in Chapter 5. In our distributed scheduling simulations, the traffic demand of each small-cell BS is set as 3.33 Gbps, and the aggregated traffic demand surpasses the network capacity. As we can see in Figure 6.3, in both MIER and LILR(2) scenarios, the aggregated through-

put achieved using the modified algorithm is close to the maximized traffic demand that can be supported by the backhaul network. It shows that our proposed algorithm can schedule the backhaul traffic efficiently.

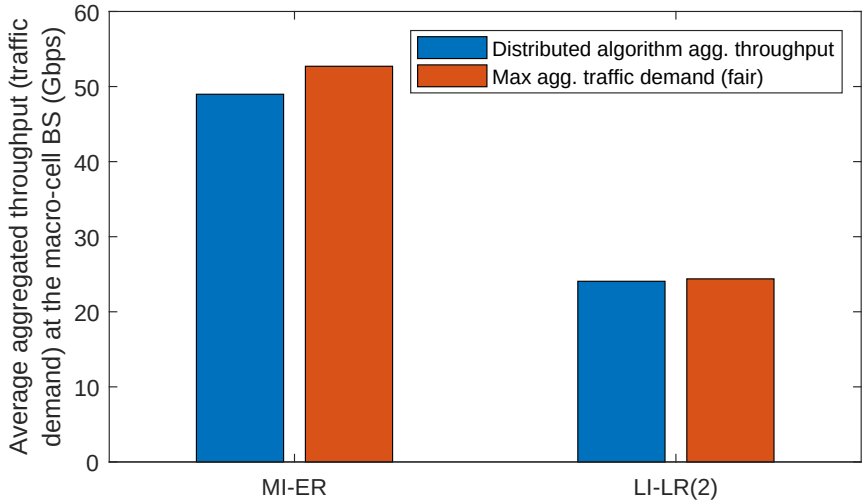

Figure 6.3: Comparison between the aggregated throughput achieved using the distributed algorithm and the maximized aggregated traffic demand

Moreover, as the input traffic demand is the same on each small-cell BS, we also calculate the Jain's fairness index of the set of throughput values of all small-cell BSs obtained in the distributed scheduling simulation. Figure 6.4 shows that our algorithm can provide better fairness than the case in the theoretical analysis in Chapter 5 can. Because in Chapter 5, the optimization does not address the fairness issue in the allocation of the extra to be supported traffic demand among small-cell BSs. In the solution to the optimization problem obtained in the theoretical analysis, usually the extra traffic demand is allocated to only a few BSs, which leads to an unfair situation. In contrary, using our distributed algorithm, the extra traffic demand is allocated locally fairly due to the procedure of determining final valid schedule at small-cell BSs.

6.5.3 Track the dynamic traffic demand of a small-cell BS

In the practical backhaul system, the traffic demand of each small-cell BS may be fluctuating within a small range in most of the time or it changes gradually with a slow speed;

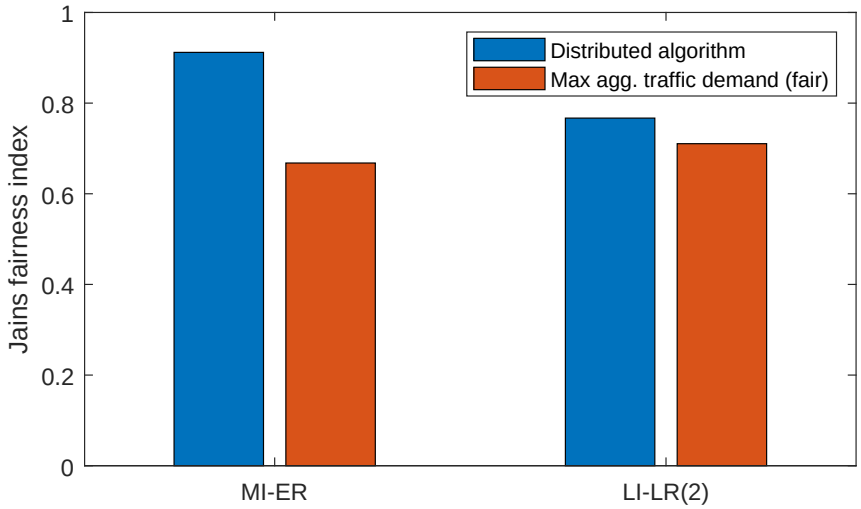

Figure 6.4: Comparison on the achieved fairness index values between applying the distributed algorithm and maximizing the aggregated traffic demand

therefore, during a relatively long period of time, only a few BSs are likely to experience sharp traffic demand change. In this simulation, we aim to explore the feature of our proposed distributed scheduling algorithm on tracking the dynamic traffic demand (with sharp demand change) of a small-cell BS in the backhaul network. The topology used in the simulation is shown in Figure 6.5, where the targeting BS is marked as B^*. In the simulation,

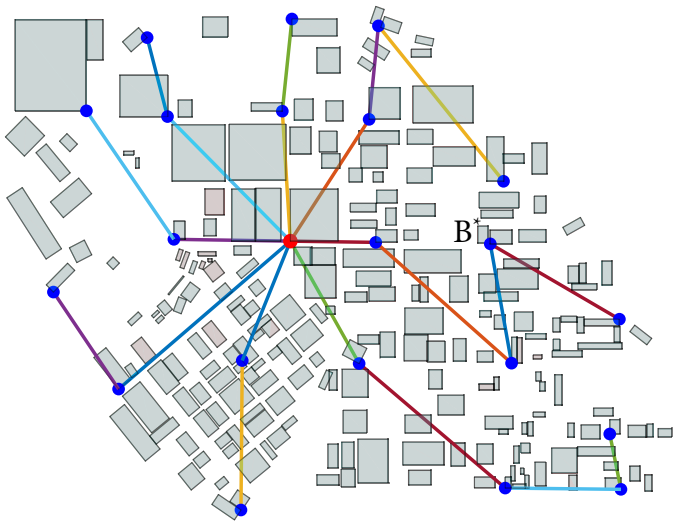

Figure 6.5: Backhaul topology (logical links) used in the simulation

the traffic demand of all small-cell BSs is initialized as 0.67 Gbps for downlink and 0.33

Gbps for uplink. When time arrives at the 250-th subframe, the downlink traffic demand of B^* is doubled to 1.34 Gbps; while its uplink traffic demand is unchanged until the 400-th subframe. Starting from the 400-th subframe, the uplink traffic demand of B^* is doubled. The downlink and uplink traffic demands of B^* are set back to their initial values at the 600-th and 750-th subframe, respectively.

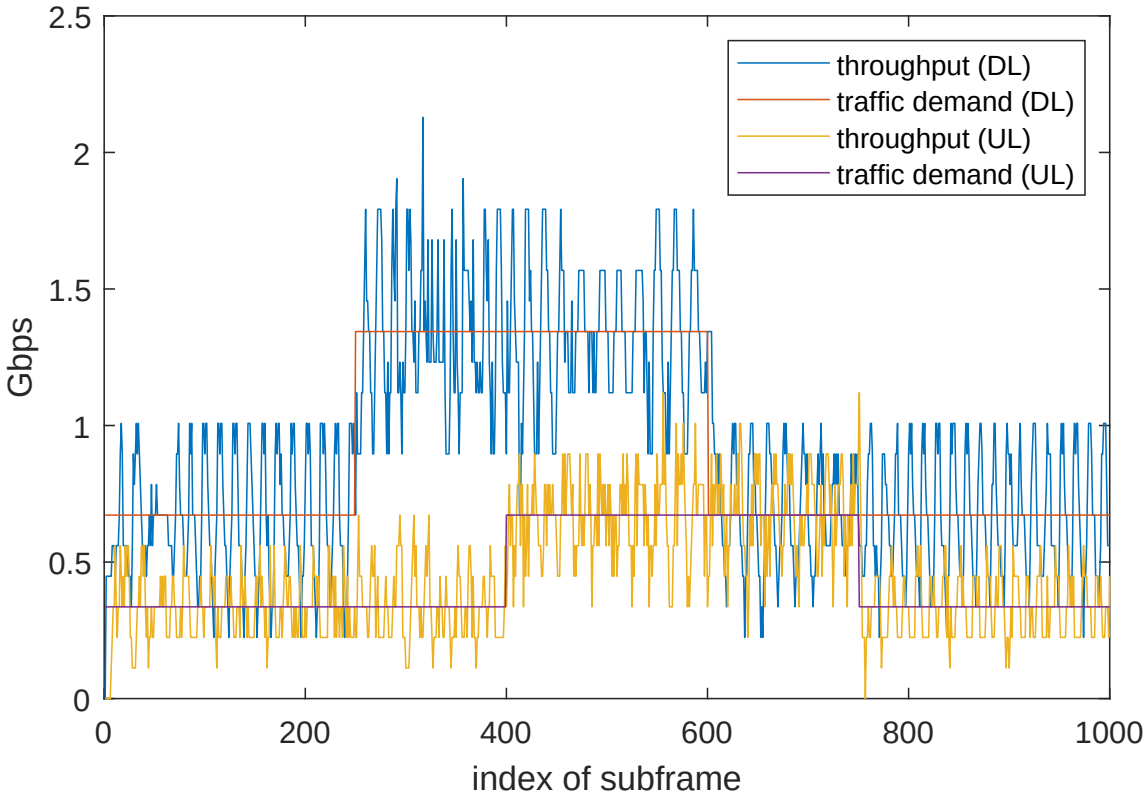

Figure 6.6: Dynamic throughput within each subframe at a BS

Figure 6.6 shows the dynamic throughput within each subframe of B^*. From the figure, we can see that the proposed distributed scheduling algorithm can track the sharp traffic demand change quickly and accurately. In fact, when the downlink traffic demand doubles, it takes 8 subframes for the instantaneous downlink throughput to jump to the new stage; while it takes 13 subframes for the instantaneous downlink throughput to drop back to the old stage, after the downlink traffic demand sets back to the original value. Correspondingly, the two values of number of subframes used to track the uplink traffic demand

changes are 4 and 8. The selected BS has a height of 4 in the topology. In the downlink traffic demand change case, the traffic demand change has to first propagate to the macro-cell BS to increase the "desired" time slots for the logical links in the route. After that, more packets can be transferred to the targeting BS. However, in the uplink case, the increased uplink traffic flows together with the "traffic increasing" message to the macro-cell BS, which is a one-way trip intuitively. When the traffic demand drops, it takes a bit longer time for the throughput to drop, because the packets from the heavy traffic queued in the intermediate BSs need time to be absorbed by B^*.

6.6 Chapter summary

In this chapter, a novel distributed scheduling algorithm is created, which aims to efficiently schedule both the uplink and downlink backhaul traffic in the mmWave backhaul network with a tree topology. The handshaking of control messages, calculation of local schedules, and the determination of final valid schedule are all discussed. Simulation results show that the performance of the distributed algorithm can reach very close to the aforementioned maximum traffic demand of the backhaul network, and it can also adapt to the dynamic traffic with sharp traffic demand change of small-cell BSs quickly and accurately.

CHAPTER 7
OPTIMIZING MMWAVE BACKHAUL NETWORKS IN ROADSIDE ENVIRONMENTS

7.1 Introduction

The demand for high-speed wireless communications in vehicles, e.g. video streaming for the entertainment of vehicle passengers, is rapidly increasing. Given the small cells that will be used in 5G and increased demand from vehicles, it is very likely that many base stations (BSs) will need to be placed very close to roadways, e.g. highways. This will be true in heavily trafficked road sections even outside of major urban areas. Connecting fiber backhaul networks to such roadside networks will be costly and difficult, and therefore it is expected that wireless backhaul networks will be used in segments to connect to a limited number of network nodes having fiber connections. mmWave communication is the most attractive candidate for wireless backhaul due to its ability to support very high data rates.

Note that, in the dense urban environment, interference between different mmWave links is almost completely eliminated due to the presence of many large obstacles [54]. In more wide open areas, such as along roadsides or in rural areas,[1] interference is not limited by obstacles and must be taken into account when designing the backhaul network. Even though the interference footprint is reduced due to the use of narrow beamwidth directional antennas, concurrent transmissions of multiple links along a network path may cause mutual interference, because the beam directions of all antennas are close to the road direction. We show later that, without specific arrangement and coordination, mutual interference greatly reduces link capacity in this setting.

In this chapter, we investigate the design of interference-minimal and throughput-optimal

[1] Some of the work described in this chapter could be useful in rural backhaul deployments also. However, in the remainder of the chapter, we focus solely on roadside network deployments.

mmWave backhaul topologies that can be deployed along a roadside, e.g. by mounting nodes on regularly-spaced lampposts that are already present on most roads and highways. We propose and analyze the triangular-wave topology, which is a regular topology well-suited for this problem setting. We first derive the conditions necessary for the triangular-wave topology to produce interference-minimal transmissions that can be easily and optimally scheduled. For a given antenna beamwidth, we also derive conditions on the height and spacing of lampposts that are necessary to support an interference-minimal triangular-wave topology and show that, if these conditions are satisfied, the topology is throughput optimal. We also investigate how well the proposed topology performs using actual lamppost positions taken from a 12 km stretch of highway in Atlanta using Google Earth. The results show that the proposed topology can achieve network throughputs very close to the ideal case and can support backhaul throughputs of 10+ Gbps in real roadside scenarios.

7.2 Relay-assisted mmWave backhaul on roadsides

In the 5G era, mmWave small cell BSs will be deployed along roads and highways to provide ultra high speed data service for communications with vehicles. mmWave small cells in dense urban environments can only sustain a radius of around 100 meters due to the presence of many obstacles. However, in a roadside deployment, a mmWave small cell BS should be able to easily support a radius of at least 500 meters, because of the relatively obstacle-free environment. This means a BS separation of 1 km is sufficient to provide full coverage to the roadway and the length of a self-backhaul link will then be about 1 km. In Fig. 7.1, we can see that a mmWave link with 1 km length at 60 GHz can reach a capacity of around 0.9 Gbps[2].

We assume that the relationship between SNR and link capacity obeys the well-known Shannon equation,

$$C = B \log_2(1 + \min\{\mathrm{SNR}, T_{max}\}) \ , \tag{7.1}$$

[2]The detailed simulation setting can be found in Section 7.4.

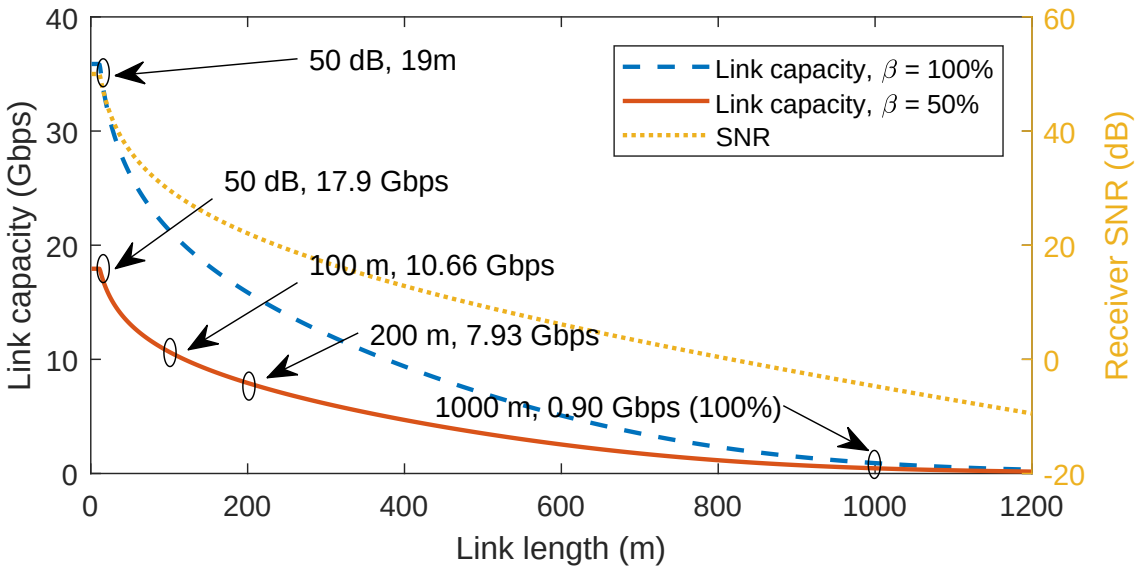

Figure 7.1: mmWave link capacity against link length.

where C is the link capacity, B is bandwidth, SNR is the signal-to-noise ratio, and T_{max} (e.g., 50 dB) is the SNR that produces the link's maximum rate. In practice, capacity cannot be increased without limit and this is captured by T_{max}.

As mentioned above, mmWave small cell BSs are expected to be deployed about every 1 km along a roadway. Moreover, considering the cost of running fiber to small cell BSs, having a separation of around 10-20 km between anchored-BSs (A-BSs) that are wire-connected to the broader network is a reasonable assumption. We also assume that a single mmWave node cannot transmit and receive at the same time, commonly referred to as the *primary interference constraint*. Define the *link utility ratio* β as the percentage of time that a link is active out of the total time. Due to the primary constraint, backhaul links have a utility ratio of 50% intuitively, which means it halves the average throughput of a backhaul link (see Fig. 7.1). To deal with the high path loss in mmWave band, we assume that two high-gain directional antennas with narrow beam width are equipped, and one is used to transmit, while the other is used to receive.

7.2.1 mmWave backhaul in a "straight-line" topology

A segment of a roadside mmWave backhaul network is shown in Fig. 7.2 with small cell BSs mounted on the tops of lampposts. Lamppost mounting provides easy access to power, good access tier coverage for vehicles on the road, and ease of deployment. Adjacent BSs are connected by mmWave backhaul links (shown in red), which use beamforming to achieve signal directionality. The left-most BS, also shown in red, has a fiber connection to the Internet, thus it is an A-BS. Fig. 7.2 shows one simple traffic pattern in the backhaul network, where data is disseminated from left to right (i.e., from B_0 to B_1 ... B_{10}), or data is aggregated from right to left. All data is consumed/generated by vehicles on the road and the access tier links operate on a different frequency from the backhaul links. Obviously, the left-most backhaul link (B_0, B_1) has the largest traffic load of about 10 Gbps.

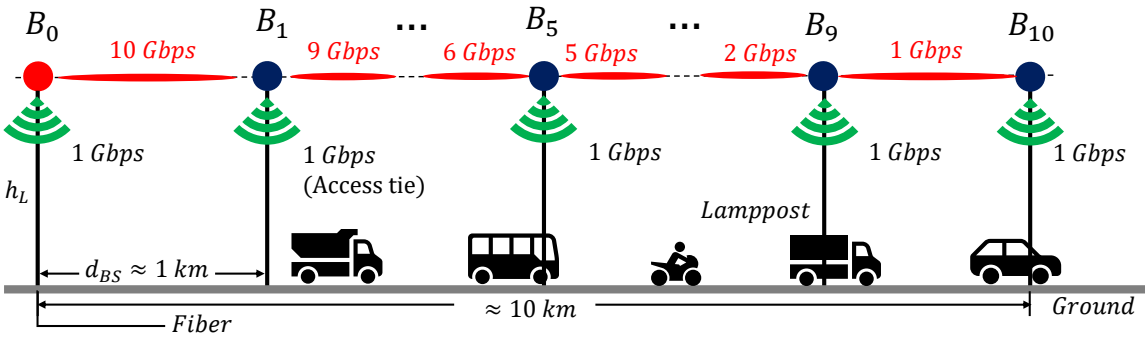

Figure 7.2: A segment of mmWave backhaul network along the highway.

The "straight-line" topology for *self-backhaul* is simple but it has two fatal issues preventing it from achieving high throughput. First, the link length is around 1 km which is too long to support more than 1 Gbps traffic as shown in Fig. 7.1. Second, the signal directions for the antennas on a sequence of BSs are colinear, which will cause severe mutual interference leading to poor system throughput when concurrent transmissions occur on multiple links. In [42], all backhaul links use orthogonal frequency bands to get rid of mutual interference in a street canyon scenario, however the system can only support 4 hops with the access tier data rate at 1 Gbps and hop distance at 200m for each hop. The system capacity

is limited to 3-4 Gbps, because it does not fully use the frequency resource. We introduce relays to the backhaul network and show that, through optimizing the relay placement and scheduling, both issues are resolved and a 10+ Gbps throughput objective can be met.

7.2.2 "Triangular-wave" topology for relay-aided backhaul

As mentioned above, deploying relays can resolve the two issues impeding the performance of straight-line networks without relays. With relays in between BSs, the length of each hop shrinks, which results in a higher single hop data rate. However, the introduction of relays raises two new issues: how to place relays and how to schedule the transmissions of relay links. If relays are still mounted on the top of lampposts following the "straight-line" topology, the backhaul network performance will still be poor due to the mutual interference. To eliminate mutual interference, we propose to deploy relays using a "triangular-wave" topology, as shown in either Fig. 7.3 or Fig. 7.4. In Fig. 7.3, all BSs and relays are deployed on the same side of the road in case the road only has lampposts on one side or in the median. If lampposts are present on both sides of a road, we can deploy relays according to Fig. 7.4.

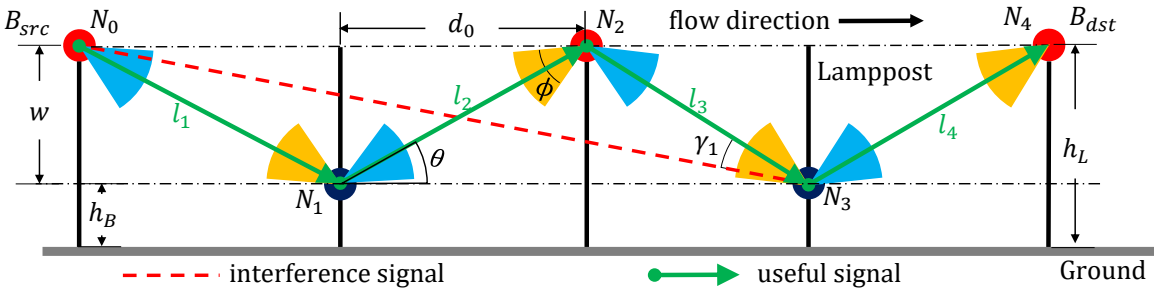

Figure 7.3: A segment of relay-aided mmWave backhaul (One side).

In the "one-side" case, BSs are mounted on the top of lampposts with a height denoted by h_L. The BS on the left-most lamppost is the source node, denoted as B_{src} (also as N_0 in Fig. 7.3). As shown in Fig. 7.3, the separation between consecutive lampposts that host a relay is d_0. A destination BS, denoted as B_{dst} (also as N_5), is mounted on the top of the right-most lamppost. The first relay N_1 to the right of B_{src} is mounted at a specific height

denoted as h_B where $h_B < h_L$. The next relay along the road N_2 is mounted on the top of the lamppost which is d_0 away from the lamppost hosting N_1. From N_1, every $2d_0$ there is one relay deployed at height h_B, while from N_2, every $2d_0$ there is one relay mounted at height h_L, and this forms the so called "triangular wave" topology. Fig. 7.3 shows an example of 3 relays deployed between two adjacent BSs along the road. It is expected that in the "one-side" case, an odd number of relays are deployed between two adjacent BSs. When an even number of relays have to be deployed, an extra relay deployed at the height h_B on the same lamppost where B_{dst} is mounted could help to maintain the consistency of the triangular wave topology with a fiber connection established between B_{dst} and the extra relay. Due to the limited length of this paper and the similarity of analysis on both cases, we focus on the "one-side" case later on.

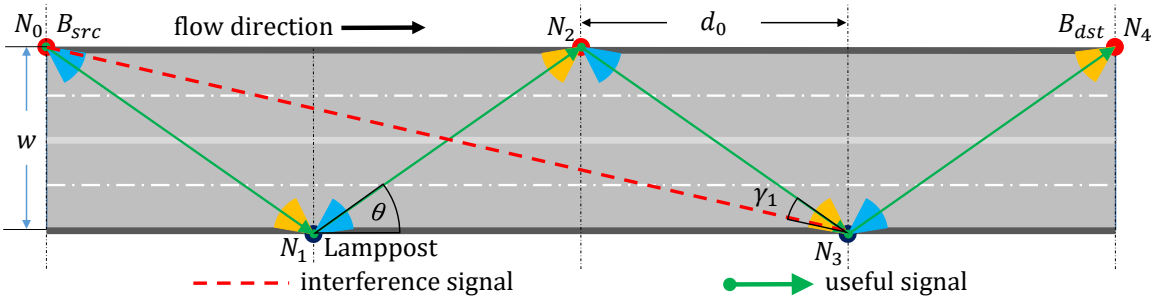

Figure 7.4: A segment of relay-aided mmWave backhaul (Two sides).

Note that, due to the static nature of the backhaul network, when wireless nodes are deployed, the beams of two adjacent nodes connected by a link are assumed to be aligned perfectly. The blue and orange beams represent transmit and receive beams respectively, and the beamwidth is denoted by ϕ. The angle θ depicted in the figures, e.g., $N_3\widehat{N_1}N_2$, is referred to as the angle of elevation. d_0 and θ together determine the triangular-wave topology. We also refer to the even nodes as Group_0 nodes and the odd nodes as Group_1 nodes.

7.2.3 Different cases of mutual interference

The following analysis adopts the *flat-top* antenna model, in which the measured antenna gain $G(\alpha)$ is shown in Eq. 7.2, where α is the angle to the antenna boresight, $G_h \gg G_l$.

$$G(\alpha) = \begin{cases} G_h & \text{if } \alpha < \frac{\phi}{2} \\ G_l & \text{if } \alpha \geq \frac{\phi}{2} \end{cases} \tag{7.2}$$

Fig. 7.5 shows three different interference cases due to the possible position relationship between the intended link and the interfering link: (a) depicts the most interference case where the interference signal experiences G_h at both Tx_1 and Rx_2. In (b), the antenna gains on interference signal are G_h and G_l, while in (c), both gains are G_l. If we assume the intended link length is 100 meters, an interferer is 300 meters away from the intended receiver, and $\beta = 50\%$, the achieved link rates are 0.72 Gbps, 6.91 Gbps, and 10.55 Gbps in case (a-c) respectively. Since in case (c), the amount of interference is smaller than the noise level, it is regarded as *interference-minimal*. The next subsection discusses the conditions under which the proposed triangular-wave topology can produce the interference-minimal case for all concurrently active links.

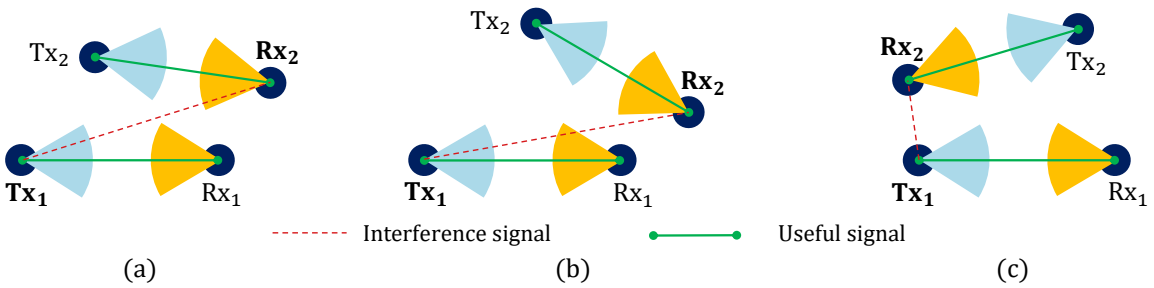

Figure 7.5: Three different interference cases of two mmWave links.

7.2.4 "Interference-minimal" condition for triangular-wave topology

As the angle θ decreases, the triangular-wave topology gets closer to the straight-line topology, which is more likely to encounter mutual interference. Also, when the beam width ϕ becomes smaller, it is more likely to generate an interference-minimal case given a fixed θ. Thus, it is intuitive to think that the conditions that enable interference-minimal communication in the triangular-wave topology are dependent on θ and ϕ.

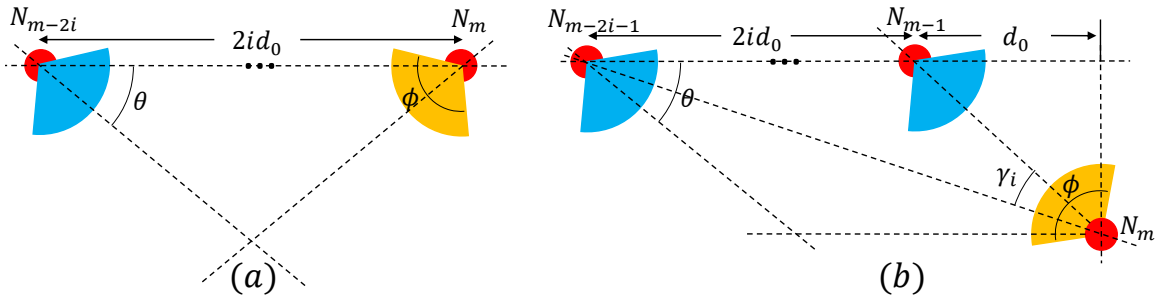

Figure 7.6: Interfering (a) within the same group; (b) across different groups.

As mentioned above, the nodes deployed in a mmWave backhaul with a triangular-wave topology can be partitioned into two groups (i.e., Group_0 and Group_1). Consider a node N_m ($3 \leq m \leq n$), as the receiving node of an intended link, where n is the total number of nodes in the backhaul network. The position relationship between the potential interferer node to N_m is depicted in Fig. 7.6. Fig. 7.6 (a) shows the case where interferer N_{m-2i} ($m > 2i > 0$) comes from the same group as N_m. It is obvious that as long as $\theta < 0.5\phi$, N_{m-2i}'s transmission interferes with the reception of N_m. Fig. 7.6 (b) depicts the scenario where interferer N_{m-2i-1} ($m > 2i+1 > 0$) and receiver N_m are in different groups. If $\frac{\phi}{2} \leq \gamma_i$, N_{m-2i-1} does not interfere with N_m. Thus, the interference-minimal condition for the triangular-wave topology can be expressed as:

Theorem 2. The condition for an interference-minimal scenario in the triangular-wave topology is

$$\gamma_1 = \theta - \arctan\left(\frac{\tan\theta}{3}\right) \geq \frac{\phi}{2} \tag{7.3}$$

Proof. It is obvious that the first three nodes from the source end in the network will be interference minimal due to the primary constraint. As for the other nodes N_m, when $\theta < 90^o$, γ_i can be found as $\theta - \arctan\left(\frac{\tan\theta}{2i+1}\right)$, which monotonically increases as i increases. Thus, $\gamma_i > \gamma_1, i = 2, 3, \ldots$, which means as long as Eq. 7.3 is satisfied, the nodes from different group will not interfere with N_m. In addition, since $\theta > \gamma_i$ is always true, the nodes from the same group of N_m will not interfere N_m as well. Since the analysis can be applied to any node N_m in the network, Eq. 7.3 ensures that a receiver will not be interfered by any other node in the network. □

Note that in the proof, we do not consider the potential interference caused by one-time reflections off the ground, because the potential reflected interference is controlled through optimal scheduling and topology design. Specifically, for the case shown in Fig. 7.6 (a), our optimal scheduling presented next will prevent the depicted transmitter and receiver from being active in the same time slot. For the case in Fig. 7.6 (b), since the receiving antenna of N_m is pointing up, the possible interference from a ground-reflected signal corresponds to the "single-gain" case as shown in Fig. 7.5 (b). However, due to to the large reflection attenuation of mmWave signals (about 15 dB [65]), which is quite close to the antenna gain (e.g., 21.87 dBi in our simulation), the interference strength is close to the interference-minimal case (i.e., the interference level is smaller than the noise level). Thus the interference can still be ignored.

7.2.5 Optimal scheduling for triangular-wave topology

Due to the introduction of relays that produce multi-hop transmissions between consecutive BSs in the mmWave backhaul, link scheduling must be considered. We refer to the multi-hop path between a pair of BSs as a relay path. We assume that relay paths operate in TDMA fashion so that their performance can be maximized. We also assume that traffic flows in only one direction at a time across a given relay path.

If the relationship in Theorem 2 stands, a triangular wave deployment of mmWave

backhaul is free-of-interference (i.e., interference is way smaller than the noise level). If thermal noise is considered and every node uses the same transmit power, the SNR value at every receiver is equal. Thus, the rates of all links are identical based on Eq. 7.1, and we denote that rate by R_{max}. We refer to the following schedule as the *"by-2" schedule*. There are two time slots of equal length in the schedule. In time slot 0, all even-numbered nodes transmit and in time slot 1, all odd-numbered nodes transmit.

Theorem 3. For interference-minimal triangular-wave topologies, the "by-2" schedule is optimal with a throughput of $R_{max}/2$.

The proof is simple, and to save space we leave the details to the journal version of this work.

We will see in Section 7.4 that, given a typical highway scenario and with narrow beamforming ($\phi \leq 15^o$), the throughput of a relay path can exceed 10 Gbps, which satisfies the requirement of backhaul in the highway scenario for future 5G networks. In the next section, we show that the triangular-wave topology is throughput-optimal under certain conditions.

7.3 Optimality of triangular-wave topology

The triangular-wave topology has several advantages due to its symmetric deployment of relays and BSs along the highway. The links are the same length and, therefore, assuming the propagation environment is consistent along the road, the analysis of each link is identical, thereby reducing network analysis complexity. The symmetric and homogeneous properties allow the analysis to be extended to any length of topology in a straightforward way. It also allows several virtual BS-to-BS long links to directly cascade together without mutual interference between them, which eases the network deployment. With symmetry, the analysis of the single-directional flow case can be easily applied to the reverse direction. It eases analysis of bi-directional flows (e.g., assigning time slots to the links in each direction by TDMA).

In addition to these practical advantages, it is possible to show that, if the lamppost configurations satisfy certain minimum conditions, the triangular-wave topology achieves the maximum end-to-end (i.e. BS-to-BS) throughput possible. These conditions are provided by Theorem 4.

Theorem 4. In the "one-side" deployment with at least 3 hops, given system parameters d_0, h_L, and ϕ, select h_B so that the equality of Eq. 7.3 holds. Assume $d_0 = ah_L$, $a > 1$, if $h_B = b^{-1}h_L$, $b > 1$, when the following condition is satisfied,

$$\begin{cases} a > \sqrt{\frac{3(b-1)^3}{b^2(b-2)}} \\ b > 2 \end{cases} \tag{7.4}$$

the triangular-wave topology offers the largest end-to-end throughput among any possible topologies.

Proof. Since h_B is selected so that the equality of Eq.2 holds, the triangular wave topology is interference-minimal. If a certain topology can outperform the triangular wave one, it must be interference-minimal as well, due to the great loss of link capacity if mutual interference exists. Hence, the theorem is proved if we can prove that given the proposed condition, any other topology requires a beam width ϕ' smaller than the given ϕ to achieve interference-minimal.

Consider a minimum segment with 4 nodes N_0 to N_3 deployed. N_0 is a BS mounted on the top of a lamppost, N_1 to N_3 can be deployed at any height in the range of $[h_B, h_L]$. There are four possible interference-minimal scenarios when the "by-2" schedule is applied, as depicted in Fig. 7.7. Note that if a topology is interference-minimal and offers the maximum throughput, the "by-2" schedule is a necessity for it offers the largest link utility ratio. Thus in this segment, N_0 must not interfere N_3, when data flows from N_0 to N_3.

As for case (a), to eliminate interference, the half beam width must be no larger than the largest possible angle $N_3\widehat{N_0}N_1$ and angle $N_0\widehat{N_3}N_2$. $N_3\widehat{N_0}N_{1max} = \arctan(\frac{\tan\theta}{3})$ is

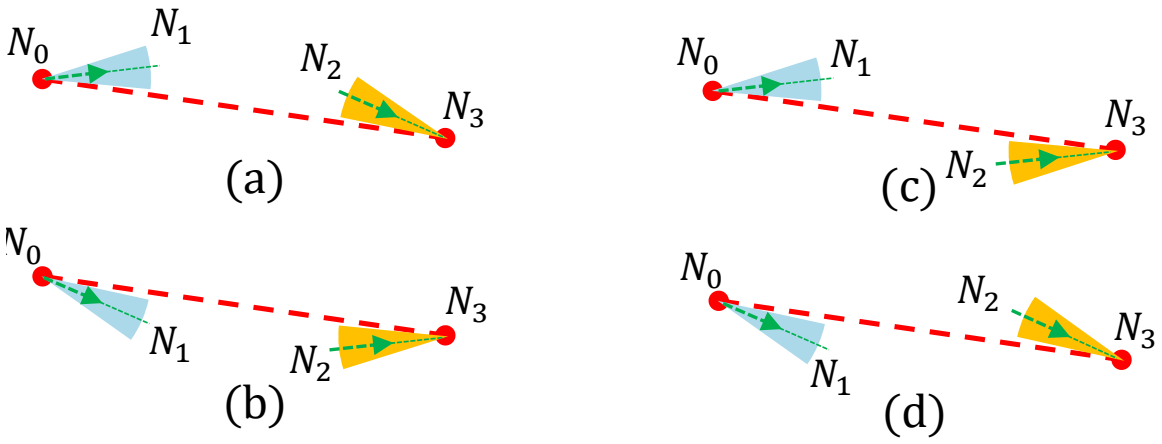

Figure 7.7: Four possible interference-minimal scenarios.

obtained when N_1 and N_3 are at h_L and h_B, respectively. $N_0\widehat{N_3}N_{2max} = \theta - \arctan(\frac{\tan\theta}{3})$ is achieved when N_2 and N_3 are at h_L and h_B, respectively. Thus, when $\theta < 60^o$,

$$\phi' \leq 2\arctan(\frac{\tan\theta}{3}) < 2(\theta - \arctan(\frac{\tan\theta}{3})) \leq \phi \tag{7.5}$$

Similarly, in case (c), due to angle $N_3\widehat{N_0}N_1$, Eq. 7.5 can upper bound ϕ', i.e., $\phi' < \phi$.

In case (d), $\phi' \leq \phi$ can be derived, as to achieve interference-minimal,

$$\frac{\phi'}{2} \leq \min\{N_3\widehat{N_0}N_{1max}, N_0\widehat{N_3}N_{2max}\}$$

stands. The equality holds only when N_1, N_3 are at h_B, and N_2 is at h_L, which is exactly the triangular wave topology.

Based on the above analysis, any other possible interference-minimal topology following the pattern of case (a), (c), or (d) requires a beam width ϕ' smaller than ϕ in the triangular-wave topology.

As for case (b), $\frac{\phi'}{2} \leq \theta$ can be easily derived similarly. However, N_3 may be interfered by the reflected signal from N_0 against the ground. Thus, to be interference-minimal, $\phi' \leq \max\{N_0'\widehat{N_3}N_0, N_3'\widehat{N_0}N_3\}$, where N_0', N_3' are the mirror reflections of N_0, N_3 against

the ground, respectively. Otherwise, the reflected interference signal is amplified by G_h on both N_0 and N_3, and its power is significantly larger than the noise level. It can be proved that $N_3'\widehat{N_0}N_3 \leq N_0'\widehat{N_3}N_0$. Thus, assume N_3 is deployed at $h_M \in [h_B, h_L]$,

$$\phi' \leq \arctan(\frac{h_L - h_M}{3d_0}) + \arctan(\frac{h_L + h_M}{3d_0}) \tag{7.6}$$

In case (b), to have $\phi' < \phi$, the right side of Eq. 7.6 must be smaller than ϕ. After processing, we have,

$$\frac{h_L - 2h_B}{3} - \frac{(h_L - h_B)^3}{d_0^2} > 0 \tag{7.7}$$

Applying $d_0 = ah_L$, $h_L = bh_B$, Eq. 7.7 can be further processed, and the relationship in Eq. 7.4 can be derived. □

Given d_0, h_L, and ϕ, selecting h_B to have $\gamma_1 = \frac{\phi}{2}$ leads to the maximum throughput achievable by the triangular wave topology, due to the achieved minimum link length. In practice, typically h_L is about 12 m, d_0 is around 40 m, and $a = 3.33$. If $\phi = 15^o$, $\theta = 11.3^o$, thus $h_B = 4$ m. Since $b = 3 > 2$, $a > \sqrt{\frac{3(b-1)^3}{b^2(b-2)}} = 1.63$, based on Theorem 4, the triangular wave topology offers the optimal throughput among any possible topologies in a typical roadside setting as well.

7.4 Numerical results and simulations

In this section, numerical and simulation results are provided to show the performance of our proposed schemes and to verify our mathematical analyses.

All evaluations are done at 60 GHz with a 2.16 GHz bandwidth. The transmit power of each wireless node is 1 watt and the antenna gains are $G_h = 21.87$dBi (generated from Matlab using 16 element circular panel array antenna) and $G_l = 0$dBi. The pathloss exponent is 2 in the Friis pathloss model used, the attenuation due to oxygen absorption is 16 dB/km, and the reflection attenuation against the ground is 15 dB. We also consider a 15 dB link margin which covers the noise figure and rain attenuations.

In this paper, we focus on the linear backhaul network topology such as the deployment along a straight-line highway, or a near straight-line scenario with a slight curve and/or surface height variation due to the practical terrain. As for a specific road trajectory with circles, sharp curves, etc., it would likely need a customized backhaul design to control mutual interference and is outside the scope of this paper.

7.4.1 The impact of relay distance and antenna beam width on BS-to-BS throughput

Assuming that all antennas have a common beam width ϕ, this evaluation shows the trend of BS-to-BS throughput as the distance, d_0, between two relays increases. A 3 km straight line highway segment with a flat road surface and lampposts evenly deployed is considered. The data from [94] is used where h_L is 15.3 m. h_B is set to 3.0 m. A freeway with 6 lanes and a total width of 22.2 m is considered. The range of d_0 considered is within $[30, 1000]$ m, and d_0 is an integer times the distance between two adjacent lampposts d_L. Typically, d_L is within $[30, 100]$ m. If $d_0 > d_L$, relays are deployed every several lampposts.

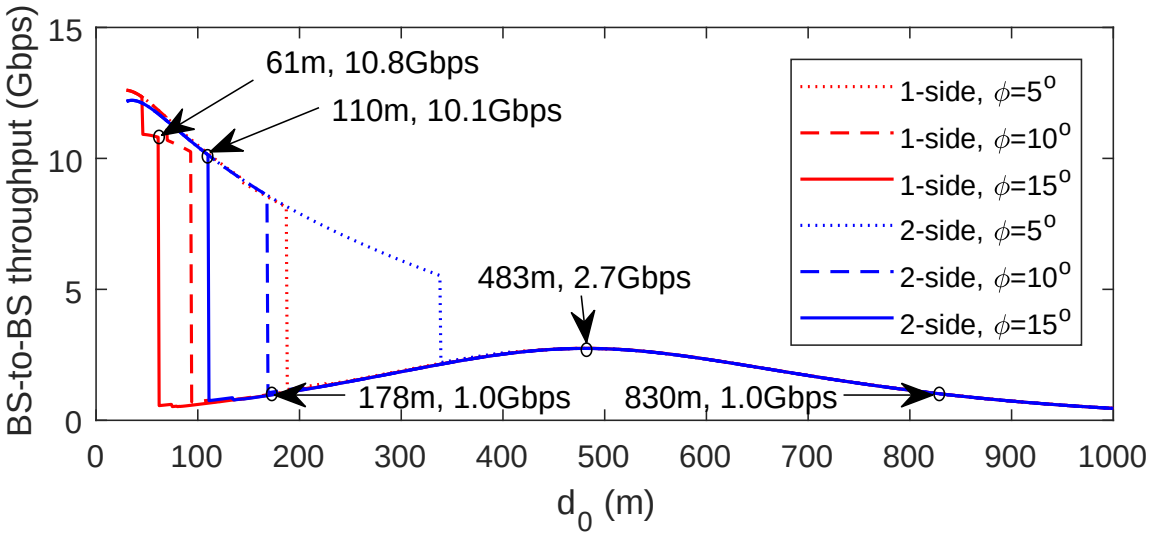

Figure 7.8: Throughput vs. d_0

As shown in Fig. 7.8, for beam width $\phi = 15^o$, the BS-to-BS throughput is above 10 Gbps when $d_0 \leq 61$ for the one-side case and when $d_0 \leq 110$ for the two sides case. If d_0

increases beyond this threshold, then the throughput drops substantially to below 1 Gbps, because as d_0 increases, the elevation angle θ decreases given fixed span w as shown in Fig. 7.3 and Fig. 7.4. When θ is small enough, Eq. 7.3 does not hold, and the significant mutual interference reduces the throughput. It is also shown that, the threshold of d_0 to eliminate interference increases when the beam width decreases, which is consistent with Theorem 4.

An interesting phenomenon in Fig. 7.8 is, after the severe drop due to mutual interference, the throughput gradually increases as d_0 further increases, and it reaches a local maximum of 2.7 Gbps when d_0 is 483m, while after that, the throughput decreases again gradually. This is because due to the use of "by-2" scheduling, the propagation distance of the interference signal increases 3 times faster than d_0, which means the impact of interference on the throughput is alleviated until interference becomes small enough and the system becomes noise-limited.

These data show that as the BS-to-BS throughput requirement varies, as discussed in Section 7.2.1, the network topology can use different d_0 values and can therefore adapt the number of relays in between different BS pairs. For example, with $\phi = 5^o$ and the two-sides deployment, d_0 can smoothly vary as the BS-to-BS throughput requirement varies between 6 Gbps and 12 Gbps, meaning that the number of relays can be varied from about 3 (at 6 Gbps) to about 20 (at 12 Gbps), assuming BSs are placed every 1 km. Three relays are necessary down to about 2.7 Gbps and then 2 relays are sufficient at that throughput and below. If base stations are spaced around every 800 meters and the throughput requirement is 1 Gbps or less, then no relays are necessary at all.

7.4.2 The performance of mmWave backhaul deployment based on real highway data

In practice, the road may not be a perfectly straight line. Thus, in this evaluation, we conduct simulations where the proposed mmWave backhaul network is deployed based on real highway data. To carry out this evaluation, we extracted the lamppost locations in a 12

km segment of highway I-75/85 going through downtown Atlanta, GA from Google Earth. There are 291 lampposts deployed in the median of the highway, which separates the two directions of traffic on the road. Thus, this scenario corresponds to the one-side deployment case in our framework. The average lamppost interval is 41.4 m with a standard deviation σ of 3.32 m and the height h_L of lampposts deployed in Atlanta is about 12 m. Using this real data, we investigate the performance of the triangular-wave topology in non-ideal scenarios.

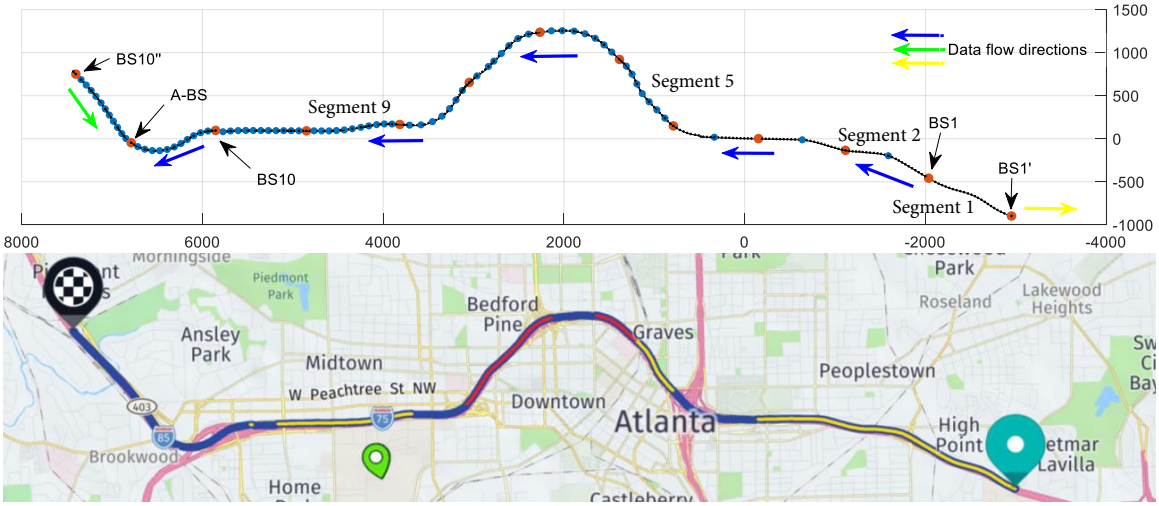

Figure 7.9: The modeled segment of highway I75/85 in Atlanta, GA

In the portion of Fig. 7.9 above the map, the location of each lamppost is marked with a small black circle. We deploy 13 BSs at the locations marked with red dots, achieving a distance between adjacent BSs of about 1 km. The 12 segments have a mean length of 1000.5 m and $\sigma = 19.21$ m. The BS second to the left in Fig. 7.9 is assumed to be an anchored BS with a fiber backhaul connection, while the other BSs do not have any wired connection. BS1 is the farthest BS associated with this A-BS. We additionally deploy BS10$''$ on the left end which is associated with this A-BS and BS1$'$ on the right end is a BS associated with a different A-BS. The arrows indicated data flow direction for each BS. It is observed that, despite the fact that the highway segment already includes a significant curve, the deployment of BSs partitions the topology into close-to-straight-line segments.

This observation supports our use of a straight-line road model in the analytical evaluations.

We first simulate the self-backhaul design as mentioned in the related work, where BSs connect to each other directly in a linear topology. Even though this topology should experience interference due to the linear topology, the long distances involved cause each backhaul link to be noise-limited to a rate of around 0.4 Gbps. Thus, narrowing the beamwidth to reduce the interference footprint does not affect the results, as shown in Fig. 7.10 (a). Clearly, this topology is not sufficient to meet 5G backhaul requirements. In addition, this result is generated assuming that there is a LOS path between each pair of adjacent BSs. However, due to the existence of obstacles (buildings, tunnels, etc.) alongside the road, the LOS path may be blocked if there is a large curve and this would lead to the total failure of the self-backhaul network.

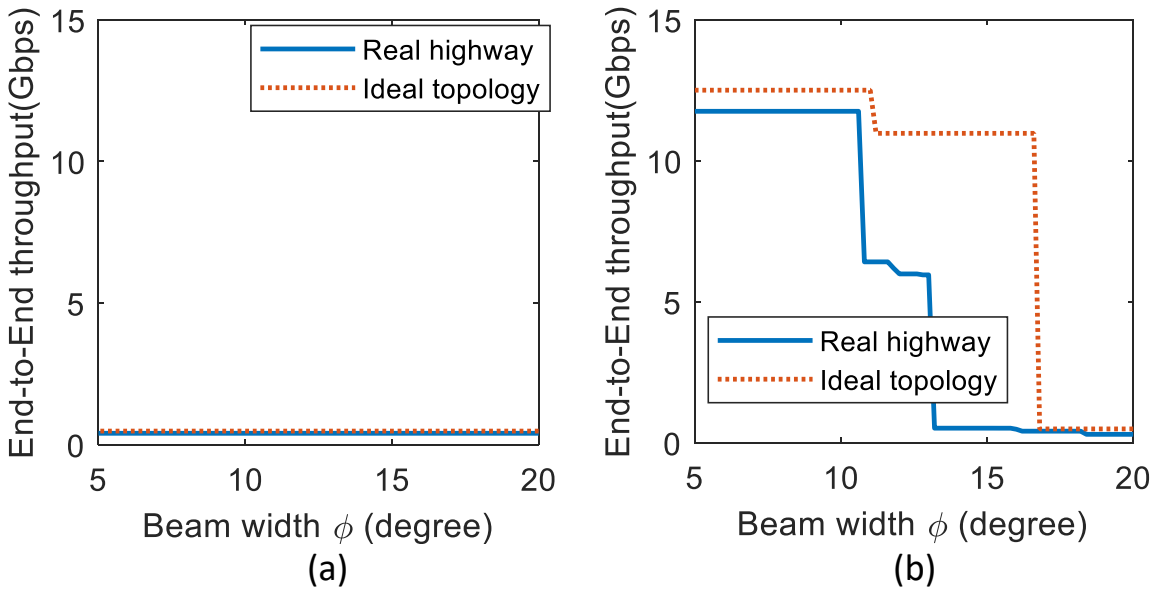

Figure 7.10: Comparison on throughput between real topology and ideal topology. (a) Self-backhaul; (b) Backhaul with the maximum number of relays deployed.

Next, we investigated the end-to-end throughput for the triangular-wave topology on the same highway segment with a relay deployed on every lamppost. A comparison between this real road scenario and the ideal scenario is also conducted. As shown in Fig. 7.10, when beam width is larger than 17^o, both cases have very bad throughput, due to the large mutual

interference. When beam width is no larger than 10.6^o, both cases have high throughput, 11.77 Gbps and 12.5 Gbps for the real deployment and the ideal deployment, respectively. Between these two thresholds of beam width, the throughputs decrease in both cases as the beam width increases. We simulated the real road scenario on each segment, and the result of the "worst" segment which provides the worst throughput performance is shown in Fig. 7.10. The performance on the real highway scenario is worse than for the ideal case, because the by-2 schedule is not perfect since the non-ideal topology is not perfectly symmetric and there are several long links (the maximum interlamppost separation is 52.8 m).

As mentioned in Section 7.2.1, there is no need for every BS-to-BS connection in the backhaul network to achieve more than 10 Gbps data rate, especially for those connections far away from an anchor BS. From the perspective of reducing the number of relays to control the cost, it is intuitive to think that for connection with a lower rate required, relays can be deployed further apart (every several lampposts). Thus, on the highway segment of Fig. 7.9, we simulate the deployment of different triangular-wave topologies between different BS pairs using as few relays as possible. The result in Fig. 7.11 shows that when the antenna beam width $\phi = 5^o$, deploying 75 relays as blue dots depicted in Fig. 7.9 can satisfy the throughput requirements from segment 2 to 11. This is significantly smaller than the 232 relays that would be used if a relay were deployed on every lamppost. Note that the maximum throughput in Fig. 7.11 is slightly lower than that in Fig. 7.10 (b), because we deploy relays every two lampposts here which corresponds to relatively longer link lengths.

7.5 Chapter summary

In this chapter, we investigate backhaul topologies deployed along roadsides to provide 5G service to vehicles. To support high backhaul data rates, relay nodes between small cell base stations will be necessary. Also, self-interference among backhaul links has to be accounted for since roadsides are relatively clear of obstacles and many transmissions are

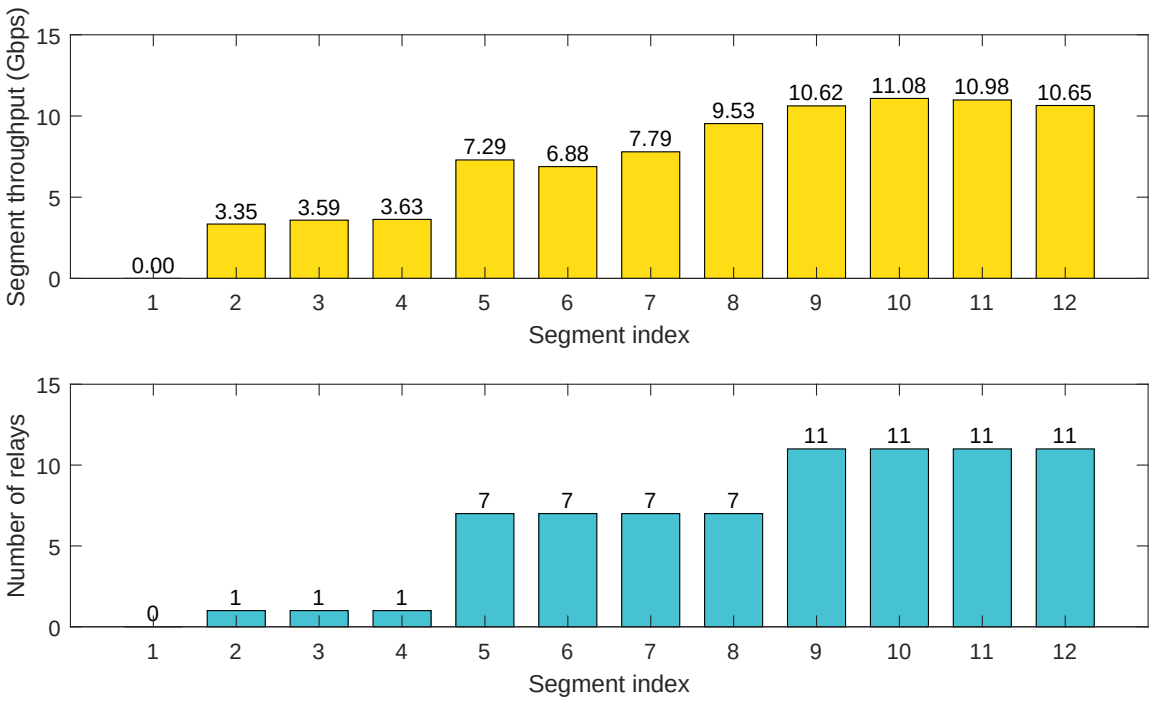

Figure 7.11: Backhaul deployment based on real data. (a) Segment throughput; (b) Number of relays in each segment.

in the same direction since they follow the roadway. We investigate the design of wireless backhaul topologies that can be deployed on regularly-spaced lampposts alongside a road. We propose the triangular-wave topology, which is a regular topology well-suited for this setting. We derive conditions necessary for the triangular-wave topology to be interference-minimal and throughput-optimal. We also investigate how the proposed topology performs using lamppost positions taken from a 12 km stretch of highway in Atlanta. Results show that the topology can achieve throughputs very close to the ideal case and supports backhaul throughputs of 10+ Gbps in real roadside environments.

CHAPTER 8
END-TO-END SIMULATION OF OUT-OF-BAND MMWAVE BACKHAUL NETWORKS

8.1 Introduction

In early 2019, the 3GPP release 15 on 5G NR was released [95] and the telecommunication industry began preparing for commercial launches of 5G. Meanwhile, as we are still in the early stages of the 5G rollout, both industry and academia continue to evolve and innovate new 5G technologies. Since it is challenging for small research groups to afford expensive 5G hardware, analytic methods and simulation tools are crucial to 5G research and development activities. Considering that the simplifications and assumptions made in analytic models limit the generality of the results, simulation tools that can provide accurate results are in great demand. As a result, 5G millimeter-wave (mmWave) related modules in ns-3 are gaining attention from the research community, because they are expected to be able to evaluate the performance of 5G mmWave cellular systems in a flexible, accurate and cost-effective way.

Although multiple mmWave modules for ns-3 have been released, most focus on implementing access tier features, while very few touch the backhaul tier. With the pervasive deployment of small cells in dense urban areas for 5G, the backhaul challenge has become critical due to the enormous amount of data that needs to be forwarded between small-cell base stations (BSs), where wired fiber connections may not be available easily due to the cost and construction limits. Moreover, since it has not yet been standardized, there is an opportunity for research on 5G mmWave backhaul. Note that mmWave backhaul can be categorized into two types, in-band and out-of-band, depending on whether the access and backhaul tiers use the same frequency band or not. Currently, an integrated-access-

and-backhaul (IAB, which is in-band) module is available in ns-3; while no solution to the mmWave out-of-band backhaul has been released to date.

In this paper, we introduce our approach to realize end-to-end simulation of mmWave out-of-band backhaul networks in ns-3. In Section 8.3.1, we propose a novel design for integrating mmWave out-of-band backhaul in ns-3, which includes a custom network backhaul device. In Section 8.3.2, we describe an extension we have implemented to the existing IAB (in-band backhaul) module to simulate the basic functionalities of out-of-band backhaul. The modified IAB module was used to produce preliminary simulation results, which are reported in Section 8.3.2.

8.2 Related Work

Several modules have been developed for simulating mmWave networks. The most well-known work [96] is from NYU Wireless and University of Padova, which is the first module developed for the end-to-end simulation of mmWave access networks. Within the EPC module from the ns-3 LTE-LENA project[97, 98], the authors added several customized models covering mmWave MAC and PHY layers, and mmWave channels. Since this work focuses on the access tier of mmWave networks, it lacks the ability to simulate backhaul communication between eNBs. To address this issue, researchers from University of Padova have developed a module which can be used to evaluate the performance of mmWave integrated-access-and-backhaul (IAB) networks [99]. An IAB node can directly communicate with an eNB or other IAB nodes. The authors also proposed a distributed scheduling mechanism to support backhaul and access data transmissions in the multi-hop scenario. Although it is the first ns-3 module to support mmWave backhaul, it only covers in-band backhaul, where access and backhaul share the same frequency band, and hence it cannot simulate out-of-band backhaul scenarios. Recently, based on the 5G NR standard, CTTC has started the 5G-LENA project [100], the goal of which is to deliver a simulator incorporating fundamental PHY-MAC NR features aligned with NR Release 15 TS 38.300.

Similar to [96], currently the 5G-LENA project focuses on the access tier rather than the backhaul tier. Besides, Assasa, et al., implemented a WLAN 802.11ad module [101] in ns-3. As stated above, we are the first to tackle the end-to-end simulation of mmWave out-of-band backhaul networks.

8.3 mmWave out-of-band backhaul simulation

8.3.1 New mmWave out-of-band backhaul module for ns-3

The ultimate goal of this work is to develop a new module in ns-3 that can be used by the community to simulate mmWave out-of-band backhaul networks and boost research in this area. To align this contribution with industry standards, we plan to build our backhaul module based on the ns-3 5G NR module, being developed by CTTC, which will incorporate fundamental PHY-MAC NR features aligned with NR Release 15 TS 38.300, while other existing mmWave modules lack this feature. In this paper, we provide the high-level architecture of our proposed module design.

Figure 8.1 provides an overview of the end-to-end classes in our design. One of our objectives is to create a new network device, `NRBhNetDevice`, which will enable the full functionalities of the mmWave out-of-band backhaul. This net-device will be installed into three types of nodes in the simulator, including gNB, small-cell BS, and mmWave relay. Note that the latter two types of nodes will also be introduced for the first time in the ns-3 system. ”Small-cell BS” is different from the gNB serving as the macro-cell BS in the 5G cellular system, because it will not have the wired connection to the SGW/PGW node as gNB does. In fact, mmWave backhaul is proposed because of the existence of a large number of small-cell BSs within each macro-cell in 5G era and it aims to resolve the issue of forwarding the large amount of backhaul traffic between these small-cell BSs without wired connections. In our design, both `NREnbNetDevice` and `NRBhNetDevice` are installed on a small-cell BS node to take care of access and backhaul transmissions, respectively, and the packet exchange between them is realized by the new `EnbBhApp` class.

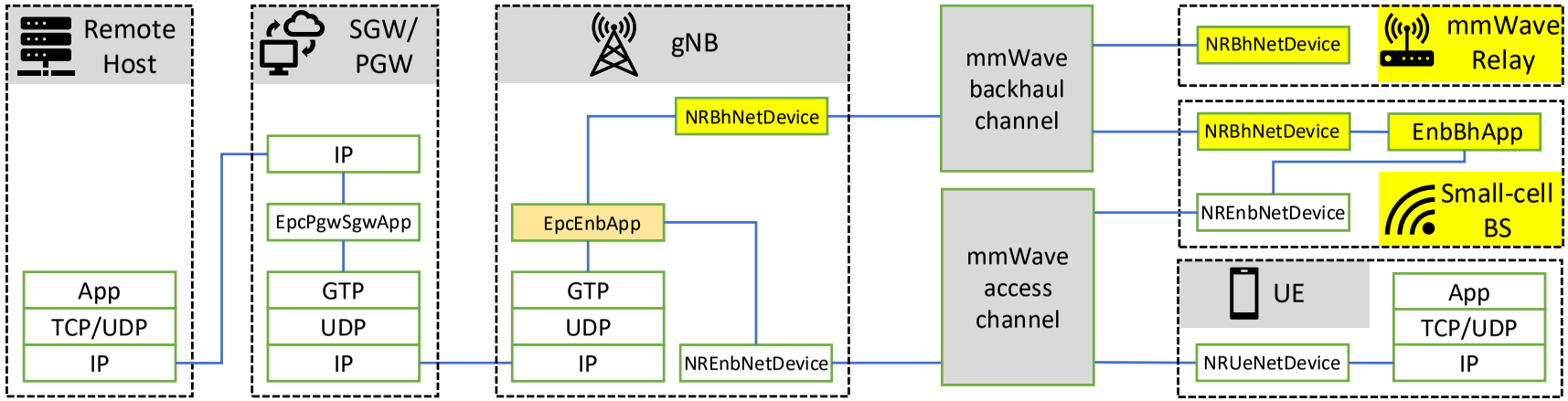

Figure 8.1: End-to-end class overview. In white, we present the existing and unmodified ns-3, LTE-LENA and 5G-LENA modules. In gold, we present the modified LTE-LENA module. In yellow, we present the newly created 5G-backhaul modules.

Since the gNB node should also support the backhaul functionality, an `NRBhNetDevice` will be installed in it as well. We also plan to modify the `EpcEnbApp` class so that it can handle packet switching between EPC, access, and backhaul.

As for "mmWave relay" nodes, they are an essential component in relay-assisted mmWave backhaul networks that are deployed to construct a multi-hop line-of-sight (LoS) relaying path between a pair of BSs where the single-hop LoS path is not available due to blockage [54, 55]. Since relays are simple devices dedicated to the backhaul network, only `NRBhNetDevice` will be installed on them.

Note that in Figure 8.1, the mmWave channel class is split into two instances, mmWave backhaul channel and mmWave access channel, to model the "out-of-band" feature of our system. Signals in different channels do not affect each other as they have different frequencies. This differentiates out-of-band backhaul from in-band backhaul, where backhaul links and access links compete for the same channel resource. The existing ns-3 mmWave backhaul module, known as integrated-access-and-backhaul (IAB) module [99], implements the in-band backhaul scenario with a single shared channel.

The stack of the proposed `NRBhNetDevice` is shown in Figure 8.2. Similar to existing net-devices in the NR module, there are corresponding `NRBhMac` and `NRBhPhy` modules, which implement most of the functionalities and features of MAC and PHY layers of `NRBhNetDevice`. Different from the net-devices in LENA modules, since the backhaul net-device does not need to support any access tier specific functionalities, we choose not to include `LteRrc`, `LtePdcp`, or `LteRlc` classes in our `NRBhNetDevice`. Instead, we will provide a `BhApp` class, which implements function blocks that abstract backhaul higher level features such as QoS, guaranteed data transmission, relay path construction and re-configuration, etc.

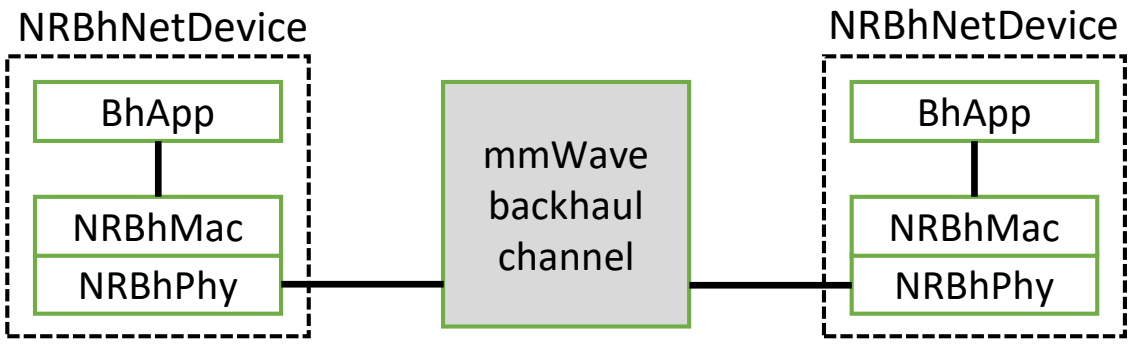

Figure 8.2: NRBhNetDevice class overview.

8.3.2 Simulating mmWave out-of-band backhaul using the existing IAB module

While our long-term focus is on development of the dedicated module introduced above, we have also implemented an expedient method to extend the existing mmWave IAB module in ns-3 to simulate the basic functionalities of mmWave *out-of-band* backhaul to get some preliminary results on its throughput performance.

This method is inspired by the fact that the IAB module has already implemented a complete framework for mmWave backhaul simulation, including extending the mmWave eNB in [96] to support backhaul transmissions. Integrating both mmWave UE and eNB net-devices on an IAB net-device to enable both backhaul and access capability was crucial to the fast development of the IAB backhaul module, as it allowed the reuse of mmWave PHY and channel models from [96]. For the same purpose, as we take advantage of the backhaul framework constructed in the IAB module, we could focus on the topology construction and MAC scheduling modifications necessary for out-of-band backhaul without being concerned with other aspects that have been resolved in the IAB module, such as the data bearer set-up along multi-hop backhaul paths.

In the following two subsections, we introduce the details about using mmWave IAB module to set-up the topology for out-of-band backhaul simulations and the modifications to the scheduler to realize the concept of out-of-band backhaul transmissions.

Topology construction

Several network elements need to be deployed in an end-to-end mmWave out-of-band backhaul system, and they can be categorized into two main sets, i.e., the EPC elements and the cellular elements. We directly adopt the EPC module in the ns-3 LTE module as was the case in both [96] and [99]. A remote host connects with the PGW node through a point-to-point wired connection. The PGW is connected with a mmWave gNB (i.e.,mmWave eNB in [96, 99]) through functions defined in `EpcEnbApp`. The cellular part of the topology starts from the gNB node, which serves as the gateway to the EPC part.

In the cellular part, if the self-backhaul is simulated, where mmWave BSs are connected with each other directly by mmWave wireless links, IAB nodes are installed to serve as the small-cell BSs. In this case, the key difference between the topology of an out-of-band backhaul network and that of an in-band backhaul network in [99] is that no mmWave UE node is deployed to connect with these IAB nodes, except that one mmWave UE node is attached to the IAB node at the end of each path. In fact, that UE also simulates a small-cell BS, which serves as the sink of the backhaul traffic from the gNB. Currently, we are still working on enabling data absorption on the intermediate IAB nodes without attaching access tier UEs, in order to virtually simulate the access tier.

As proposed in [54, 55], it is of interest to us to simulate the multi-hop relaying path of a backhaul logical link, which is constructed by dedicated mmWave backhaul relays between a pair of BSs. In fact, IAB nodes can be deployed as mmWave backhaul relays if no UEs are attached to them, because relays are assumed to be dedicated to the backhaul use, which means no data is consumed at each relay. Starting from the gNB, IAB nodes are connected sequentially with each other, and a UE attached to the last IAB node along the path serves as the destination small-cell BS of a multi-hop backhaul path.

Note that in [99], the attachment of an IAB or UE to a gNB or IAB is based on a distance metric. The `MmWaveHelper` class only implemented several "`AttachToClosest*`" functions, which means a node could only attach to its nearest neighbor. Thus, it does

not allow us to freely construct a topology in which the connection construction does not depend on distances. We added helper methods "`AttachTo*`" to address this issue and allow the attachment to happen according to the input argument of net-device ID.

Scheduler modification

To make the simulation correctly reflect the feature of out-of-band backhaul, we must modify the scheduling within both gNB and IAB net-devices. In the original IAB net-device, the TDMA-based scheduling allocates part of the time resource to access and the rest is assigned to backhaul. In the out-of-band backhaul, however, as we do not need to explicitly simulate the access tier, all the frequency and time resource can be dedicated to the backhaul usage. For an IAB or gNB node without UE attached, all the time slots within a subframe can be allocated for backhaul; while for the last IAB node of each backhaul path, all the time slots can be allocated for transmissions to its attached UE.

In the default scheduler of IAB, "`MmWaveFlexTtiMacScheduler`", the round-robin style scheduler constrains that backhaul transmissions cannot use more than half of the total available time slots in a subframe, as the other half is reserved for access tier. Our first attempt is to remove this constraint, and to allow all available time slots to be assigned for the backhaul tier. However, due to the highest priority of scheduling retransmissions and the inherent limits from a round-robin scheduler, the throughput performance is not as good as we expected, which is shown later in section 8.3.2.

Actually, in urban environments, small-cell base stations tend to have fixed locations at a higher elevation, which means the topology of mmWave backhaul networks is quite stable. Different from the access links, the channel condition of backhaul links also tends to be stable. Based on these features, we can calculate the optimal schedule of a mmWave backhaul network in the planning stage (the optimal schedule is detailed in [54]) and the pre-calculated optimal schedule can then be pre-loaded into each node in the backhaul network. To do so, we implement a method to install the scheduling decision on each

node. We create a new pair of attributes "`symAvailStart`" and "`symAvailEnd`" for "`MmWaveFlexTtiMacSch-eduler`" to record the range of time slots available for the transmission from the current node to each of its downlink peer node. The time slots assigned for either retransmitting corrupted data or transmitting new data to a specific UE cannot exceed its pre-set range of available time slots. During the simulation, if channel conditions change significantly on some backhaul links, the optimal schedule could change. We are currently developing a method to collect the MCS used on each link as well as a method for the gNB to disseminate the updated optimal schedule to each node.

Example simulations

In this subsection, we provide the results of several example simulations. In all simulations, we consider a Manhattan-like urban environment, where 5 vertical and 5 horizontal streets with the same width of 10 meters intersect with each other. The distance between adjacent streets in the same direction is 60 meters. In each blank area surrounded by 4 streets, a building with the size 50×50 m^2 is deployed. The height of each building is 30 meters. We set up a gNB node in the center of the area, and all IABs or UEs are deployed at the intersections of streets. To simplify the analysis, we assume every node is at the same height of 20 meters, which results in a `UMi-StreetCanyon` scenario since buildings are higher than wireless nodes and most of the secondary interference due to the concurrent transmissions on different links is blocked by those buildings. In the simulations, we choose to use the `MmWave3gppChannel` model and the `MmWave3gppBuildingsPropagationLossModel`. As for the traffic generation, we adopt the `UdpClientServer` application. For each UE node attached to the end IAB node of a backhaul path, a `UdpServer` application is installed, and correspondingly a `UdpClient` application is installed at the remote host, which takes the responsibility of generating UDP packet stream controlled by the `Interval` attribute. The UDP packet size is 1400 bytes. The backhaul frequency band is at 28 GHz with a total bandwidth of

1 GHz. The subframe duration is 1 ms and each subframe contains 24 OFDM symbols. The code of extended IAB module is available at: `https://github.com/hqfrank/ns3-mmwave-relay`.

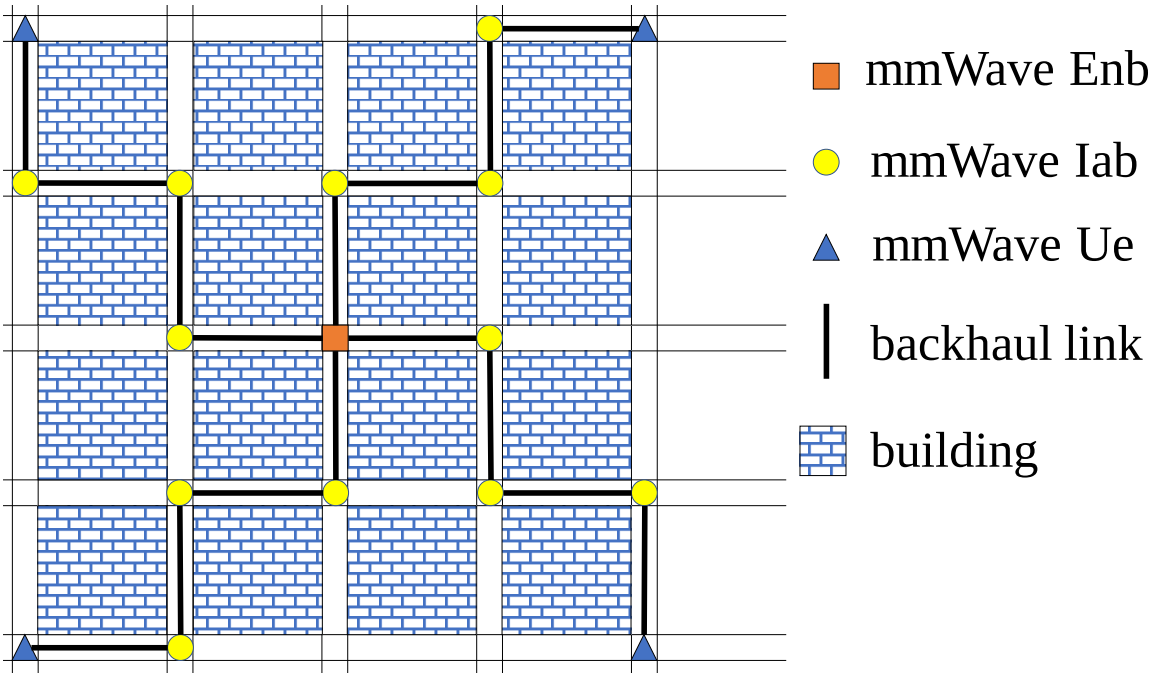

Figure 8.3: A mmWave out-of-band backhaul with 4 paths.

We first simulate the single backhaul logical link case to see how high a throughput can be achieved by the out-of-band backhaul under the default setting of IAB module. If the backhaul logical link only contains one hop, it is referred to as the case "1-hop"; while if an IAB node is deployed between the gNB and a UE, it is considered as the "2-hop" case. In both cases, each hop is LoS with a length of 60 meters. Figure 8.4a shows that as the UDP packet interval shrinks (i.e., "traffic rate" increases), the "1-hop" path can reach a maximum end-to-end throughput close to 3 Gbps when the packet interval is 3 us, which is slightly below the maximum PHY rate of 3.2 Gbps defined in the IAB module. Also, the MCS reaches the maximum value of 28 for the transmission in each time slot. However, in the "2-hop" case, the maximum throughput is halved due to the fact that an IAB node cannot transmit and receive at the same time.

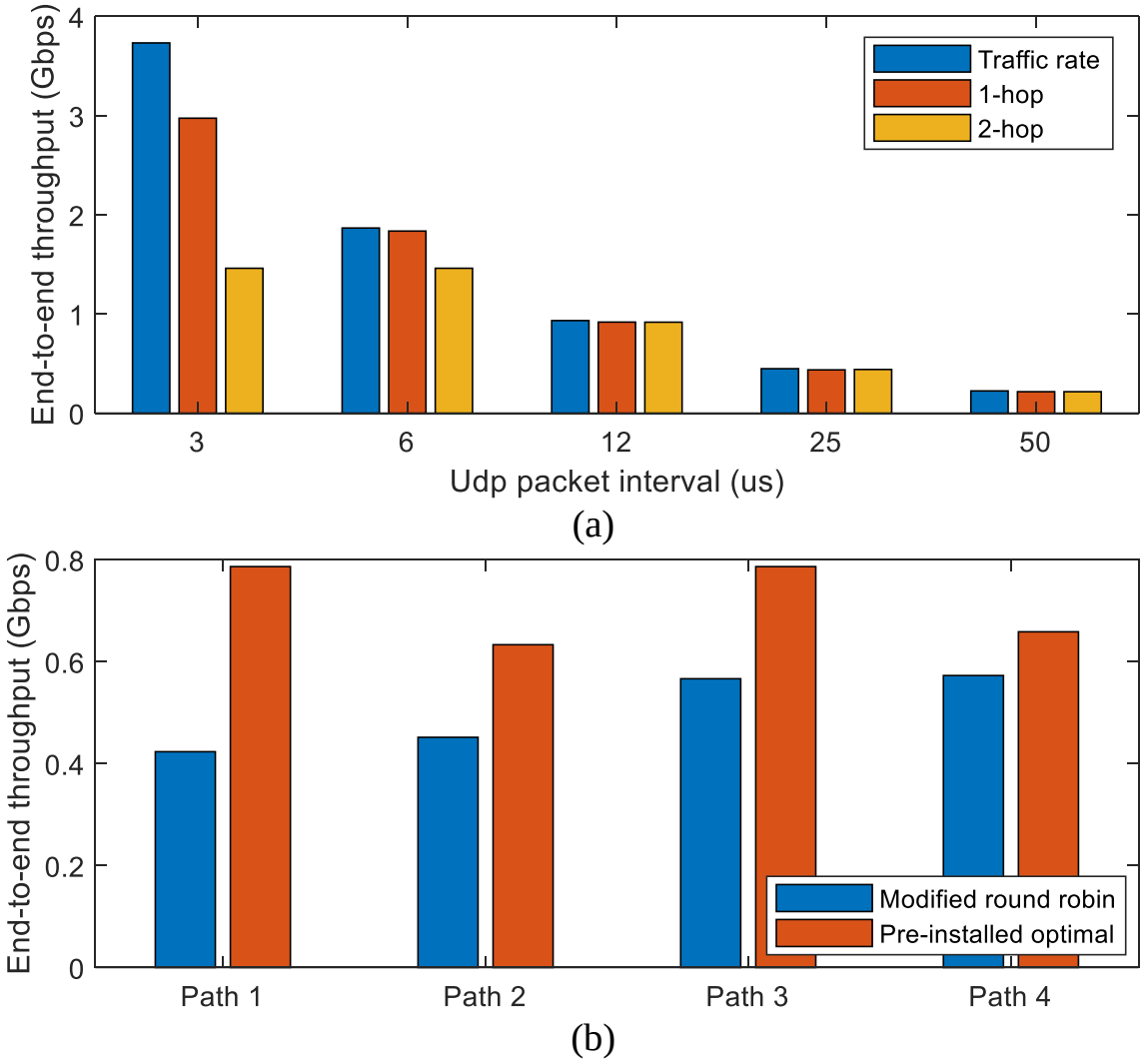

Figure 8.4: (a) Single path scenario. (b) Multiple paths scenario.

Figure 8.4b depicts the impact of the MAC scheduling on the throughput performance of an out-of-band backhaul network. As shown in Figure 8.3, there are four 4-hop backhaul paths in the topology. The blue bars in Figure 8.4b indicate the end-to-end backhaul throughput of each path, when the round-robin based "`MmWaveFlex-TtiMacScheduler`" in the IAB net-device is modified to support the out-of-band backhaul; while the red bars shows the end-to-end backhaul throughput of each path when the optimal scheduling calculated for the topology is pre-installed in the scheduler. It is seen that, the optimal scheduling scheme helps increase the total throughput by about 40% as compared to the modified round-robin scheduling scheme. Note that in the topology shown in Figure 8.3, the mmWave Enb connects 4 backhaul links; however, as there is only one radio chain on the Enb, in the optimal scheduling, the 4 links obtain time slots in the numbers of $\{6,5,6,5\}$. That is to say, the PHY rate has been divided into 4 parts almost evenly. If we sum the throughput of 4 paths in the optimal scheduling case, it gives 2.87 Gbps, which is slightly smaller than the maximum throughput of the "1-hop" case shown in Figure 8.4a.

8.3.3 Changes to the base mmWave Iab module

During our development, we found and fixed several minor problems with the base IaB module:

1) In `MmWaveFlexTtiMacScheduler::CalcMinTbSizeNumSym()` the bisection line search does not consider the case that the temporarily calculated `tbSize` equals to `bufSize`, and it would result in a wrong Transmission Block (TB) size occasionally, which would further affect the scheduling performance.

2) In `MmWaveAmc::GetTbSizeFromMcsSymbols()` the calculation of the number of code blocks does not follow the process in [102] exactly. The total size of data should be `tbSize + m_crcLen`, while each code block contains at most `cbSize - m_crcLen` bits.

8.4 Chapter summary

In this chapter, we focus on the end-to-end simulation of mmWave out-of-band backhaul networks in ns-3. We first introduce a design for an out-of-band backhaul module in ns-3. A custom backhaul network device is proposed that can be added to nodes to enable out-of-band backhaul transmissions. Since the new backhaul module is still under development, we extended the existing mmWave IAB module to enable mmWave out-of-band backhaul simulation and produce some preliminary results on throughput performance. We also modified the existing scheduler in the IAB module to support customizable scheduling for logical links in out-of-band backhaul networks. We used the customizable scheduler to implement an optimal scheduling algorithm from prior work and demonstrate that it increases throughput performance by up to 40% in certain scenarios.

CHAPTER 9
CONCLUSIONS

9.1 Conclusions

In the 5G era, the cell size becomes smaller, and the operators are to deploy a large number of small-cell base stations BSs, which cooperate with the legacy macro-cell BSs, aiming to provide better coverage and higher data rate to cellular users. However, most of the small-cell BSs have no wired Internet connections due to the construction restrictions and prohibitive cost, so that small-cell BSs can only connect to Internet with the help from nearby macro-cell BSs acting as gateway nodes. Thus, this small-cell trend brings the backhaul challenge of transferring huge amount of data between small-cell BSs and macro-cell BSs. Being able to support multi-Gbps wireless links, mmWave backhauling has been regarded as an essential use case in 5G cellular systems. Different from most related work on mmWave backhaul networks, a unique relay-assisted mmWave backhaul network architecture is proposed, which aims to provide a feasible solution to the critical backhaul challenge.

Our focus is on the system design and performance optimization of the relay-assisted mmWave backhaul network in the urban environment. The objective of this thesis is to address the challenges therein and establish the fundamentals of the relay-assisted mmWave backhauling for 5G cellular systems. The contribution of each chapter is summarized as follow,

- In chapter 3, with the use of a 3D model for buildings targeted at urban environments, we provide optimal and efficient algorithms both for scheduling communications along a single mmWave relay-assisted path and for choosing the relay-assisted path with maximum throughput among all candidate paths connecting a given base

station pair. In addition to proving optimality of these algorithms, we evaluate their performance through simulations based on a real urban topology. Simulation results show that our algorithms can produce short relay paths with end-to-end throughputs of around 10 Gbps and higher that are capable of providing virtual mmWave links for a wireless backhaul use case.

- In chapter 4, we investigate the problem of constructing multiple mmWave backhaul logical links between a set of BSs in urban areas. We propose an algorithm to find high-throughput LoS relaying paths for all logical links by minimizing interference within and between paths. We also propose methods to modify the backhaul topology to increase the probability of finding high-throughput paths using our algorithm. Extensive simulations, based on a 3-D model of a section of downtown Atlanta, are conducted to show the effectiveness of our algorithms and models. Some insights on the network design problem are also provided.

- In chapter 5, a novel interference model is proposed which reflects the characteristic of the proposed relay-assisted mmWave backhaul architecture. Based on the proposed interference model, we can obtain the maximum downlink or uplink traffic demand of each small-cell BS supported by the tree-style backhaul network through linear programming, considering different interference and radio chain resource conditions.

- In chapter 6, an efficient distributed scheduling algorithm is also proposed, which can be easily implemented in practice. The simulation results show that the throughput performance of the proposed scheduling algorithm is very close to the maximized traffic demand calculated in certain traffic settings, and it can adapt to the scenario where dynamic traffic demand is applied to the small-cell BSs in the backhaul network.

- In chapter 7, we investigate mmWave backhaul networks that use relay nodes and a

regular triangular-wave topology to meet the very high data rates necessary to handle backhaul traffic in the roadside scenario. The challenge is to manage the self interference that can occur due to the near- straight-line topology that arises from a roadside deployment. The triangular-wave is a regular topology that can be deployed on regularly-spaced lampposts alongside a road. We derive conditions necessary for the triangular-wave topology to be interference-minimal and throughput-optimal. We also investigate how the proposed topology performs using lamppost positions taken from a 12 km stretch of highway in Atlanta. Results show that the topology can achieve throughputs very close to the ideal case and is capable of supporting backhaul throughputs of 10+ Gbps in real roadside environments.

- In chapter 8, we address the issue of realizing end-to-end simulation of mmWave out-of-band backhaul networks in ns-3. A novel design for integrating mmWave out-of-band backhaul in ns-3 is proposed, which includes a custom network backhaul device that can be added to nodes to enable the out-of-band backhaul transmissions. We also implement an extension to the existing mmWave IAB module in ns-3 to simulate the basic functionalities of the out-of-band backhaul and produce some preliminary results on the throughput performance. The existing scheduler in the IAB module is modified to support customizable scheduling for logical links in out-of-band backhaul networks.

9.2 Future Work

In this thesis, we address the design and optimization issues of relay-assisted mmWave backhaul networks in the urban environment. Although we try to cover as many aspects of the topic as we can, there are still some work for us to complete in the near future.

In chapter 3 and chapter 4, the problem of selecting relays from a set of candidate relay locations to form mmWave backhaul logical links are investigated; however, when the mutual interference issue is addressed, the possible interference signals due to reflections

are not considered. It is meaningful to conduct measurements using real devices in the 3D urban environment to see how likely and in what extent the reflected interfering signals affect the reception of useful signals in different scenarios.

In chapter 4, the given backhaul topology is a tree style topology, which is generated through a simple spanning-tree algorithm. It is interesting to develop different tree-topology generation algorithms so that different types of tree-topologies can be obtained. Upon these new topologies it is possible to find out the crucial factors on the topology design which greatly impact the feasibility of constructing interference-minimal relay-assisted mmWave backhaul networks and the throughput performance of the backhaul.

In chapter 5, when the traffic demand of small-cell BSs are maximized using linear programming, either the downlink or the uplink case is considered. Therefore, next step could be investigating the throughput performance upper bound of the mmWave backhaul network in a downlink and uplink hybrid scenario. This task is quite challenging in the case where mutual interference exists between some logical links, since the interference relationship between two logical links may vary according to the different combinations of logical link directions.

In chapter 8, a new design of the out-of-band mmWave backhaul module in ns-3 is proposed. It is expected that this module can be fully developed and added to ns-3 in the near future, so that it could benefit the research community of mmWave backhaul.

9.3 Publications

As part of the research conducted in this dissertation, we have written several documents that are either published, submitted, or in progress as follows:

- Q. Hu and D. Blough, "On the Feasibility of High Throughput mmWave Backhaul Networks in Urban Areas," submitted to 2020 International Conference on Computing, Networking and Communications (ICNC).

- Y. Yan, Q. Hu, and D. Blough, "Optimal Path Construction with Decode and Forward Relays in mmWave Backhaul Networks," submitted to 2020 International Conference on Computing, Networking and Communications (ICNC).

- Y. Liu, Q. Hu, and D. Blough, "Joint Link-level and Network-level Reconfiguration for mmWave Backhaul Survivability in Urban Environments," to appear, 22nd ACM International Conference on Modeling, Analysis and Simulation of Wireless and Mobile Systems, 2019.

- Q. Hu, Y. Liu, Y. Yan, and D. Blough, "End-to-end Simulation of mmWave Out-of-band Backhaul Networks in ns-3" Proc. of the Workshop on Next-Generation Wireless with ns-3, 2019.

- Y. Yan, Q. Hu, and D. Blough, "Path Selection with Amplify and Forward Relays in mmWave Backhaul Networks," Proc. of IEEE Int'l Symposium on Personal, Indoor, and Mobile Radio Communications, 2018.

- Y. Liu, Q. Hu, and D. Blough, "Blockage Avoidance in Relay Paths for Roadside mmWave Backhaul Networks," Proc. of IEEE Int'l Symposium on Personal, Indoor, and Mobile Radio Communications, 2018.

- Q. Hu and D. Blough, "Optimizing Millimeter-Wave Backhaul Networks in Roadside Environments," Proc. of IEEE International Conference on Communications, 2018.

- Q. Hu and D. Blough, "Relay Selection and Scheduling for Millimeter Wave Backhaul in Urban Environments," Proc. of IEEE International Conference on Mobile Ad-hoc and Sensor Systems, pp. 206-214, 2017.

REFERENCES

[1] Z. Pi and F. Khan, "An introduction to millimeter-wave mobile broadband systems," *IEEE communications magazine*, vol. 49, no. 6, 2011.

[2] R. J. Weiler, M. Peter, W. Keusgen, E. Calvanese-Strinati, A. De Domenico, I. Filippini, A. Capone, I. Siaud, A.-M. Ulmer-Moll, A. Maltsev, *et al.*, "Enabling 5G backhaul and access with millimeter-waves," in *Networks and Communications (EuCNC), 2014 European Conference on*, IEEE, 2014, pp. 1–5.

[3] L. Verma, M. Fakharzadeh, and S. Choi, "Backhaul need for speed: 60 GHz is the solution," *IEEE Wireless Communications*, vol. 22, no. 6, pp. 114–121, 2015.

[4] M. Jaber, M. A. Imran, R. Tafazolli, and A. Tukmanov, "5G backhaul challenges and emerging research directions: A survey," *IEEE Access*, vol. 4, pp. 1743–1766, 2016.

[5] T. L. Frey, "The effects of the atmosphere and weather on the performance of a mm-Wave communication link," *Applied Microwave and Wireless*, vol. 11, pp. 76–81, 1999.

[6] J. Zhang, J. Wang, Y. Xu, M. Xu, F. Lu, L. Cheng, J. Yu, and G.-k. Chang, "Fiber–wireless integrated mobile backhaul network based on a hybrid millimeter-wave and free-space-optics architecture with an adaptive diversity combining technique," *Optics letters*, vol. 41, no. 9, pp. 1909–1912, 2016.

[7] F. Lu, M. Xu, S. Shen, Y. M. Alfadhli, H. J. Cho, and G.-K. Chang, "Demonstration of inter-dimensional adaptive diversity combining and repetition coding in converged mmw/fso links for 5g and beyond mobile fronthaul," in *2018 Optical Fiber Communications Conference and Exposition (OFC)*, IEEE, 2018, pp. 1–3.

[8] Y. Alfadhli, P.-C. Peng, H. Cho, S. Liu, R. Zhang, Y.-W. Chen, and G.-K. Chang, "Real-time fpga demonstration of hybrid bi-directional mmw and fso fronthaul architecture," in *2019 Optical Fiber Communications Conference and Exhibition (OFC)*, IEEE, 2019, pp. 1–3.

[9] D Hogg, "Path diversity in propagation of millimeter waves through rain," *IEEE Transactions on Antennas and Propagation*, vol. 15, no. 3, pp. 410–415, 1967.

[10] G. E. Weibel and H. O. Dressel, "Propagation studies in millimeter-wave link systems," *Proceedings of the IEEE*, vol. 55, no. 4, pp. 497–513, 1967.

[11] R. Crane, "Propagation phenomena affecting satellite communication systems operating in the centimeter and millimeter wavelength bands," *Proceedings of the IEEE*, vol. 59, no. 2, pp. 173–188, 1971.

[12] S. L. Johnston, "Millimeter wave radar," *Dedham, MA, Artech House, Inc., 1980. 671 p*, 1980.

[13] Z. Qingling and J. Li, "Rain attenuation in millimeter wave ranges," in *2006 7th International Symposium on Antennas, Propagation & EM Theory*, IEEE, 2006, pp. 1–4.

[14] R. Humpleman and P. Watson, "Investigation of attenuation by rainfall at 60 GHz," in *Proceedings of the Institution of Electrical Engineers*, IET, vol. 125, 1978, pp. 85–91.

[15] *E-band technology*, `http://www.e-band.com/index.php?id=86`, [Online; accessed 17-Dec.-2017].

[16] T. S. Rappaport, S. Sun, R. Mayzus, H. Zhao, Y. Azar, K. Wang, G. N. Wong, J. K. Schulz, M. Samimi, and F. Gutierrez, "Millimeter wave mobile communications for 5G cellular: It will work!" *IEEE access*, vol. 1, pp. 335–349, 2013.

[17] T. S. Rappaport, S. Sun, and M. Shafi, "5G channel model with improved accuracy and efficiency in mmWave bands," *IEEE 5G Tech Focus*, vol. 1, no. 1, pp. 1–6, 2017.

[18] T. S. Rappaport, F. Gutierrez, E. Ben-Dor, J. N. Murdock, Y. Qiao, and J. I. Tamir, "Broadband millimeter-wave propagation measurements and models using adaptive-beam antennas for outdoor urban cellular communications," *IEEE transactions on antennas and propagation*, vol. 61, no. 4, pp. 1850–1859, 2012.

[19] J. Esch, "Prolog to" state of the art in 60-GHz integrated circuits and systems for wireless communications"," *Proceedings of the IEEE*, vol. 99, no. 8, pp. 1386–1389, 2011.

[20] G. R. MacCartney and T. S. Rappaport, "73 GHz millimeter wave propagation measurements for outdoor urban mobile and backhaul communications in New York City," in *ICC*, 2014, pp. 4862–4867.

[21] M. R. Akdeniz, Y. Liu, M. K. Samimi, S. Sun, S. Rangan, T. S. Rappaport, and E. Erkip, "Millimeter wave channel modeling and cellular capacity evaluation," *IEEE journal on selected areas in communications*, vol. 32, no. 6, pp. 1164–1179, 2014.

[22] M. Kyro, V.-M. Kolmonen, and P. Vainikainen, "Experimental propagation channel characterization of mm-wave radio links in urban scenarios," *IEEE Antennas and Wireless Propagation Letters*, vol. 11, pp. 865–868, 2012.

[23] K. Haneda, J. Zhang, L. Tan, G. Liu, Y. Zheng, H. Asplund, J. Li, Y. Wang, D. Steer, C. Li, *et al.*, "5G 3GPP-like channel models for outdoor urban microcellular and macrocellular environments," in *2016 IEEE 83rd Vehicular Technology Conference (VTC Spring)*, IEEE, 2016, pp. 1–7.

[24] F. Gutierrez Jr, K. Parrish, and T. S. Rappaport, "On-chip integrated antenna structures in CMOS for 60 GHz WPAN systems," in *GLOBECOM 2009-2009 IEEE Global Telecommunications Conference*, IEEE, 2009, pp. 1–7.

[25] S. Emami, R. F. Wiser, E. Ali, M. G. Forbes, M. Q. Gordon, X. Guan, S. Lo, P. T. McElwee, J. Parker, J. R. Tani, *et al.*, "A 60GHz CMOS phased-array transceiver pair for multi-Gb/s wireless communications," in *2011 IEEE International Solid-State Circuits Conference*, IEEE, 2011, pp. 164–166.

[26] D. Liu and R Sirdeshmukh, "A patch array antenna for 60 GHz package applications," in *2008 IEEE Antennas and Propagation Society International Symposium*, IEEE, 2008, pp. 1–4.

[27] J. Wang, Z. Lan, C.-W. Pyo, T. Baykas, C.-S. Sum, M. A. Rahman, R. Funada, F. Kojima, I. Lakkis, H. Harada, *et al.*, "Beam codebook based beamforming protocol for multi-Gbps millimeter-wave WPAN systems," in *GLOBECOM 2009-2009 IEEE Global Telecommunications Conference*, IEEE, 2009, pp. 1–6.

[28] Y. M. Tsang, A. S. Poon, and S. Addepalli, "Coding the beams: Improving beamforming training in mmwave communication system," in *2011 IEEE Global Telecommunications Conference-GLOBECOM 2011*, IEEE, 2011, pp. 1–6.

[29] J. Qiao, X. Shen, J. W. Mark, and Y. He, "MAC-layer concurrent beamforming protocol for indoor millimeter-wave networks," *IEEE Transactions on Vehicular Technology*, vol. 64, no. 1, pp. 327–338, 2014.

[30] S. Singh, R. Mudumbai, and U. Madhow, "Interference analysis for highly directional 60-GHz mesh networks: The case for rethinking medium access control," *IEEE/ACM Transactions on Networking (TON)*, vol. 19, no. 5, pp. 1513–1527, 2011.

[31] S. Singh, F. Ziliotto, U. Madhow, E Belding, and M. Rodwell, "Blockage and directivity in 60 GHz wireless personal area networks: From cross-layer model to multihop MAC design," *IEEE Journal on Selected Areas in Communications*, vol. 27, no. 8, 2009.

[32] S. Collonge, G. Zaharia, and G. El Zein, "Influence of the human activity on wide-band characteristics of the 60 GHz indoor radio channel," 2004.

[33] C. Dehos, J. L. González, A. De Domenico, D. Ktenas, and L. Dussopt, "Millimeter-wave access and backhauling: The solution to the exponential data traffic increase in 5G mobile communications systems?" *IEEE Communications Magazine*, vol. 52, no. 9, pp. 88–95, 2014.

[34] R. Taori and A. Sridharan, "Point-to-multipoint in-band mmwave backhaul for 5G networks," *IEEE Communications Magazine*, vol. 53, no. 1, pp. 195–201, 2015.

[35] Z. Gao, L. Dai, D. Mi, Z. Wang, M. A. Imran, and M. Z. Shakir, "MmWave massive-MIMO-based wireless backhaul for the 5G ultra-dense network," *IEEE Wireless Communications*, vol. 22, no. 5, pp. 13–21, 2015.

[36] Z. Pi, J. Choi, and R. Heath, "Millimeter-wave gigabit broadband evolution toward 5G: Fixed access and backhaul," *IEEE Communications Magazine*, vol. 54, no. 4, pp. 138–144, 2016.

[37] K. Zheng, L. Zhao, J. Mei, M. Dohler, W. Xiang, and Y. Peng, "10 Gb/s hetsnets with millimeter-wave communications: Access and networking-challenges and protocols," *IEEE Communications Magazine*, vol. 53, no. 1, pp. 222–231, 2015.

[38] Y. Zhu, Y. Niu, J. Li, D. O. Wu, Y. Li, and D. Jin, "QoS-aware scheduling for small cell millimeter wave mesh backhaul," in *Communications (ICC), 2016 IEEE International Conference on*, IEEE, 2016, pp. 1–6.

[39] A. Ahmed and D. Grace, "A dual-hop backhaul network architecture for 5G ultra-small cells using millimetre-wave," in *Ubiquitous Wireless Broadband (ICUWB), 2015 IEEE International Conference on*, IEEE, 2015, pp. 1–6.

[40] R. Ford, F. Gómez-Cuba, M. Mezzavilla, and S. Rangan, "Dynamic time-domain duplexing for self-backhauled millimeter wave cellular networks," in *Communication Workshop (ICCW), 2015 IEEE International Conference on*, IEEE, 2015, pp. 13–18.

[41] X. Xu, W. Saad, X. Zhang, X. Xu, and S. Zhou, "Joint deployment of small cells and wireless backhaul links in next-generation networks," *IEEE Communications Letters*, vol. 19, no. 12, pp. 2250–2253, 2015.

[42] J. Du, E. Onaran, D. Chizhik, S. Venkatesan, and R. A. Valenzuela, "Gbps user rates using mmwave relayed backhaul with high-gain antennas," *IEEE Journal on Selected Areas in Communications*, vol. 35, no. 6, pp. 1363–1372, 2017.

[43] M. Bennai, L. Talbi, J. Le Bel, and K. Hettak, "Medium range backhaul feasibility under NLOS conditions at 60 GHz," in *Millimeter Waves (GSMM), 2015 Global Symposium On*, IEEE, 2015, pp. 1–3.

[44] L. Chen, F. R. Yu, H. Ji, V. C. Leung, X. Li, and B. Rong, "A full-duplex self-backhaul scheme for small cell networks with massive MIMO," in *Communications (ICC), 2016 IEEE International Conference on*, IEEE, 2016, pp. 1–6.

[45] R.-A. Pitaval, O. Tirkkonen, R. Wichman, K. Pajukoski, E. Lahetkangas, and E. Tiirola, "Full-duplex self-backhauling for small-cell 5G networks," *IEEE Wireless Communications*, vol. 22, no. 5, pp. 83–89, 2015.

[46] V. K. Sakarellos, C. I. Kourogiorgas, D. Skraparlis, A. D. Panagopoulos, and J. D. Kanellopoulos, "End-to-end performance analysis of millimeter wave triple-hop backhaul transmission systems," *Wireless personal communications*, vol. 71, no. 4, pp. 2725–2740, 2013.

[47] J. Zhao, T. Q. Quek, and Z. Lei, "Coordinated multipoint transmission with limited backhaul data transfer," *IEEE Transactions on Wireless Communications*, vol. 12, no. 6, pp. 2762–2775, 2013.

[48] Y. Shi, M. Li, X. Xiong, and G. Han, "A flexible wireless backhaul solution for emerging small cells networks," in *2014 IEEE International Conference on Signal Processing, Communications and Computing (ICSPCC)*, IEEE, 2014, pp. 591–596.

[49] X. Ge, H. Cheng, M. Guizani, and T. Han, "5G wireless backhaul networks: Challenges and research advances," *IEEE Network*, vol. 28, no. 6, pp. 6–11, 2014.

[50] S. Samarakoon, M. Bennis, W. Saad, and M. Latva-aho, "Backhaul-aware interference management in the uplink of wireless small cell networks," *IEEE Transactions on Wireless Communications*, vol. 12, no. 11, pp. 5813–5825, 2013.

[51] M. N. Islam, A. Sampath, A. Maharshi, O. Koymen, and N. B. Mandayam, "Wireless backhaul node placement for small cell networks," in *2014 48th annual conference on information sciences and systems (CISS)*, IEEE, 2014, pp. 1–6.

[52] J. Zhao, T. Q. Quek, and Z. Lei, "Heterogeneous cellular networks using wireless backhaul: Fast admission control and large system analysis," *IEEE Journal on Selected Areas in Communications*, vol. 33, no. 10, pp. 2128–2143, 2015.

[53] X. Yi, P. de Kerret, and D. Gesbert, "The dof of network mimo with backhaul delays," in *2013 IEEE International Conference on Communications (ICC)*, IEEE, 2013, pp. 3318–3322.

[54] Q. Hu and D. M. Blough, "Relay selection and scheduling for millimeter wave backhaul in urban environments," in *2017 IEEE 14th International Conference on Mobile Ad Hoc and Sensor Systems (MASS)*, IEEE, 2017, pp. 206–214.

[55] Q. Hu and D. M. Blough, "Optimizing millimeter-wave backhaul networks in roadside environments," in *Communication (ICC), 2018 IEEE International Conference on*, IEEE, 2018.

[56] Q. Hu and D. M. Blough, "High throughput relay-assisted millimeter-wave backhaul networks in urban areas," in *to be submitted*, 2019.

[57] Y. Yan, Q. Hu, and D. M. Blough, "Path selection with amplify and forward relays in mmWave backhaul networks," in *2018 IEEE 29th Annual International Symposium on Personal, Indoor and Mobile Radio Communications (PIMRC)*, IEEE, 2018, pp. 1–6.

[58] Q. Hu, Y. Liu, Y. Yan, and D. M. Blough, "End-to-end simulation of mmWave out-of-band backhaul networks in ns-3," in *Proceedings of the 2019 Workshop on Next-Generation Wireless with ns-3*, ACM, 2019, pp. 1–4.

[59] Y. Yang, H. Hu, J. Xu, and G. Mao, "Relay technologies for WiMAX and LTE-advanced mobile systems," *IEEE Communications Magazine*, vol. 47, no. 10, pp. 100–105, 2009.

[60] S. W. Peters, A. Y. Panah, K. T. Truong, and R. W. Heath, "Relay architectures for 3GPP LTE-advanced," *EURASIP Journal on Wireless Communications and Networking*, vol. 2009, no. 1, p. 618 787, 2009.

[61] Z. Lan, L. A. Lu, X. Zhang, C. Pyo, and H. Harada, "A space-time scheduling assisted cooperative relay for mmWave WLAN/WPAN systems with directional antenna," in *Global Telecommunications Conference (GLOBECOM 2011), 2011 IEEE*, IEEE, 2011, pp. 1–6.

[62] G. Zheng, C. Hua, R. Zheng, and Q. Wang, "Toward robust relay placement in 60 GHz mmwave wireless personal area networks with directional antenna," *IEEE Transactions on Mobile Computing*, vol. 15, no. 3, pp. 762–773, 2016.

[63] Y. Niu, Y. Li, D. Jin, L. Su, and D. Wu, "Blockage robust and efficient scheduling for directional mmWave WPANs," *IEEE Transactions on Vehicular Technology*, vol. 64, no. 2, pp. 728–742, 2015.

[64] J. Qiao, B. Cao, X. Zhang, X. Shen, and J. W. Mark, "Efficient concurrent transmission scheduling for cooperative millimeter wave systems," in *Global Communications Conference (GLOBECOM), 2012 IEEE*, IEEE, 2012, pp. 4187–4192.

[65] E. J. Violette, R. H. Espeland, R. O. DeBOLT, and F. Schwering, "Millimeter-wave propagation at street level in an urban environment," *IEEE Transactions on Geoscience and Remote Sensing*, vol. 26, no. 3, pp. 368–380, 1988.

[66] S. Singh, M. N. Kulkarni, A. Ghosh, and J. G. Andrews, "Tractable model for rate in self-backhauled millimeter wave cellular networks," *IEEE Journal on Selected Areas in Communications*, vol. 33, no. 10, pp. 2196–2211, 2015.

[67] Y. Liu, Q. Hu, and D. M. Blough, "Blockage avoidance in relay paths for roadside mmWave backhaul networks," in *2018 IEEE 29th Annual International Symposium on Personal, Indoor and Mobile Radio Communications (PIMRC)*, IEEE, 2018, pp. 1–7.

[68] Y. Liu and D. M. Blough, "Analysis of blockage effects on roadside relay-assisted mmWave backhaul networks," in *2019 IEEE International Conference on Communications (ICC)*, IEEE, 2019.

[69] Y. Liu, Q. Hu, and D. M. Blough, "Joint link-level and network-level reconfiguration for mmWave backhaul survivability in urban environments," in *22nd ACM International Conference on Modeling, Analysis and Simulation of Wireless and Mobile Systems*, ACM, 2019.

[70] Y. Niu, C. Gao, Y. Li, L. Su, D. Jin, and A. V. Vasilakos, "Exploiting device-to-device communications in joint scheduling of access and backhaul for mmwave small cells," *IEEE Journal on Selected Areas in Communications*, vol. 33, no. 10, pp. 2052–2069, 2015.

[71] Y. Niu, C. Gao, Y. Li, L. Su, D. Jin, Y. Zhu, and D. O. Wu, "Energy-efficient scheduling for mmWave backhauling of small cells in heterogeneous cellular networks," *IEEE Transactions on Vehicular Technology*, vol. 66, no. 3, pp. 2674–2687, 2017.

[72] J. García-Rois, F. Gómez-Cuba, M. R. Akdeniz, F. J. González-Castaño, J. C. Burguillo, S. Rangan, and B. Lorenzo, "On the analysis of scheduling in dynamic duplex multihop mmwave cellular systems," *IEEE Transactions on Wireless Communications*, vol. 14, no. 11, pp. 6028–6042, 2015.

[73] J. G. Rois, B. Lorenzo, F. J. González-Castaño, and J. C. Burguillo, "Heterogeneous millimeter-wave/micro-wave architecture for 5G wireless access and backhauling," in *Networks and Communications (EuCNC), 2016 European Conference on*, IEEE, 2016, pp. 179–184.

[74] Z. Shi, Y. Wang, L. Huang, and T. Wang, "Dynamic resource allocation in mmwave unified access and backhaul network," in *Personal, Indoor, and Mobile Radio Com-*

munications (PIMRC), 2015 IEEE 26th Annual International Symposium on, IEEE, 2015, pp. 2260–2264.

[75] V. M. Vishnevsky, A. A. Larionov, R. E. Ivanov, and M. Dudin, "Applying graph-theoretic approach for time-frequency resource allocation in 5G MmWave backhaul network," in *Advances in Wireless and Optical Communications (RTUWO), 2016*, IEEE, 2016, pp. 221–224.

[76] B. Hajek and G. Sasaki, "Link scheduling in polynomial time," *IEEE transactions on Information Theory*, vol. 34, no. 5, pp. 910–917, 1988.

[77] A. Thornburg, T. Bai, and R. W. Heath, "Interference statistics in a random mmwave ad hoc network," in *2015 IEEE International Conference on Acoustics, Speech and Signal Processing (ICASSP)*, IEEE, 2015, pp. 2904–2908.

[78] I. A. Hemadeh, K. Satyanarayana, M. El-Hajjar, and L. Hanzo, "Millimeter-wave communications: Physical channel models, design considerations, antenna constructions, and link-budget," *IEEE Communications Surveys & Tutorials*, vol. 20, no. 2, pp. 870–913, 2018.

[79] P. Gupta and P. R. Kumar, "The capacity of wireless networks," *IEEE Transactions on information theory*, vol. 46, no. 2, pp. 388–404, 2000.

[80] C. Bron and J. Kerbosch, "Algorithm 457: Finding all cliques of an undirected graph," *Communications of the ACM*, vol. 16, no. 9, pp. 575–577, 1973.

[81] A. Yonis, M. Abdullah, and M. Ghanim, "LTE-FDD and LTE-TDD for cellular communications," *Proceeding, Progress in*, 2012.

[82] G. Ku, "Resource allocation in LTE," *Adaptive Signal Processing and Information Theory Research Group*, 2011.

[83] B. T. Scheme, "LTE: The evolution of mobile broadband," *IEEE Communications magazine*, vol. 45, pp. 44–51, 2009.

[84] D. D. Coleman and D. A. Westcott, *CWNA Certified Wireless Network Administrator Study Guide: Exam CWNA-107*. John Wiley & Sons, 2018.

[85] S Ramanathan, "A unified framework and algorithm for (T/F/C) DMA channel assignment in wireless networks," in *Proceedings of INFOCOM'97*, IEEE, vol. 2, 1997, pp. 900–907.

[86] S. C. Ergen and P. Varaiya, "TDMA scheduling algorithms for wireless sensor networks," *Wireless Networks*, vol. 16, no. 4, pp. 985–997, 2010.

[87] Y. Yi, A. Proutière, and M. Chiang, "Complexity in wireless scheduling: Impact and tradeoffs," in *Proceedings of the 9th ACM international symposium on Mobile ad hoc networking and computing*, ACM, 2008, pp. 33–42.

[88] G. Sharma, R. R. Mazumdar, and N. B. Shroff, "On the complexity of scheduling in wireless networks," in *Proceedings of the 12th annual international conference on Mobile computing and networking*, ACM, 2006, pp. 227–238.

[89] T. Moscibroda, R Rejaie, and R. Wattenhofer, "How optimal are wireless scheduling protocols?" In *IEEE INFOCOM 2007-26th IEEE International Conference on Computer Communications*, IEEE, 2007, pp. 1433–1441.

[90] D. M. Blough, S. Das, G. Resta, and P. Santi, "A framework for joint scheduling and diversity exploitation under physical interference in wireless mesh networks," in *2008 5th IEEE International Conference on Mobile Ad Hoc and Sensor Systems*, IEEE, 2008, pp. 396–403.

[91] D. M. Blough, G. Resta, and P. Santi, "Approximation algorithms for wireless link scheduling with SINR-based interference," *IEEE/ACM Transactions on Networking (ToN)*, vol. 18, no. 6, pp. 1701–1712, 2010.

[92] R. Jain, A. Durresi, and G. Babic, "Throughput fairness index: An explanation," in *ATM Forum contribution*, vol. 99, 1999.

[93] R. Ferrus, O. Sallent, J. Perez-Romero, and R. Agusti, "On 5g radio access network slicing: Radio interface protocol features and configuration," *IEEE Communications Magazine*, vol. 56, no. 5, pp. 184–192, 2018.

[94] C Lopez, "Highway illumination manual," *Austin, TX: Texas Department of Transportation Traffic Operations Division*, 2003.

[95] 3GPP, *Release 15*, `https://www.3gpp.org/release-15`, [Online; accessed 8-Apr.-2019].

[96] M. Mezzavilla, M. Zhang, M. Polese, R. Ford, S. Dutta, S. Rangan, and M. Zorzi, "End-to-end simulation of 5G mmWave networks," *IEEE Communications Surveys & Tutorials*, vol. 20, no. 3, pp. 2237–2263, 2018.

[97] G. Piro, N. Baldo, and M. Miozzo, "An LTE module for the ns-3 network simulator," in *Proceedings of the 4th International ICST Conference on Simulation Tools and Techniques*, ICST (Institute for Computer Sciences, Social-Informatics and, 2011, pp. 415–422.

[98] N. Patriciello, S. Lagen, L. Giupponi, and B. Bojovic, "An improved MAC layer for the 5G NR ns-3 module," in *Proceedings of the 2019 Workshop on ns-3*, ACM, 2019, pp. 41–48.

[99] M. Polese, M. Giordani, A. Roy, S. Goyal, D. Castor, and M. Zorzi, "End-to-end simulation of integrated access and backhaul at mmwaves," in *2018 IEEE 23rd International Workshop on Computer Aided Modeling and Design of Communication Links and Networks (CAMAD)*, IEEE, 2018, pp. 1–7.

[100] N. Patriciello, S. Lagen, B. Bojovic, and L. Giupponi, "An E2E simulator for 5G NR networks," *Simulation Modelling Practice and Theory*, vol. 96, p. 101 933, 2019.

[101] H. Assasa and J. Widmer, "Implementation and evaluation of a WLAN IEEE 802.11 ad model in ns-3," in *Proceedings of the Workshop on Ns-3*, ACM, 2016, pp. 57–64.

[102] 3GPP, *Medium access control (MAC) protocol specification*, `https://www.3gpp.org/DynaReport/36321.htm`, [Online; accessed 7-Apr.-2019].